國 立 交 通 大 學

材料科學與工程研究所

博 士 論 文

含雜環之新型窄能隙共軛高分子於有機光伏電池應用
之合成與鑑定

Synthesis and Characterization of Novel Narrow-Band-Gap
Conjugated Copolymers Containing Heterocyclic Moieties
for Organic Photovoltaic Cells Applications

研 究 生：李光潔

指導教授：林宏洲 博士

中華民國九十八年四月

含雜環之新型窄能隙共軛高分子於有機光伏電池應用

之合成與鑑定

Synthesis and Characterization of Novel Narrow-Band-Gap Conjugated Copolymers Containing Heterocyclic Moieties for Organic Photovoltaic Cells Applications

研 究 生 ：李光潔　　　　　　　Student: Kuang-Chieh Li

指導教授 ：林宏洲　　　　　　　Advisor: Prof. Hong-Cheu Lin

國立交通大學

材料科學與工程學系

博士論文

A Thesis
Submitted to Department of Materials Science and Engineering
College of Engineering
National Chiao Tung University
In Partial Fulfillment of the Requirement
For the Degree of Doctor of Philosophy of Science
In Materials Science and Engineering
April 2009
Hsinchu, Taiwan

中華民國九十八年四月

Synthesis and Characterization of Novel Narrow-Band-Gap Conjugated Copolymers Containing Heterocyclic Moieties for Organic Photovoltaic Cells Applications

Student: Kuang-Chieh Li   Advisor: Prof. Hong-Cheu Lin

Department of Materials Science and Engineering National Chiao Tung University

Abstract

First, novel twelve narrow-band-gap conjugated copolymers consisting of the comonomers alkyl-substituted fluorene and mono- and bis-(2-aryl-2-cyanovinyl)-10-hexylphenothiazine were copolymerized by a padallium-catalyzed Suzuki coupling reaction with two different feed ratios. The polymers showed broad optical absorption from 400 to 800 nm with optical band gaps at 1.55-2.10 eV. Second, other novel groups of five cyclopentadithiophene-based copolymers employing arylcyanovinyl and keto groups in different molar ratios were also synthesized successfully by palladium (0)-catalyzed Suzuki coupling reactions. Finally, six novel conjugated copolymers containing coplanar cyclopentadithiophene units (incorporated with bithiazole/thienyl-based monomers) were synthesized and developed for the applications of polymer solar cells (PSCs). For these cyclopentadithiophene-based copolymers, they showed broad optical absorption from 400 to 900 nm with optical band gaps at 1.38-1.94 eV. Powder X-ray diffraction

(XRD) analyses suggested that these copolymers formed highly self-assembled π-π stackings. Under 100 mW/cm^2 of AM 1.5 white-light illumination, as blended with [6,6]-phenyl C$_{61}$ butyric acid methyl ester (PCBM) as an electron acceptor in bulk heterojunction photovoltaic devices, narrow-band-gap polymers as electron donors showed significant photovoltaic performance which varied with the intramolecular donor-acceptor interaction and their mixing ratios to PCBM. The PSC device in the weight ratio of 1:2 with PCBM gave the best preliminary result with an overall power conversion efficiency (PCE) of 3.04%, an open-circuit voltage of 0.70 V, a short-circuit current of 8.00 mA/cm^2, and a fill factor of 53.7%

含雜環之新型窄能隙共軛高分子於有機光伏電池應用之合成與鑑定

學　生：李光潔　　　　　　　　　指　導　教　授：林宏洲　博士

國立交通大學材料科學與工程研究所

博士班

摘　要

　　本論文研究方向為探討一系列包含窄能隙共軛高分子之合成與其在有機太陽能電池的應用，並以三大方向為研究主軸。第一個部份，包含了以烷基取代的莽 (Flourene) 單元與雜環 bis-(2-aryl-2-cyanovinyl)-10-hexylphenothiazine 衍生物之單體為高分子主鏈結構，成功的以 Suzuki coupling 聚合出 12 個新的高分子。第二，另一些新的雜環包含 arylcyanovinyl 與 keto 取代基的 cyclopentadithiophene 單體，也成功地以 Suzuki coupling 聚合出 5 個新的共軛高分子。最後一個部份，將另一些新型之 bithiazole/thienyl

基團的單體與 cyclopentadithiophene 單體做為研究的主題，共聚出六

個共軛高分子。在鑑定方面，藉由 ^{1}HNMR 光譜圖上的積分值可輕易

的鑑定出共軛高分子的主鏈結構是由上同的單體所建構。然而，利用

紫外光-可見光光譜儀，這些共軛高分子顯示了從 400 至 900 nm 如此

寬廣的吸收能帶，且其光學能隙大約在 1.38-2.10 eV 之間。而利用 X

光繞射圖譜（XRD）可以更進一步證明這些共軛高分子本身就具有高

度的自我堆疊的效果。結果發現，在 AM1.5G、100 mW/cm^2 的模擬

太陽光下，將合成出之高分子與 PCBM ([6,6]-phenyl C$_{61}$-butyric acid

methyl ester)混合(blend)為主動層材料，成功地以 1:2w/w 的混合比例

得到一具有短路電流 8.00 mA/cm^2、開路電壓 0.70 V、填充因子 0.537

及最高之光電轉換效率 3.04%之有機太陽能電池。

ACKNOWLEDGEMENTS

Table of Contents

Table Lists

Figure Lists

Chapter 1 Introduction

1.1 Introduction to organic photovoltaic cells

The discovery of the photovoltaic (PV) effect is commonly ascribed to Becquerel (see Figure 1.1[1]), who discovered a photocurrent when platinum electrodes, covered with silver bromide or silver chloride, was illuminated in aqueous solution (strictly speaking this is a photo electrochemical effect).[2] Smith and Adams made the first reports on photoconductivity, in 1873 and 1876, respectively, working on selenium.[3] Anthracene was the first organic compound in which photoconductivity was observed by Pochettino in 1906[4] and Volmer in 1913[5]. In the late 1950s and 1960s the potential use of organic materials as photo receptors in imaging systems was recognized.[6] The scientific interest as well as the commercial potential led to increased research into photoconductivity and related subjects. In the early 1960s it was discovered that many common dyes, such as methylene blue, had semiconducting properties.[7] Later, these dyes where among the first organic materials exhibited the PV effect.[8] Also, the PV effect was observed in many important molecules such as carotenes, chlorophylls and other porphyrins, as well as the structural related phthalocyanines (PC).

The potential of organic photovoltaic cells (OPVs) is related to the idea of low-cost photovoltaic materials such as polymers (plastics), which could be easily manufactured as large area films, cut from rolls and installed onto permanent structures. Inspired by the significant progress in solar cell efficiencies with some organic materials such as dyes in the case of dye-sensitized solar cells and the discovery of efficient charge transfer between certain organic electron donor and acceptor molecules, the research on organic photovoltaic materials has grown rapidly during the last decade and is very active at the moment. Organic materials used presently in solar cells include for example conducting polymers, dyes, pigments, and

liquid crystals. Among these, the conductive polymers are perhaps the best known for their photo-physical properties.
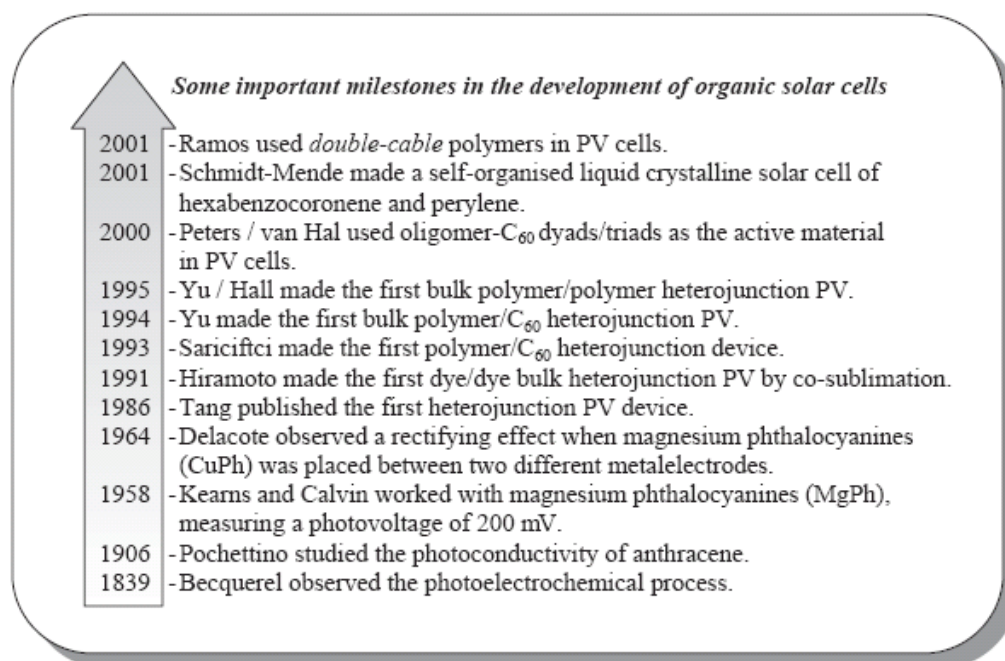
Figure 1.1 Some important milestones in the development of organic solar cells.[1]

Sorts of solar cell		Semiconductor Materials	Power conversion efficiency
Silicon	Crystalline silicon	Single crystal silicon (wafer type)	13~20%
		Polycrystal silicon (wafer type、thin film type)	10~15%
	Amorphous silicon	α-Si、α-SiO、α-SiGe	5~10%
Compound Semiconductor	Two element	GaAs(wafer type)	GaAs18~30%
		CdS、CdTe(thin film type)	7~10%
	Three elememt	CuInSe$_2$(thin film type)	8~10%
Dye Senzitized Solar Cell			11%
Organic Thin Film Solar Cell			~5% Single Cell 6.5% Tandem Cell

Figure 1.2 Current status of solar cells.

The current status of solar cells is shown in Figure 1.2. In the more than 20 years since the seminal work of Tang,[9] organic solar cells have undergone a gradual evolution that has led to power conversion efficiencies (PCE) of about 5%. To attain efficiencies approaching 10% in such organic solar cells, much effort is required to understand the fundamental electronic interactions as well as the complex interplay of device architecture, morphology, processing, and the fundamental electronic processes.

1.1.1 Conjugated polymer semiconductors

Conjugated polymers are organic molecules with repeating structural units attached to each other by alternating single and double carbon-carbon (sometimes carbon-nitrogen) bonds. The single bond is so-called σ-bond, while the double bond contains a σ-bond and a π-bond. In this alternating chain of single and double bonds, the molecular p_z orbitals constituting the π-bonds are actually overlapped and spread over the entire molecule, and the electrons in this molecular orbital are respectively delocalized along the whole molecular chain.

One of the most studied photoconducting polymers is poly(vinyl carbazole) (PVK). The first report came in 1958 by Hoegel et al.[10] who proposed its practical use as an electrophotographic agent. In the 1970s it was discovered that certain conjugated polymers, notably poly(sulphur nitride) and polyacetylene (see Figure 1.3), could be made highly conducting in the presence of certain dopants.[11] In 1982 Weinberger et al.[12] investigated polyacet ylene as the active material in an Al/polyacetylene/graphite cell. The cell had a low open-circuit voltage of only 0.3V and a low QE of only 0.3%. Later Glenis et al.[13] investigated different polythiophenes. Again the systems suffered low efficiencies and low open-circuit voltages in the 0.4 V range. The low open-circuit voltages have been ascribed to the formation of polarons

3

(delocalised excitons) that energetically relax in the energy gap, which then becomes smaller than the π-π^* gap. This relaxation results in a large spectral shift when the luminescence spectra are compared to the absorption spectra (Stokes' shift). The result of the relaxations is that it limits the attainable voltage and the maximum PCE. Different electrode material have been used but not with success.
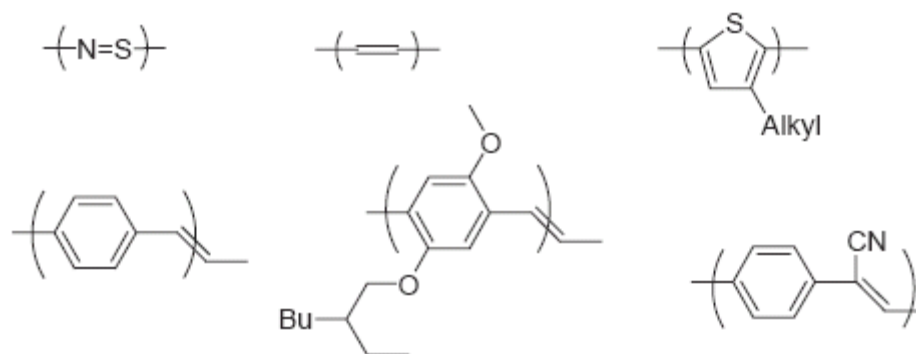
Figure 1.3 Some conjugated polymers investigated in PV cells. Top: poly(sulpher nitride) (SNx), polyacetylene, and poly(3-alkyl-thiophene). Bottom: poly(p-phenylene vinylene) (PPV), poly(2-methoxy-5-(2'-ethylhexyloxy)-1,4-phenylvinylene) (MEH–PPV), and cyano-PPV (CN-PPV).

Followed by the poly(alkyl-thiophenes) (PATs), PPV and its derivatives is the most investigated conjugated polymer in PV cells. Unlike polyacetylene and polythiophene there is only limited energy relaxation. Karg et al.[14] was the first to investigate PPV in ITO/PPV/Al LEDs and PV devices in 1993. Karg measured V_{oc} of 1 V and a PCE of 0.1% under white light illumination. In 1994 both Marks et al.[15] and Antoniad is et al.[16] also investigated this system. Interestingly enough they had different views on the depletion width in the cells. Marks found that their cells were completely depleted while Antoniadis' cells formed Schottky type barriers at the Al-interface. This divergent behavior is probably related to the fact that PPV is very sensitive to atmospheric oxygen as an efficient dopant for PPV. Other investigated PPV derivatives include M3EH–PPV[17] and poly(2,5-diheptyloxy-pphenylenevinylene) (HO–PPV)[18].

1.1.2 Photovoltaic effect in conjugated polymers

The situation in molecular or polymeric organic solar cells is however much more complex because of the absence of three dimensional crystal lattice, different intramolecular and intermolecular interactions, local structural disorders, amorphous and crystalline regions, and chemical impurities. Figure 1.4 illustrates the mechanism by which light energy is converted into electrical energy in the devices. The energy conversion process has four fundamental steps in the commonly accepted mechanism:[19] 1) Absorption of light and generation of excitons, 2) diffusion of the excitons, 3) dissociation of the excitons with generation of charge, and 4) charge transport and charge collection.
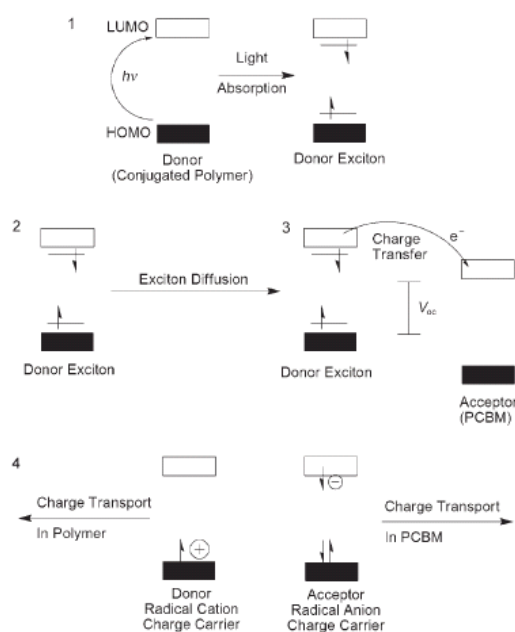
Figure 1.4 General mechanism for photoenergy conversion in excitonic solar cells.[20]

The current-voltage characteristics of a solar cell in the dark and under illumination are shown in Figure 1.5. In the fourth quandrant (between (a) and (b)), the device generates power under light. At maximum power point (MPP), the product of current and voltage is the largest.[21]
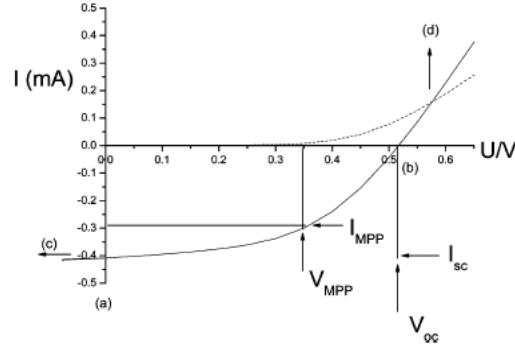
Figure 1.5 Current-voltage (*I-V*) curves of an organic solar cell (dark, - - -; illuminated, -). The characteristic intersections with the abscissa and ordinate are the open circuit voltage (V_{oc}) and the short circuit current (I_{sc}), respectively. The largest power output (P_{max}) is determined by the point where the product of voltage and current is maximized. Division of P_{max} by the product of I_{sc} and V_{oc} yields the fill factor FF.[22]

The photovoltaic power conversion efficiency of a solar cell is determined by the following formula:

$$\eta_e = \frac{V_{oc} * I_{sc} * FF}{P_{in}}$$

$$FF = \frac{I_{mpp} * V_{mpp}}{V_{oc} * I_{sc}}$$

where V_{oc} is the open circuit voltage, I_{sc} is the short circuit current, FF is the fill factor, and P_{in} is the incident light power density. This light intensity is standardized at 1000 W/m^2 with a spectral intensity distribution matching that of the sun on the earth's surface at an incident angle of 48.2°, which is called the AM 1.5 spectrum.[23] I_{mpp} and V_{mpp} are the current and voltage at the maximum power point.

Open Circuit Voltage

Generally, the open circuit voltage of a metal-insulator-metal (MIM) device is determined by the difference in work functions of the two metal contacts. [24] However, in a p-n junction, the maximum available voltage is determined by the difference of the quasi Fermi levels of the two charge carriers, that is, n-doped semiconductor energy level and p-doped semiconductor energy level, respectively. In organic solar

6

cells, the open circuit voltage is found to be linearly dependent on the highest occupied molecular orbital HOMO level of the donor (p-type semiconductor quasi Fermi level) and lowest unoccupied molecular orbital LUMO level of the acceptor (n-type semiconductor quasi Fermi level).[25-26]

Gadisa et al.[27] studied the changes in the Voc with the variation of the first oxidation potential (HOMO level) of the donor conjugated polymer. Scharber et al.[26] reported for 26 different bulk heterojunction solar cells that there is a linear relation between the oxidation potential (HOMO level) of the conjugated polymer and the V_{oc} (see Figure 1.6).
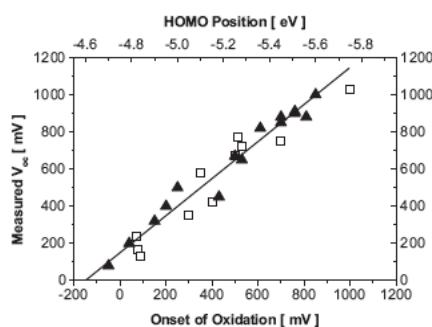
Figure 1.6 V_{oc} of different bulk heterojunction solar cells plotted versus the oxidation potential/HOMO position of the donor polymer used in each individual device. The straight line represents a linear fit with a slope of 1.[26]

Charge carrier losses at electrodes lower the V_{oc}.[27] Open circuit voltage is also affected by the nanomorphology of the active layer in the polymer fullerene bulk heterojunction solar cells.[28] To achieve a better match between the energy levels of the anode and the HOMO of the hole conducting material, the commonly used indium tin oxide (ITO) anode can be modified by plasma etching[29] or by coating with a higher work function organic hole transport layer.[30] The cathode is generally modified by deposition of a thin layer of LiF between the metal electrode and the organic semiconductor. This improves the charge injection in organic light emitting diodes OLEDs and also increases V_{oc} in organic solar cells.[31] Therefore, the open circuit

potential is a sensitive function of energy levels of the used materials as well as their interfaces.[21]

Short Circuit Current

In the ideal, loss free contacts, the short circuit current, I_{sc}, is determined by the product of the photoinduced charge carrier density and the charge carrier mobility within the organic semiconductors:

$$I_{sc} = ne\mu E$$

where n is the density of charge carriers, e is the elementary charge, μ is the mobility, and E is the electric field. Assuming the 100% efficiency for the photoinduced charge generation in a bulk heterojunction mixture, n is the number of absorbed photons per unit volume.

For a given absorption profile of a given material, the bottleneck is the mobility of charge carriers. It is sensitive to the nanoscale morphology of the organic semiconductor thin film.[32-33] Parameters such as solvent type, the solvent evaporation (crystallization) time, the temperature of the substrate, and/or the deposition method can change the nanomorphology.[34] Organic semiconductors generally are materials exhibiting low mobilities, ranging between $\mu \approx 10^{-5}$ to 10^{0} cm^2/Vs.[35] This directly limits the active layer thickness of organic photovoltaic devices. Beyond a certain thickness, the charge carriers will not reach the electrodes before recombination. Therefore, high mobility/low band gap materials are the general route for improving the short circuit current.

The external quantum efficiency or incident photon to current efficiency (IPCE) is simply the number of electrons collected under short circuit conditions, divided by the number of incident photons. IPCE is calculated using the following formula:

$$IPCE = \frac{1240 I_{sc}}{\lambda P_{in}}$$

where λ [nm] is the incident photon wavelength, I_{sc} [μA/cm^2] is the photocurrent of

the device, and P_{in} [W/m^2] is the incident power.

Fill Factor

The filling factor FF is determined by the fraction of the photogenerated charge

carriers that actually reach the electrodes, when the built-in field is lowered toward

the open circuit voltage. There is a competition between charge carrier recombination

and transport. Hence, the product of the lifetime τ times the mobility μ determines the

distance d that charge carriers can drift under a certain electric field E:[36]

$$d = \mu \times \tau \times E$$

This product $\mu \times \tau$ has to be maximized.[37] Furthermore, the series resistances

influence the filling factor considerably and should be minimized. Finite conductivity

of the ITO substrate clearly limits the FF on large area solar cells.[38] Finally, the device

should be free of "shorts" between electrodes to maximize the parallel shunt

resistance.

1.1.3 Photovoltaic narrow-band-gap heterocyclic polymer-based materials

There are several factors that influence the efficiency of OPVs, e.g. the structure

of the polymer, the morphology of the film, and the choice of electron acceptor and

the ratio between this and the polymer.[39] A band gap is defined as the difference

between the highest occupied molecular orbital (HOMO) and the lowest unoccupied

molecular orbital (LUMO) energy levels in the polymer. Narrow band gap polymers

are loosely defined as polymers of band gaps < 2 eV.

Thus, the representation of the solar spectrum in photon flux as a function of

wavelength give a better picture of how many photons that are available for conversion into electrons under ideal conditions. Figure 1.7 shows a displacement of the maximum towards the infrared wavelengths when considering the number of photons rather than the energy. From this point of view it is of great interest to harvest photons at the longer wavelengths. The view taken in this account is experimental and the practical efficiencies that can be obtained for low band gap materials may not coincide with the theoretically predicted value for the optimum band gap. Based on these simple considerations the low band gap polymers have the possibility to improve the efficiency of OPVs due to a better overlap with the solar spectrum.[41]
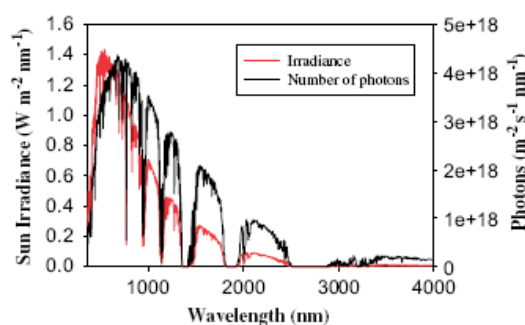
Figure 1.7 Sun irradiance (red) and number of photons (black) as a function of wavelength. The sun intensity spectrum is based on data from NREL.[40]

Structural Factors and Band Gap

Due to a unique combination of stability, moderate aromatic character and structural versatility, thiophene-based linear π-conjugated systems still represent the most widely investigated basic structure for the synthesis of molecular or polymeric materials with a narrow band gap. There are several factors that influence the band gap of a conjugated polymer material. Among these are: (1) intra-chain charge transfer; (2) bond-length alternation; (3) aromaticity; (4) substituents effects; (5) intermolecular interactions; (6) π-conjugation length.[42-43]

Most of the low band gap polymers described in the literature are based on thiophene either as a polythiophene (PT), in a copolymer or as part of a fused ring

system which can be achieved by modifying the electronic properties of existing polymer units.[44] Identical for these copolymers are the alternation between electron donor (electron rich) and electron acceptor (electron deficient) units.[43,45] The high energy level for the HOMO of the donor and the low energy level for the LUMO of the acceptor results in a lower band gap due to an intra-chain charge transfer from donor to acceptor.[43,45] By mathematical simulation it was shown that the electron affinity was higher around the acceptor units compared with the donor units in these types of copolymers.[46]

Planarity along the aromatic backbone results in a low band gap, due to a high degree of delocalization of the pelectrons.[47] A reduction of the difference in bond length alternation is achieved by the alternation of donor and acceptor units along the conjugated polymer chain thus lowering the band gap. In essence this concept suppresses the Peierls effect.[48] The alternation between donor and acceptor results in two resonance forms: D-A and $D^+ = A^-$.[47] As described interactions between acceptor and donor enhance double bond character between the repeating units, this stabilizes the quinoid form of e.g. benzo-bis(thiadiazole) (see Figure 1.8) formed within the polymer backbone, and hence a reduction in band gap is achieved.[48]
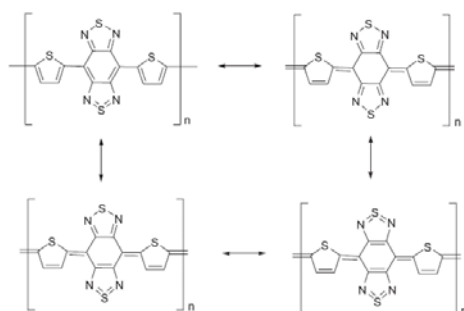
Figure 1.8 Resonance structures in benzo-bis-thiadiazole.

If the HOMO level of the donor and the LUMO level of the acceptor are close in energy it results in a low band gap as shown in Figure 1.9. This is efficiently achieved

by using electron withdrawing groups (EWG) on the acceptor and electron donating groups (EDG) on the donor. EWG such as CN, NO_2, quinoxalines, pyrazines, thiadiazoles or bithiazoles lower the energy levels (and thereby LUMO) of the acceptor. EDG such as thiophene or pyrrole raise the energy levels (and thereby HOMO) of the donor.[48]
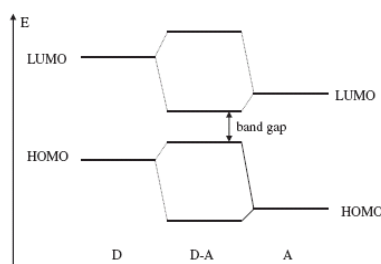
Figure 1.9 Alternating donor-acceptor units lower the band gap by orbital mixing.

Heterocyclic structures for OPVs

The first examples of solar cells based on PT were reported in 1984 by Garnier and coworkers, who described Schottky diodes with 0.15% efficiency under white-light irradiation at low intensity.[49] In 1992 Sariciftci et al. demonstrated that photo-excitation of a mixture of poly[2-methoxy,5-(20-ethyl-hexyloxy)-p-phenylene vinylene] (MEH-PPV) and C_{60} fullerene results in an ultra-fast, photo-induced electron transfer from the π-conjugated system to C_{60} with a quantum efficiency for charge separation close to unity and a lifetime of the charge-separated state in the millisecond-range.[50] However, these efforts have generated a continuous improvement in performance and power-conversion efficiencies of 3.5% have been obtained based on PPV derivatives.[19] The replacement of PPV derivatives with poly(3-hexylhiophene) (P3HT) represents an important step in the optimization and several groups have recently reported power conversion efficiencies in the 4.5 to 5% range.[51-53]

It is generally admitted that a conjugated system serving as donor in OPVs

should have a band gap lower than 1.80 eV in order to achieve a better harvesting of solar photons, whose maximum flux is around 1.77 eV.[26] Although this E_g value is relatively easy to obtain, the problem is complicated by the fact that, besides having the appropriate band gap, the conjugated donor must fulfill other prerequisites regarding the absolute position of the HOMO and LUMO levels, the absorption coefficient and the hole mobility. Furthermore, since the open-circuit voltage of the cell depends on the difference between the HOMO of the donor and the LUMO of the acceptor material, the donor must possess a relatively low HOMO level.[25-26]

As shown in previous work, introduction of acceptor groups such as nitro, carboxy or cyano at the 3-position of the thiophene unit induces a large increase in the oxidation potential.[54] Work carried out in many groups have shown that the introduction of a cyano group at the vinylene linkage of dithienylethylene could lead to a considerable reduction of the band gap of the corresponding polymers.[55-57] Thus E_g values as low as 0.60 eV have been observed for **P1** (Figure 1.10). However due to solubility problems, the polymer contains only a limited fraction of low band gap material. Reynolds and coworkers synthesized a cyanovinylenedioxythiophene **P2** (Figure 1.10) with a band gap of 1.70 eV. OPVs were fabricated with PCBM in a ratio of 1:4. The action spectrum of the cell shows an EQE peak of 11% at 600 nm, and a 0.10% efficiency under white-light illumination in AM 1.5 conditions.[55] More recently, Vanderzande and coworkers synthesized a series of polymers from bis-(cyano-2-thienylvinylene)phenylene precursors (**P3**-**P4**) (Figure 1.10). The polymers show E_g values of 1.72 and 1.59 eV for **P3** and **P4** respectively.[56]

In the past decade, the π-conjugated polymers containing of the five- or six-membered heterocyclic molecules have been dramatically attracted for OPV applications. Fused ring derivatives of aromatic or heteroaromatic molecules lead to

13

more extended conjugation in the ground state, more planar molecular geometries and more rigid structures. The rigid fused ring structure also lowers the reorganisation energy, a factor that has been shown to strongly affect the rate of intermolecular hopping and hence the mobility of charges in organic semiconductors.[58]
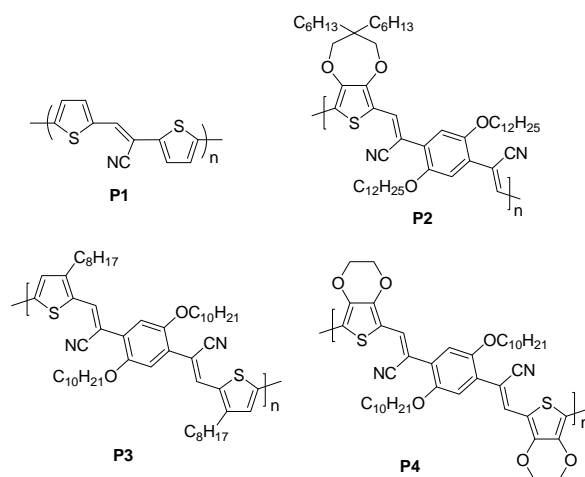
Figure 1.10 Introduction of electron-withdrawing groups cyano groups in polymers **P1-P4** can reduce the band-gap energy.[55-57]

Phenothiazine is a well-known heterocyclic compound with electron-rich sulfur and nitrogen heteroatoms. Polymers and organic molecules containing phenothiazine units as the electron-donating moieties have lately attracted considerable research interests on account of the unique electro-optical properties originated from their electron-rich sulfur and nitrogen heteroatoms on the heterocyclic compounds, which can make these molecules potential materials for the applications of photovoltaic devices,[59-60] and organic field effect transistors (OFETs).[61]

Kraak *et al.* coworkers first reported cyclopentadithiophene (CPDT) units in 1968[62], and the resulting polymers showed relatively high conductivity[63-65], which compared to that polythiophene or polyfluorene, etc.[64-65] Recently, Mülbacher et al. synthesized a copolymer of dialky-cyclopentabithiophene and benzothiadiazole (Figure 1.11), which showed an absorption maximum at 705 nm and a PCE value of 2.67%.[66] Quite recently, Peet et al. have shown that incorporation of a few percent of

alkanedithiol in the solution used to spin-cast films of the copolymer and C_{60} led to an increase of the PCE of the cell to 5.5%.[67]

Recently, thiazole is one of the strongest electron-accepting azaheterocycles because it contains one electron-withdrawing imine –C=N nitrogen in place of the carbon atom at the 3-position of thiophene. Therefore, polymers with incorporation of the bithiazole moieties have been demonstrated to be new materials as n-type transporters.[68-69] Wong et al. synthesized platinum(II) polyynes containing bithiazole-oligo(thienyl) rings (Figure 1.11), which displayed the OPVs with PCE up to 2.7% and a peak external quantum efficiency (EQE) to 83% under AM 1.5 simulated solar illumination.[70]

(a)   (b)
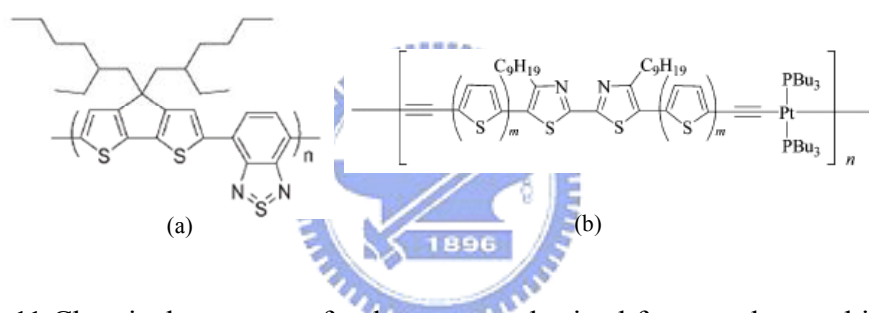
Figure 1.11 Chemical structure of polymers, synthesized from cyclopentabithiophene and benzothiadiazole (a) and platinum(II) polyynes (b).

1.1.4 Organic photovoltaic device architectures

The organic solar cells reported in the literature can be categorized by their device architecture as having single layer, bilayer, disordered bulk heterojunction, or ordered bulk heterojunction.structure (Figure 1.12).

OPVs base on the bulk heterojunction (BHJ)[72] concept are particularly attractive, mainly due to their potential for low cost, ease of fabrication, and mechanical flexibility. For the polymer solar cells highest efficiencies reaching up to 5% have been reported.[51-52]   The bulk hetero-junction is to intimately mix the donor and acceptor components in bulk, and it is different from the bilayer device due to it

exhibits a largely increased interface area where charge separation occurs and each donor–acceptor interface is within a distance less than the exciton diffusion length of each absorbing site, no loss due to too small exciton diffusion lengths is expected because ideally all excitons will be dissociated within their lifetime. However, the collection efficiency of photo-generated carriers in the bulk heterojunction cell is critically dependent on the transport properties of the interpenetrating network of the donor and acceptor materials.
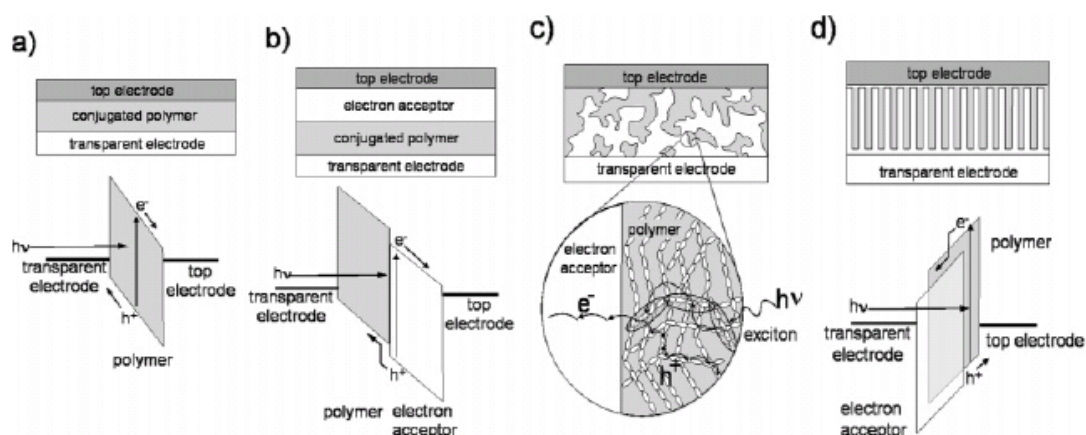
Figure 1.12 Four device architectures of conjugated polymer-based photovoltaic cells: (a) single-layer PV cell; (b) bilayer PV cell; (c) disordered bulk heterojunction; (d) ordered bulk heterojunction.[71]

To achieve high quantum efficiency, all photo-generated excitons have to reach and dissociate at a donor-acceptor interface, and subsequently all created charges have to reach the respective electrodes. Photoluminescence quenching and photocurrent modeling indicate that only photogenerated excitons in proximity to the D-A interface within less than the exciton diffusion length can be dissociated. To ensure the most intimate mixing, D-A dyads and D-A polymers (double cables)[73] were synthesized and used as photoactive materials in organic solar cells. This leads to the conclusion, that too intimate mixing may result in too small mean free paths. Thus, the critical issue will not only be the relationship between molecular structure and device properties but also between nanomorphology and device properties (Figure 1.13).
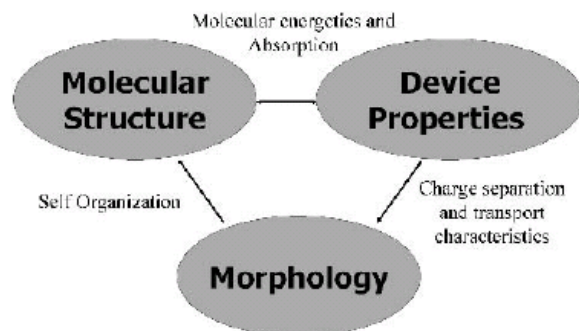
Figure 1.13 In organic or hybrid bulk heterojunction solar cells, the molecular structure, nanoscale morphology, and device properties are closely interrelated. Hence, the design of advanced organic solar cells requires the simultaneous optimization of these closely interconnected parameters.[21]

When these results are considered together, they suggest that an optimum domain size of the phase separation between donor and acceptor is needed, to balance exciton dissociation and charge transport requirements. Morphological stability in organic solar cells is an issue to be addressed, as under operating conditions elevated temperatures must be expected.[51-52] In conclusion, the optimal morphology of a bulk heterojunction device requires stable, nanometersized interpenetrating donor and acceptor domains.

Chapter 2 Novel Narrow-Band-Gap Conjugated Copolymers Containing Phenothiazine-Arylcyanovinyl Units for Organic Photovoltaic Cell Applications

2.1 Introduction

Since energy harvesting directly from sunlight by using photovoltaic cells (PVCs) is a very important way to utilize renewable energy of the nature, especially for the development of organic solar cells, it has increasingly attracted intensified attention recently.[22,42] Among several types of organic solar cell materials investigated so far, semi-conducting conjugated polymers with electron donor-acceptor architectures are one of the most effective ways to build intramolecular charge transfer (ICT) interaction between the electron donor (D) and electron acceptor (A) units.[56,66-67] Conjugated D-A copolymers with strong ICT effects are promising materials for the development of high performance polymer-based PVCs due to the merits of narrow bandgaps,[56,66-67] broad absorption bands extending into the near-infrared spectral range, efficient photoinduced charge transfer and separation, pronounced charge photogeneration and collection, and high mobility of ambipolar charge transport.[56,66-67]

It is noticeable that a well-known design of the electron-withdrawing unit would be an aryl-substituted cyano or nitro group, because the cyano and nitro groups are among the most widespread electron withdrawing groups in organic chemistry.[74] On the other hand, polymers and organic molecules[75] containing phenothiazine units or their derivatives as the electron-donating moieties have lately attracted considerable research interests on account of the unique electro-optical properties originated from their electron-rich sulfur and nitrogen heteroatoms on the heterocyclic compounds,

which can make these molecules potential materials for the applications of light-emitting diodes, photovoltaic devices,[59-60] and organic field effect transistors (OFETs).[61] In the past years, various attempts to reduce the band gaps of conjugated polymers have been studied by constructing conjugated systems more planar which will increase the delocalization of π–electrons on the backbones, and thus to reduce the band gaps of the polymers. Another approach to a series of narrow-band-gap (NBG) conjugated heterocyclic main-chain polymers consist of electron-accepting units (A), such as cyano or nitro groups, and electron-donating units (D), such as thiophene, furan, or pyrrole functional blocks, to form resonance structures (i.e., D－A $\leftrightarrow$ D$^+$A$^-$) in the backbones.[76] Recently, only some copolymers reported by Shim et al.[59] about the basic phenothiazine-based structure and then to extend the conjugation length by inserting phenylene and cyanovinylene functionalities for applications in red-emitting and photovoltaic devices. Although a large number of phenothiazine-based copolymers have been synthesized for applications in light-emitting devices, only a very small number of phenothiazine-based copolymers have investigated about the longer conjugated relationship with heterocyclic-containing structures and the applications for photovoltaic devices.

Based on this concept, the syntheses and characterization of NBG copolymers (**P1-P12**, as shown in Figure 2.3) that utilize the donor-acceptor approach to achieve absorption in the visible range of 400-800 nm are reported. A series of narrow-band-gap copolymers **P1-P12** derived from 9,9-dihexylfluorene (FO) units and six phenothiazine-based heteroarylene-cyanovinylene monomers (**M1-M6**, as shown in Figure 2.1 and 2.2) were prepared by the palladium-catalyzed Suzuki cross-coupling reaction, and the feed in molar ratios of FO components are equal to 75% and 50%. The PVC devices consisting of an active layer, which was made of

composite thin films containing fluorene-phenothiazine (**FO-PT**) copolymers blended with a fullerene derivative, i.e., [6,6]-phenyl C_{61} butyric acid methyl ester (PCBM), show promising performance with the best ECE value up to 0.51% under AM1.5 solar simulator. In the present study, we have successfully synthesized a series of novel phenothiazine-based copolymers by incorporating different numbers of electron donors and acceptors, such as thiophene and cyano groups, respectively, with various ratios of phenothiazine (PT) units. The synthetic routes and structures of monomers **M1**-**M6** and polymers **P1**-**P12** are shown in Figures 2.1-2.3. The optical and electronic properties, such as UV absorption spectra, electrochemical properties, photoluminescence quenching effects, and photovoltaic device results, of the copolymers are evaluated.

2.2 Experimental Section

2.2.1 Materials

Compounds 5-bromo-2-thiopheneacetonitrile (**5**),[77] 2,7-dibromo-9,9-dihexylfluorene (**11**),[78] and 2,7-bis(4,4,5,5-tetramethyl-1,3,2-dioxaborolan-2-yl)-9,9-dihexylfluorene (**12**)[78] were synthesized according to known literature procedures. The others precursors of monomers are shown in Figures 2.1-2.3, and their synthetic procedures are describes as follows.

2.2.2 Synthesis

10-n-Hexylphenothiazine (1) In a flame-dried flask attached to a reflux condenser, 1.88 g of sodium hydride (60% in mineral oil and washed by hexane, 78 mmol) was dissolved in 140 mL of anhydrous THF under nitrogen. 14.1g (71 mmol) of phenothiazine dissolved in 80 mL of anhydrous THF was added into the clear solution. After refluxing for 1 h, 15 mL of 1-bromohexane (106 mmol) was added.

The mixture was refluxed for 24 h and then poured into 250 mL of water. The product was extracted with methylene chloride (150 mL × 3), and the organic layer was dried over anhydrous magnesium sulfate. After purification by silica gel column chromatography with hexane as eluent, 16.9 g of colorless oil was obtained. Yield: 85%. ^{1}H NMR (DMSO-d_6, ppm), δ: 7.16 (m, 4H), 6.94 (m, 4H), 3.83 (t, J = 7.2 Hz, 2H), 1.65 (m, 2H), 1.40-1.15 (m, 6H), 0.80 (m, 3H).

10-n-Hexylphenothiazine-3,7-dicarbaldehyde **(2)** Compound **2** was synthesized by Vilsmeier formylation from compound **1**. A three-necked flask containing 20.04 mL (264 mmol) of anhydrous DMF was cooled in an ice bath. To the solution, 20.16 mL (216 mmol) of phosphorus chloride was added dropwisely for 30 min. Compound **1** (6 g, 21.2 mmol) in 30 mL of 1,2-dichloroethane was added to the above solution and heated to ca. 90 °C for 2 days. This solution was cooled to room temperature, poured into ice water, and neutralized to pH 6-7 by dropwise addition of saturated aqueous sodium hydroxide solution. The mixture was extracted with CH$_2$Cl$_2$/water. The organic layer was concentrated under reduced pressure. The crude product was purified by column chromatography with ethyl acetate (EA)/hexane (1:4) to get 4.6 g of yellow solids. Yield: 64%. ^{1}H NMR (DMSO-d_6, ppm), δ: 9.79 (s, 2H), 7.73 (dd, J = 8.7, 2.1 Hz, 2H), 7.60 (s, 2H), 7.21 (d, J = 8.4 Hz, 2H), 3.98 (t, J = 7.2 Hz, 2H), 1.67 (m, 2H), 1.38-1.21 (m, 6H), 0.80 (m, 3H).

10-n-Hexylphenothiazine-3-carbaldehyde **(3)** The synthetic procedure of compound **3** was similar to that of compound **2**, but the reactive time was just 1 day. The crude product was purified by column chromatography with EA/hexane (1:6) to get 6.08 g of yellow solids. Yield: 92%. ^{1}H NMR (DMSO-d_6, ppm), δ: 9.77 (s, 1H), 7.70 (dd, J = 8.7, 2.1 Hz, 1H), 7.58 (s, 1H), 7.21-6.98 (m, 5H), 3.92 (t, J = 7.2 Hz, 2H), 1.66 (m, 2H), 1.36-1.21 (m, 6H), 0.81 (m, 3H).

7-Bromo-10-hexyphenothiazine-3-carbaldehyde (6) 5.4 g (17.3 mmol) of compound **3** was dissolved in 60 mL of dichloromethane and cooled to 5-10 °C with ice-water bath, and then 1.1 mL of bromine (20.8 mmol) in 5 mL of dichloromethane was added into the solution dropwise. The mixture was stirred for 2 h at room temperature. Saturated sodium hydrogen sulfite solution was added to the reaction mixture and stirred for 30 min. After this, the reaction mixture was extracted with dichloromethane and purified by silica gel column flash chromatography with EA/hexane (1:6) as eluent. A pale yellow liquid was obtained. Yield: 92%. ^{1}H NMR (DMSO-d_6, ppm), δ: 9.78 (s, 1H), 7.71 (dd, J = 8.7, 2.1 Hz, 1H), 7.57 (d, J = 1.8 Hz, 1H), 7.35 (m, 2H), 7.14 (d, J = 8.4 Hz, 1H), 6.97 (dd, J = 8.1, 0.9 Hz, 1H), 3.88 (t, J = 7.2 Hz, 2H), 1.63 (m, 2H), 1.21-1.14 (m, 6H), 0.79 (m, 3H).

7-(Thiophen-2-yl)-10-hexylphenothiazine-3-carbaldehyde (8) Compound **6** (7.2 g, 18.4 mmol), thiophen-2-yl-2-boronic acid (**7**) (3.1 g, 23.9 mmol), and tetrakis(triphenylphosphine)palladium(0) (0.64 g) were reacted in THF (120 mL) for 10 mins, and then 80 mL of 2 M aqueous Na$_2$CO$_3$ solution was added. The reaction mixture was refluxed for 48 h. The cooled solution was washed with dilute hydrochloric acid (10%) and water. The final solution was purified by column chromatography (silica gel, CH$_2$Cl$_2$/hexane 1:10) to yield a yellow solid. Yield: 80%. ^{1}H NMR (CDCl$_3$, ppm), δ: 9.78 (s, 1H), 7.61 (m, 2H), 7.35 (m, 2H), 7.25-7.19 (m, 2H), 7.04 (m, 1H), 6.86 (m, 2H), 3.87 (t, J = 7.2 Hz, 2H), 1.81 (m, 2H), 1.46-1.24 (m, 6H), 0.85 (m, 3H).

7-(5-bromothiophen-2-yl)-10-hexylphenothiazine-3-carbaldehyde   (9) Compound **8** (8.45 g, 21.47 mmol) was dissolved in dichloromethane (50 mL) under nitrogen, and *N*-bromosuccinimide (4.2 g, 23.6 mmol) was added all at once. After refluxing the reaction mixture for 1 h, the product was poured into water (200 mL).

The solution was extracted with dichloromethane and he solvent was removed under reduced pressure, and the crude product was purified by column chromatography on silica gel (EA/ hexane 1:10) to afford compound **12** (8.76 g). Yield: 86%. ^{1}H NMR (CDCl₃, ppm), δ: 9.78 (s, 1H), 7.61 (m, 2H), 7.24 (m, 2H), 6.98-6.81 (m, 4H), 3.86 (t, J = 7.2 Hz, 2H), 1.79 (m, 2H), 1.45-1.24 (m, 6H), 0.86 (m, 3H).

7-(5-formylthiophen-2-yl)-10-hexylphenothiazine-3-carbaldehyde (10) The synthetic procedure of compound **10** was similar to that of compound **2**. The crude product was purified by column chromatography with EA/hexane (1:5) to get 8.0 g of yellow solids. Yield: 58%. ^{1}H NMR (CDCl₃, ppm), δ: 9.85 (s, 1H), 9.79 (s, 1H), 7.70-7.55 (m, 3H), 7.42-7.27 (m, 3H), 6.86 (m, 2H), 3.86 (t, J = 7.2 Hz, 2H), 1.77 (m, 2H), 1.43-1.30 (m, 6H), 0.88 (m, 3H).

General Procedures for the Syntheses of Monomers M1-M6 (PT1-PT6)

There are two different synthetic routes of monomers **M1-M6** (methods **A**[77] and **B**[79]) as described as follows:
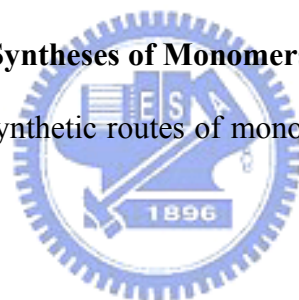
Method A

A mixture of compound **2** (or **12** or **13**), compound **4** (1-bromophenylacetonitrile), and methanol were placed in a two-neck round-bottom flask at room temperature. A catalytic amount of potassium *tert*-butoxide in methanol was added into this mixture. After 24 h, the product was filtered and dried.

Method B

A mixture of compound **2** (or **12** or **13**) and compound **5** (2-(5-bromothiophen-2-yl) acetonitrile) was dissolved in anhydrous ethanol under nitrogen in a 250 mL two-necked round-bottomed flask. A mixture of sodium hydroxide and dry ethanol was added slowly, and then the crude product was precipitated in the reaction mixture. The reaction mixture was stirred for 24 h at room temperature, and the precipitate was

filtered and washed with ethanol.

M1 (PT1) Method **A**: Compound **2** (11.48 g, 33.8 mmol), compound **4** (26.5 g, 135.2 mmol), methanol (200 mL), and a catalytic amount of potassium *tert*-butoxide were used. Chromatography on silica gel eluted with DCM/HX 3:2 afforded **M1** as a red solid (18.4 g). Yield: 78%. ^{1}H NMR (CDCl$_3$, ppm), δ: 7.78 (dd, J = 8.7, 2.1 Hz, 2H), 7.55-7.47 (m, 10H), 7.31 (s, 2H), 6.83 (d, J = 8.7 Hz, 2H), 3.83 (t, J = 7.2 Hz, 2H), 1.80 (m, 2H), 1.44-1.32 (m, 6H), 0.90 (m, 3H). ^{13}C NMR (CDCl$_3$, ppm), δ: 145.58, 140.59, 133.44, 132.12, 128.78, 128.40, 128.28, 127.17, 123.54, 123.00, 117.91, 115.24, 107.89, 48.10, 31.33, 26.47, 22.57, 22.10, 13.96. MS (EI): *m/z* [M$^+$] 695.04, calcd *m/z* [M$^+$] 695.1. Anal. Calcd for C$_{36}$H$_{29}$Br$_2$N$_3$S: C, 62.17; H, 4.20; N, 6.04. Found: C, 62.35; H, 4.60; N, 6.39.

M2 (PT2) Method **B**: Compound **2** (5.9 g, 17.35 mmol), compound **5** (14.0 g, 69.4 mmol), sodium hydroxide (1.39 g, 34.7 mmol), and ethanol (130 mL) were used. Chromatography on silica gel eluted with DCM/HX 1:3 afforded **M2** as a red solid (7.5 g). Yield: 61%. ^{1}H NMR (CDCl$_3$, ppm), δ: 7.69 (dd, J = 8.7, 1.8 Hz, 2H), 7.38 (s, 2H), 7.09-6.97 (m, 6H), 6.80 (d, J = 8.7 Hz, 2H), 3.80 (t, J = 7.2 Hz, 2H), 1.78 (m, 2H), 1.41-1.23 (m, 6H), 0.88 (m, 3H). ^{13}C NMR (CDCl$_3$, ppm), δ: 145.47, 140.56, 137.94, 130.93, 128.53, 128.13, 127.95, 126.73, 123.57, 116.48, 115.27, 112.80, 102.95, 48.13, 31.34, 26.47, 22.58, 22.13, 13.97. MS (EI): *m/z* [M$^+$] 706.96, calcd *m/z* [M$^+$] 707.1. Anal. Calcd for C$_{32}$H$_{25}$Br$_2$N$_3$S$_3$: C, 54.32; H, 3.56; N, 5.94. Found: C, 54.80; H, 4.03; N, 5.56.

M3 (PT3) Method **A**: Compound **12** (8.76 g, 18.5 mmol), compound **4** (14.5 g, 74.0 mmol), methanol (150 mL), and a catalytic amount of potassium *tert*-butoxide were used. Chromatography on silica gel eluted with dichloromethane/hexane 1:5 afforded **M3** as an orange solid (8.9 g). Yield: 74%. ^{1}H NMR (CDCl$_3$, ppm), δ: 7.80

(dd, J = 8.7, 2.1 Hz, 1H), 7.56-7.48 (m, 4H), 7.32-7.22 (m, 4H), 7.00-6.80 (m, 4H), 3.85 (t, J = 7.2 Hz, 2H), 1.80 (m, 2H), 1.45-1.32 (m, 6H), 0.89 (m, 3H). ^{13}C NMR (CDCl$_3$, ppm), δ: 146.58, 144.47, 143.16, 140.82, 133.59, 132.09, 130.82, 128.75, 128.45, 127.75, 127.14, 124.72, 124.14, 123.81, 122.87, 122.54, 118.01, 115.61, 115.01, 110.77, 107.41, 47.85, 31.36, 26.56, 26.50, 22.57, 13.97. MS (EI): m/z [M$^+$] 649.99, calcd m/z [M$^+$] 650.1. Anal. Calcd for C$_{31}$H$_{26}$Br$_2$N$_2$S$_2$: C, 57.24; H, 4.03; N, 4.31. Found: C, 57.03; H, 4.43; N, 4.70.

M4 (PT4) Method **B**: Compound **12** (2.88 g, 6.1 mmol), compound **5** (4.9 g, 24.4 mmol), sodium hydroxide (0.49 g, 12.2 mmol), and ethanol (80 mL) were used. Chromatography on silica gel eluted with EA/hexane 1:12 afforded **M4** as a red solid (2.1 g). Yield: 53%. ^{1}H NMR (CDCl$_3$, ppm), δ: 7.72 (dd, J = 8.7, 1.8 Hz, 1Hz), 7.47 (s, 1H), 7.26-7.21 (m, 3H), 7.07-6.93 (m, 5H), 6.82 (m, 2H), 3.84 (t, J = 7.2 Hz, 2H), 1.80 (m, 2H), 1.43-1.26 (m, 6H), 0.89 (m, 3H). ^{13}C NMR (CDCl$_3$, ppm), δ: 146.53, 144.47, 143.12, 140.69, 138.24, 130.89, 130.81, 128.77, 128.59, 128.13, 127.39, 126.55, 124.72, 124.15, 123.88, 122.55, 116.58, 115.60, 115.03, 112.58, 110.78, 102.49, 47.87, 31.36, 26.56, 26.50, 22.57, 13.97. MS (EI): m/z [M$^+$] 655.94, calcd m/z [M$^+$] 656.0. Anal. Calcd for C$_{29}$H$_{24}$Br$_2$N$_2$S$_3$: C, 53.05; H, 3.68; N, 4.27. Found: C, 53.45; H, 4.03; N, 4.65.

M5 (PT5) Method **A**: Compound **13** (2.5 g, 5.9 mmol), compound **4** (4.7 g, 23.6 mmol), methanol (100 mL), and a catalytic amount of potassium *tert*-butoxide were used. Finally, a pure product can be obtained by recrystallization from EA/hexane 1:3 to afford **M5** as a red solid (3.5 g). Yield: 77%. ^{1}H NMR (CDCl$_3$, ppm), δ: 7.79 (dd, J = 8.7, 2.1 Hz, 1H), 7.55-7.38 (m, 12H), 7.31 (m, 2H), 7.20 (m, 1H), 6.81 (m, 2H), 3.82 (t, J = 7.2 Hz, 2H), 1.79 (m, 2H), 1.32 (m, 6H), 0.88 (m, 3H). ^{13}C NMR (CDCl$_3$, ppm), δ: 148.19, 146.11, 143.77, 140.69, 136.18, 134.87, 134.30, 133.50, 132.84,

132.12, 132.08, 128.76, 128.40, 128.13, 127.85, 127.11, 126.87, 125.34, 124.40, 123.95, 123.49, 122.88, 122.81, 122.78, 117.99, 117.93, 115.47, 115.00, 107.44, 105.57, 47.95, 31.34, 26.62, 26.47, 22.57, 13.97. MS (EI): m/z [M$^+$] 777.03, calcd m/z [M$^+$] 777.1. Anal. Calcd for $C_{40}H_{31}Br_2N_3S_2$: C, 61.78; H, 4.02; N, 5.40. Found: C, 61.30; H, 4.52; N, 5.71.

M6 (PT6) Method **B**: Compound **13** (2.0 g, 4.8 mmol), compound **5** (3.8 g, 18.9 mmol), sodium hydroxide (0.38 g, 9.6 mmol), and ethanol (70 mL) were used. Chromatography on silica gel eluted with dichloromethane/hexane 1:5 afforded **M6** as a red solid (2.1 g). Yield: 53%. ^{1}H NMR (CDCl$_3$, ppm), δ: 7.72 (dd, J = 8.7, 1.8 Hz, 1H), 7.45-7.36 (m, 3H), 7.29-7.18 (m, 3H), 7.07-7.01 (m, 5H), 6.79 (d, J = 8.7 Hz, 2H), 3.80 (t, J = 7.2 Hz, 2H), 1.80 (m, 2H), 1.45-1.14 (m, 6H), 0.89 (m, 3H). ^{13}C NMR (CDCl$_3$, ppm), δ: 148.11, 146.00, 143.66, 140.67, 140.14, 138.08, 135.80, 134.54, 132.05, 131.00, 130.89, 130.67, 128.54, 128.11, 127.49, 126.56, 125.31, 124.32, 123.88, 123.53, 122.87, 116.56, 116.49, 115.43, 114.99, 112.64, 112.62, 102.51, 100.94, 48.00, 31.35, 29.67, 26.49, 22.59, 13.98. MS (EI): m/z [M$^+$] 788.94, calcd m/z [M$^+$] 789.0. Anal. Calcd for $C_{36}H_{27}Br_2N_3S_4$: C, 54.75; H, 3.45; N, 5.32. Found: C, 55.19; H, 3.90; N, 4.82.

General Procedures for the Syntheses of Copolymers P1-P12

The synthetic route of polymers is shown in Figure 2.3. All of the polymerizations were carried out through the palladium(0)-catalyzed Suzuki coupling reactions. Into 50 mL of two-neck flask, 1 equiv of dibromo compounds [**11** and monomers **M1-M6** (**PT1-PT6**)] and 1 equiv of **12** were added in 10 mL of anhydrous toluene. The Pd(0) complex, Pd{P(p-tolyl)$_3$}$_3$ (1 mol %), was transferred into the mixture in a dry environment. Then, 2M aqueous potassium carbonate and the phase transfer catalyst, i.e., aliquat 336 (several drops), were subsequently transferred via

cannula into the previous mixture under nitrogen. The reaction mixture was stirred at 90 °C for 2 days, and then the excess amount of iodobenzene and phenylboronic acid, the end-capper, dissolved in 1mL of anhydrous toluene was added and stirring for 4 h, respectively. The reaction mixture was cooled to 50 °C and added slowly into a vigorously stirred mixture of 300 mL of methanol. The polymers were collected by filtration and reprecipitation from methanol. The crude polymers were further purified by washing with acetone for 3 days in a Soxhlet apparatus to remove oligomers and catalyst residues. The resulting polymers were soluble in common organic solvents.

P1 (**FO$_3$-PT1**) Compounds **11** (0.25 equiv), **12** (0.5 equiv), and **M1** (0.25 equiv) were used in this polymerization. Yield: 62%. ^{1}H NMR (CDCl$_3$, ppm), δ: 8.05-7.3 (m, 32H, ArH), 6.94 (br, 2H, vinylic proton), 3.89 (weak br, CH$_2$ attached to nitrogen of phenothiazine, 2H), 2.06-0.76 (m, aliphatic, ~89H).

P2 (**FO$_1$-PT1**) Compounds **12** (0.5 equiv) and **M1** (0.5 equiv) were used in this polymerization. Yield: 88%. ^{1}H NMR (CDCl$_3$, ppm), δ: 7.90-7.32 (m, 20H, ArH), 6.97 (br, 2H, vinylic proton), 3.90 (weak br, CH$_2$ attached to nitrogen of phenothiazine, 2H), 2.17-0.76 (m, aliphatic, ~37H).

P3 (**FO$_3$-PT2**) Compounds **11** (0.25 equiv), **12** (0.5 equiv), and **M2** (0.25 equiv) were used in this polymerization. Yield: 78%. ^{1}H NMR (CDCl$_3$, ppm), δ: 7.83-7.23 (m, 28H, ArH), 6.90 (br, 2H, vinylic proton), 3.90 (weak br, CH$_2$ attached to nitrogen of phenothiazine, 2H), 2.20-0.77 (m, aliphatic, ~89H).

P4 (**FO$_1$-PT2**) Compound **12** (0.5 equiv) and **M2** (0.5 equiv) were used in this polymerization. Yield: 61%. ^{1}H NMR (CDCl$_3$, ppm), δ: 7.89-7.27 (m, 16H, ArH), 6.97 (br, 2H, vinylic proton), 3.89 (weak br, CH$_2$ attached to nitrogen of phenothiazine, 2H), 2.23-0.78 (m, aliphatic, ~37H).

P5 (**FO$_3$-PT3**) Compounds **11** (0.25 equiv), **12** (0.5 equiv), and **M3** (0.25 equiv)

were used in this polymerization. Yield: 82%. ^{1}H NMR (CDCl$_3$, ppm), δ: 7.82-7.25 (m, 30H, ArH), 6.90 (br, 1H, vinylic proton), 3.90 (weak br, CH$_2$ attached to nitrogen of phenothiazine, 2H), 2.17-0.77 (m, aliphatic, ~89H).

P6 (FO$_1$-PT3) Compound **12** (0.5 equiv) and **M3** (0.5 equiv) were used in this polymerization. Yield: 64%. ^{1}H NMR (CDCl$_3$, ppm), δ: 7.89-7.26 (m, 17H, ArH), 6.88 (br, 2H, vinylic proton), 3.88 (weak br, CH$_2$ attached to nitrogen of phenothiazine, 2H), 2.17-0.74 (m, aliphatic, ~37H).

P7 (FO$_3$-PT4) Compounds **11** (0.25 equiv), **12** (0.5 equiv), and **M4** (0.25 equiv) were used in this polymerization. Yield: 86%. ^{1}H NMR (CDCl$_3$, ppm), δ: 7.83-7.24 (m, 28H, ArH), 6.88 (br, 1H, vinylic proton), 3.89 (weak br, CH$_2$ attached to nitrogen of phenothiazine, 2H), 2.16-0.78 (m, aliphatic, ~89H).

P8 (FO$_1$-PT4) Compound **12** (0.5 equiv) and **M4** (0.5 equiv) were used in this polymerization. Yield: 71%. ^{1}H NMR (CDCl$_3$, ppm), δ: 7.79-7.13 (m, 15H, ArH), 6.86 (br, 2H, vinylic proton), 3.88 (weak br, CH$_2$ attached to nitrogen of phenothiazine, 2H), 2.17-0.74 (m, aliphatic, ~37H).

P9 (FO$_3$-PT5) Compounds **11** (0.25 equiv), **12** (0.5 equiv), and **M5** (0.25 equiv) were used in this polymerization. Yield: 87%. ^{1}H NMR (CDCl$_3$, ppm), δ: 7.83-7.25 (m, 34H, ArH), 6.90 (br, 2H, vinylic proton), 3.90 (weak br, CH$_2$ attached to nitrogen of phenothiazine, 2H), 2.17-0.77 (m, aliphatic, ~89H).

P10 (FO$_1$-PT5) Compound **12** (0.5 equiv) and **M5** (0.5 equiv) were used in this polymerization. Yield: 70%. ^{1}H NMR (CDCl$_3$, ppm), δ: 7.80-7.08 (m, 22H, ArH), 6.86 (br, 2H, vinylic proton), 3.87 (weak br, CH$_2$ attached to nitrogen of phenothiazine, 2H), 2.17-0.76 (m, aliphatic, ~37H).

P11 (FO$_3$-PT6) Compounds **11** (0.25 equiv), **12** (0.5 equiv), and **M6** (0.25 equiv) were used in this polymerization. Yield: 89%. ^{1}H NMR (CDCl$_3$, ppm), δ: 7.83-7.24

(m, 30H, ArH), 6.86 (br, 2H, vinylic proton), 3.87 (weak br, CH_2 attached to nitrogen of phenothiazine, 2H), 2.16-0.78 (m, aliphatic, ~89H).

P12 (**FO_1-PT6**) Compound **12** (0.5 equiv) and **M6** (0.5 equiv) were used in this polymerization. Yield: 75%. ^{1}H NMR (CDCl$_3$, ppm), δ: 7.85-7.27 (m, 18H, ArH), 6.89 (br, 2H, vinylic proton), 3.87 (weak br, CH_2 attached to nitrogen of phenothiazine, 2H), 2.14-0.77 (m, aliphatic, ~37H).

2.2.3 Measurements and Characterization

^{1}H NMR spectra were recorded on a Varia Unity 300 MHz spectrometer using CDCl$_3$ and DMSO solvents. Elemental analyses were performed on a HERAEUS CHN-OS RAPID elemental analyzer. Transition temperatures were determined by differential scanning calorimetry (DSC) on a Perkin-Elmer Pyris 7 thermal analyzer with a heating and cooling rate of 10 °C/min. Thermogravimetric analysis (TGA) was conducted with a TA instrument Q500 at a heating rate of 20 °C /min under nitrogen. Gel permeation chromatography (GPC) analyses were conducted on a Waters 1515 separation module using polystyrene as a standard and THF as an eluent. UV-visible absorption spectra were recorded in dilute THF solutions (10^{-6} M) on a HP G1103A spectrophotometer. Thin films of UV-vis measurements were spin-coated on a quartz substrate from chlorobenzene solutions with a concentration of 5 mg/mL. Electrochemistry measurements were performed using an Autolab Model PGSTAT30 potentiostat/galvanostat with a standard three-electrode electrochemical cell in a 0.1 M tetrabutylammonium hexafluorophosphate (TBAPF6) solution (in acetonitrile) at room temperature with a scanning rate of 50 mV/s. A platinum working electrode, a platinum wire counter electrode, and an Ag/AgCl reference electrode were used. The films of the polymers were coated onto the Pt working electrode by dipping the Pt wire into 1 wt% THF solutions. The onset potentials were determined from the

intersection of two tangents drawn at the rising current and background current of the cyclic voltammogram.

2.2.4 Device Fabrication of Polymer Photovotaic Cells

The PVC device structure used in this study was a sandwich configuration of ITO/PEDOT:PSS/active layer/LiF/Al. We fabricated the PVC devices according to the procedures similar to those of electroluminescence (EL) devices. After drying the substrate of ITO, a thin layer (ca. 50 nm) of PEDOT:PSS was spin-coated and dried. Subsequently, on the top of the PEDOT:PSS layer, the active layer was prepared by spin coating from composite solutions of **P2**, **P6**, **P8,** and **P10**/PCBM (1:4 w/w) and of **P12**/PCBM (1:1, 1:2, and 1:4 w/w) in the mixed solvents of chlorobenzene and chloroform (1:1 vol.). The spin rate was ca. 800 rpm, and the thickness of the active layer was typically ca. 100 nm. The devices were completed by deposition with 1 nm of LiF and 150 nm of Al. For PVC measurements, I-V curves were recorded under a solar simulator with AM 1.5 illumination (at 100 mW/cm^2). All cells were prepared and measured under ambient conditions.
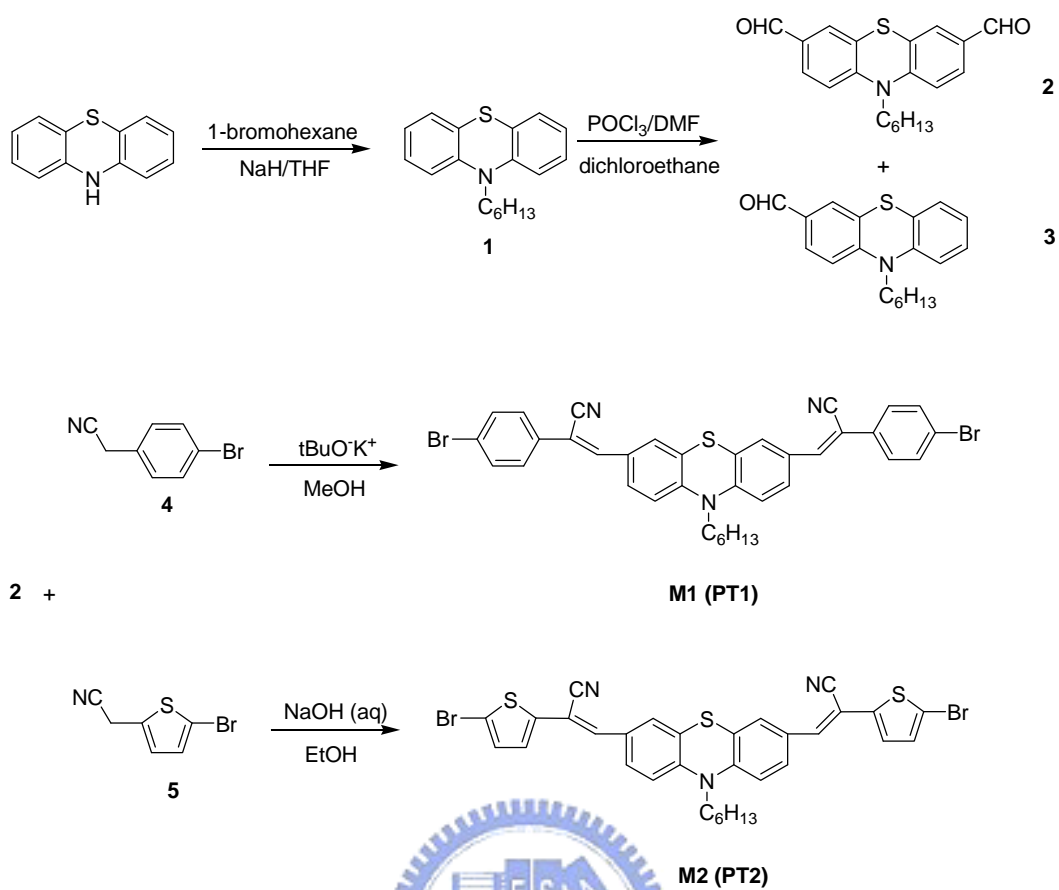
Figure 2.1 Synthetic Routes of Symmetrical Monomers **M1-M2**.
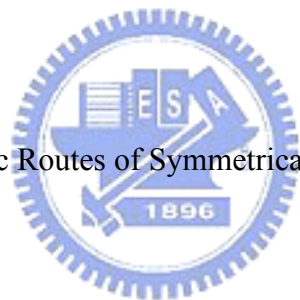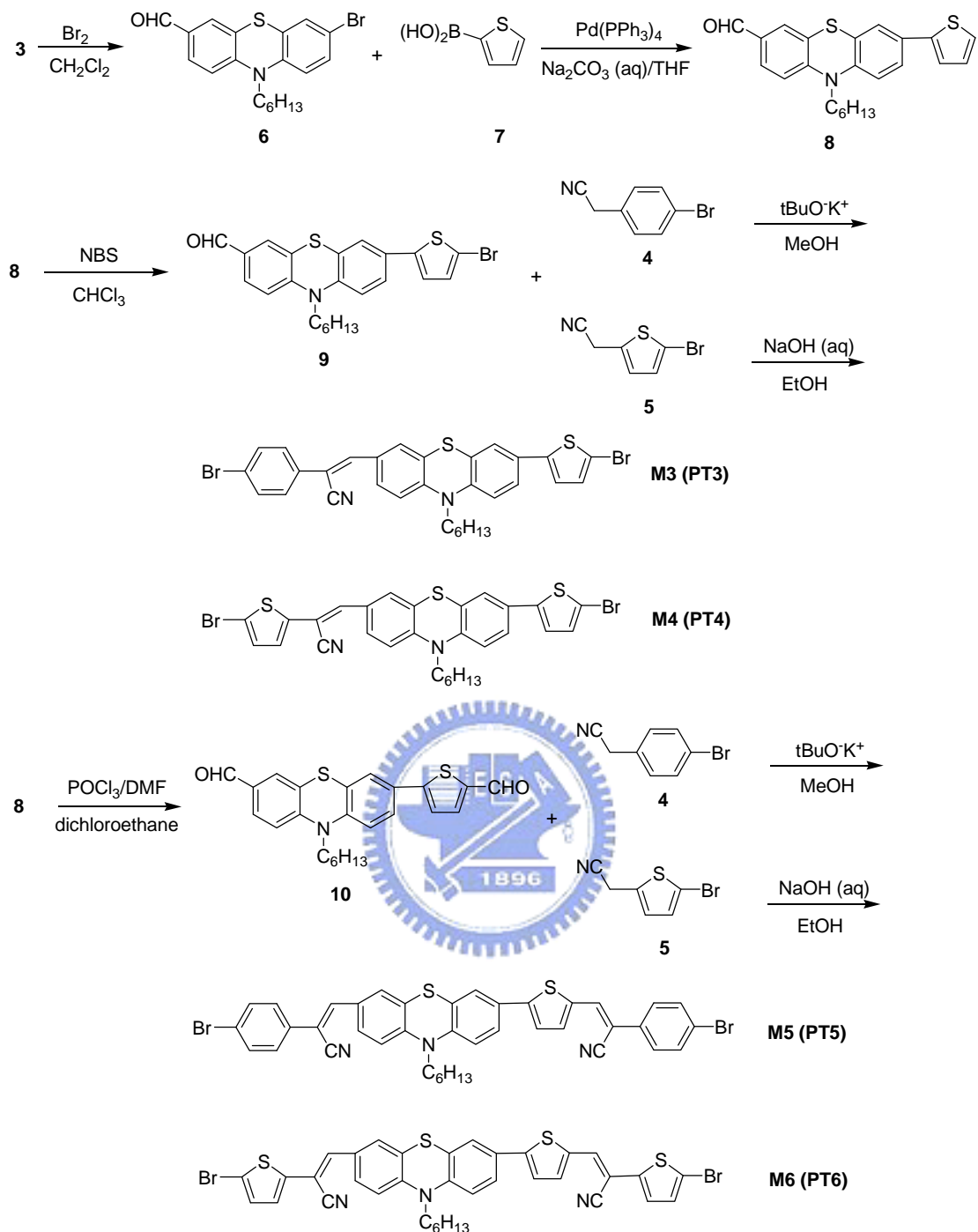
Figure 2.2 Synthetic Routes of Asymmetrical Monomers **M3-M6**.
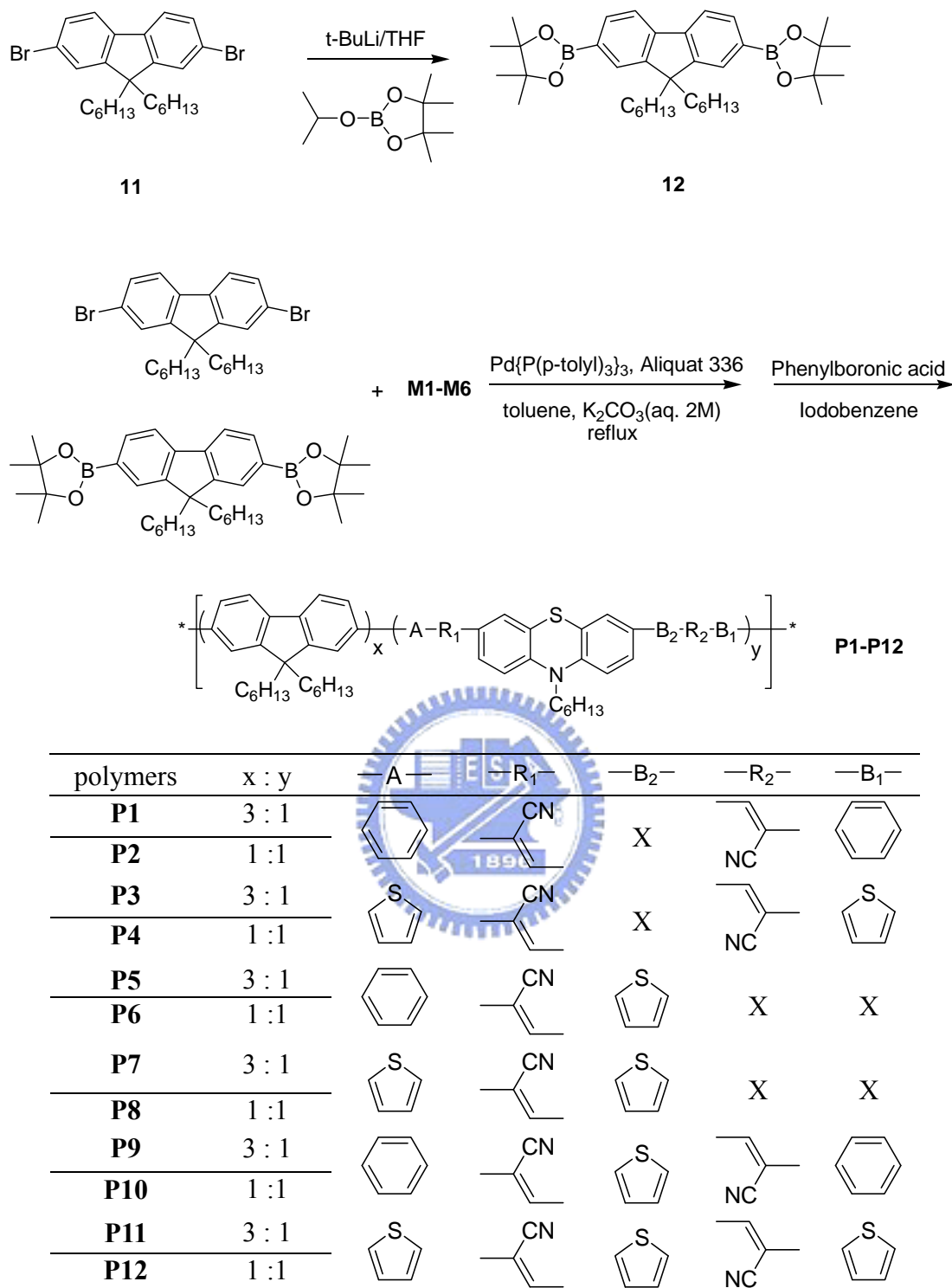
Figure 2.3 Synthetic Routes and Compositions (Molar Ratios) of Copolymers **P1-P12**.

polymers	x : y	—A—	—R₁—	—B₂—	—R₂—	—B₁—
P1	3 : 1		CN	X		
P2	1 : 1					
P3	3 : 1	S	CN	X		S
P4	1 : 1					
P5	3 : 1		CN	S	X	X
P6	1 : 1					
P7	3 : 1	S	CN	S	X	X
P8	1 : 1					
P9	3 : 1		CN	S		
P10	1 : 1					
P11	3 : 1	S	CN	S		S
P12	1 : 1					

2.3 Results and Discussion

2.3.1 Synthesis and Characterization

The general synthetic routes of monomers **M1-M6** (**PT1-PT6**) are shown in Figures 2.1-2.2. All monomers were synthesized by following the modified multistep procedures in the literature,[80] and some of them (compounds **2**, **3**, and **6**) were started from commercially available phenothiazine. Monomers (**M1-M6** and **PT1-PT6**) were satisfactorily characterized by ^{1}H NMR, ^{13}C NMR, MS spectroscopy, and elemental analyses. The synthetic procedures towards polymers **P1-P12** are outlined in Figure 3. Conjugated polymers derived from monomers **M1-M6** were prepared by palladium(0)-catalyzed Suzuki coupling reactions with an equivalent molar ratio of diboronic ester monomer **12** to dibromo monomers (**11** and **M1**-**M6**). During the polymerization, the feed in monomer ratios of fluorene units to monomers **M1-M6** were 3:1 and 1:1, respectively. The copolymers **P1-P12** were synthesized from a Suzuki coupling reaction in a biphasic system (toluene/aqueous Na$_2$CO$_3$) with freshly prepared Pd{P(p-tolyl)$_3$}$_3$ as a catalyst precursor. The obtained polymers were further purified by washing with acetone in a Soxhlet apparatus for 24 h to remove oligomers and catalyst residues and were dried under reduced pressure at room temperature. After purification and drying, all polymers were obtained as red fibrous solids in overall good yields (61% - 89%). As shown in Table 2.1, the elemental analyses indicated that the FO contents in copolymers **P1-P12** were very close to the feed in compositions. All copolymers exhibited good solubilities in common organic solvents, such as THF, chloroform, and chlorobenzene. The molecular weights of the polymers determined by gel permeation chromatography (GPC) against polystyrene standards in THF are summarized in Table 2.1. These results show that considerable molecular weights were obtained in these copolymers, which had number-average molecular

weights (M_n) ranging 8400-27900 and weight-average molecular weights (M_w) ranging 10800-102900, respectively, with polydispersity indices (M_w/M_n) ranging 1.30-3.68. In contrast to **FO₃-PT** polymer derivatives (FO:PT=3:1), the lower molecular weights of corresponding **FO₁-PT** polymer analogues (FO:PT=1:1) with higher PT contents were attributed to the lower solubilities of PT units (**PT1-PT6**) in their copolymerization processes. The PT contents of the resulting polymers can be estimated from elemental analysis (EA) results. It was found that S contents of the copolymers increased with the added PT contents during the copolymerization and were close to the monomer feed ratios of FO:PT (Table 2.1).[81] For example, the actual molar ratios of PT/FO were calculated from the S contents from the experimental EA divided by those from the calculated EA.

Table 2.1 Molecular Weights, Yields, and Thermal Data of Polymers and PT Content in the Copolymers

Polymer	$M_w{}^a$	PDI^a	Ratio of PT units		Yield (%)	$T_g{}^c$ (°C)	$T_d{}^d$ (°C)
			In the feed %	In the copolymers^b %			
P1 (FO₃-PT1)	26800	2.00	25	26.6	62	153	411
P2 (FO₁-PT1)	14600	1.55	50	48.6	88	175	401
P3 (FO₃-PT2)	18700	1.45	25	24.8	78	175	416
P4 (FO₁-PT2)	10800	1.30	50	47.8	61	189	404
P5 (FO₃-PT3)	49600	2.40	25	26.1	82	n.d.^{e}	410
P6 (FO₁-PT3)	19200	1.44	50	48.3	64	n.d.^{e}	405
P7 (FO₃-PT4)	59200	2.65	25	25.9	86	130	415
P8 (FO₁-PT4)	17400	1.43	50	53.0	71	134	408
P9 (FO₃-PT5)	102900	3.68	25	27.0	87	132	419
P10 (FO₁-PT5)	13700	1.36	50	51.0	70	137	401
P11 (FO₃-PT6)	30200	1.63	25	25.5	89	158	409
P12 (FO₁-PT6)	18100	1.40	50	50.9	75	n.d.^{e}	406

^{a} Molecular weights and polydispersity were measured by GPC, using THF as an eluent, polystyrene as a standard. M_n, number average molecular weight. M_w, weight average molecular weight. ^{b}Calculated from results of elemental analyses. ^{c}Glass transition temperature (°C) was measured by DSC at a heating rate of 10 °C/min. ^{d}Temperature (°C) at 5% weight loss measured by TGA at a heating rate of 20 °C/min under nitrogen. ^{e}No noticeable T_g was observed.

The thermal properties of the copolymers determined by thermogravimetric

analysis (TGA) and differential scanning calorimetry (DSC) are shown in Table 1. The TGA thermograms of the D-A copolymers (**P1-P12**) revealed that 5% weight loss temperatures (T_{d}s) were in the range of 401-416 °C, indicative of excllent thermal stabilities. **FO$_1$-PT** polymer derivatives (FO:PT=1:1) showed lower T_{d} values than respective **FO$_3$-PT** polymer analogues (FO:PT=3:1), which may be probably due to the lower molecular weights of the former copolymers with lower FO contents. As for DSC properties, two thermally induced phase transitions, including a glass transition (T_{g} = 158 °C) and a melting peak (T_{m} = 180 °C), were merely observed in **P11**. However, **P5**, **P6**, and **P12** exhibited no obvious phase transitions until 300 °C where slight decompositions began, and only one glass transition with T_{g} values between 130 °C and 189 °C were found in the other copolymers. Compared with **FO$_3$-PT** polymer derivatives (FO:PT=3:1), **FO$_1$-PT** polymer analogues (FO:PT=1:1) generally showed higher T_{g} values owing to the higher contents of rigid PT segments. These phenomena demonstrate that the physical properties of the copolymers, such as conformation, planarity, rigidity, and stacking, will be affected by the variation of PT structures and contents. Basically, the thermal stabilities of the copolymers are adequate for their applications in polymer solar cells and other optoelectronic devices.

The molecular structures of the copolymers were identified by FT-IR and ^{1}H NMR. Representative FT-IR spectra of copolymers **P3**, **P4**, **P11**, and **P12** are shown in Figure 2.4, where the cyano functional groups appeared at 2270-2210 cm^{-1} in the triple bond region of FT-IR spectra showed a sharp band with a medium intensity. As a result of the stretching modes of cyano groups in the copolymers, the absorption bands typically appeared at 2210 cm^{-1}, and the intensity of this band increased with higher fractions of phenothiazine units in these polymers. Figure 2.5 shows the proton NMR spectra of monomer **M4** and polymers **P7-P8** in CDCl$_3$. For example, the

characteristic signal of the CH_2 segments attached to the nitrogen atoms of phenothiazine units can be seen clearly ca. δ = 3.8 ppm for all monomers and copolymers. Compared with ^1H NMR spectra of polymers **P7-P8** in Figure 2.5, it was generally found that sharper and more splitted signals of monomer **M4** disappeared after polymerization. In addition, in contrast to polymer **P7** (**FO$_3$-PT4**), a larger integrated signal (ca. δ = 3.8 ppm) was observed in polymer **P8** (**FO$_1$-PT4**) with a higher molar ratio of phenothiazine units (FO:PT4=1:1). Similar results were observed in the FT-IR and ^1H NMR spectra for all copolymers.
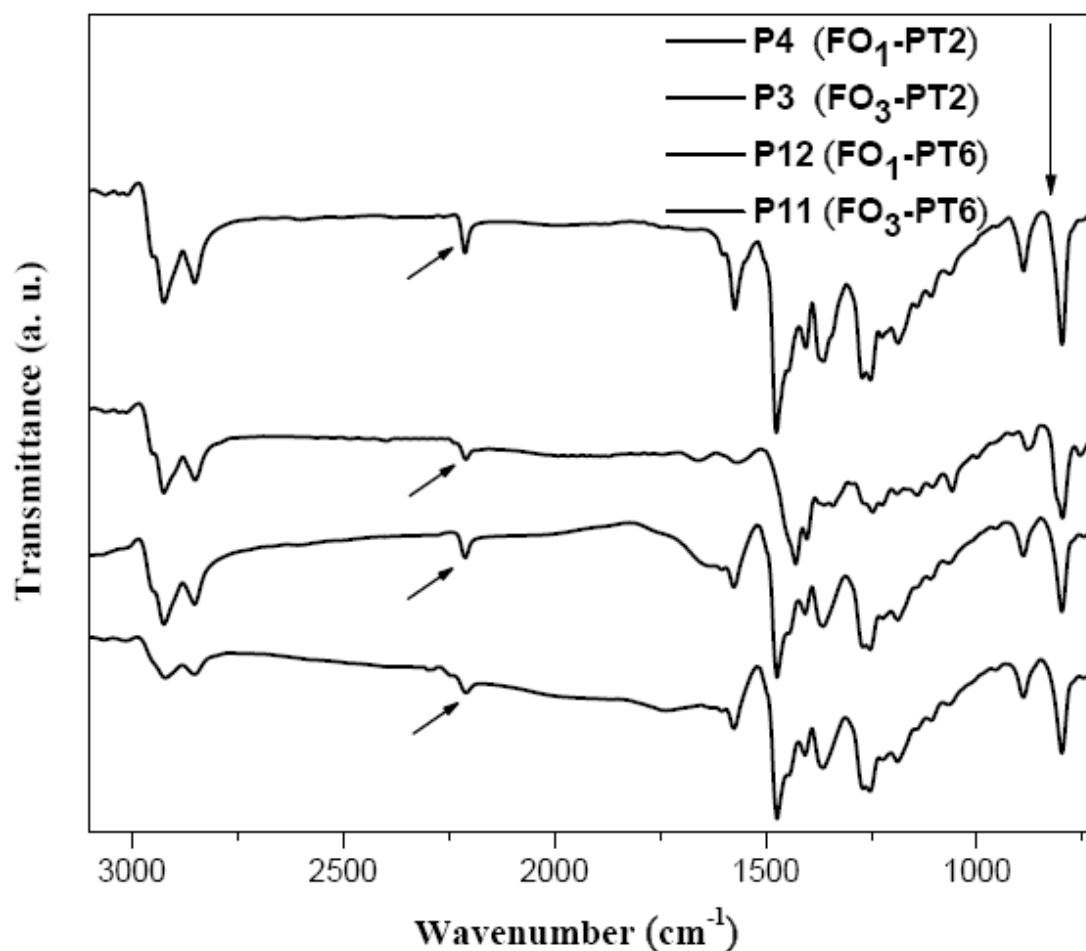
Figure 2.4 FT-IR spectra of copolymers **P3**, **P4**, **P11**, and **P12**.
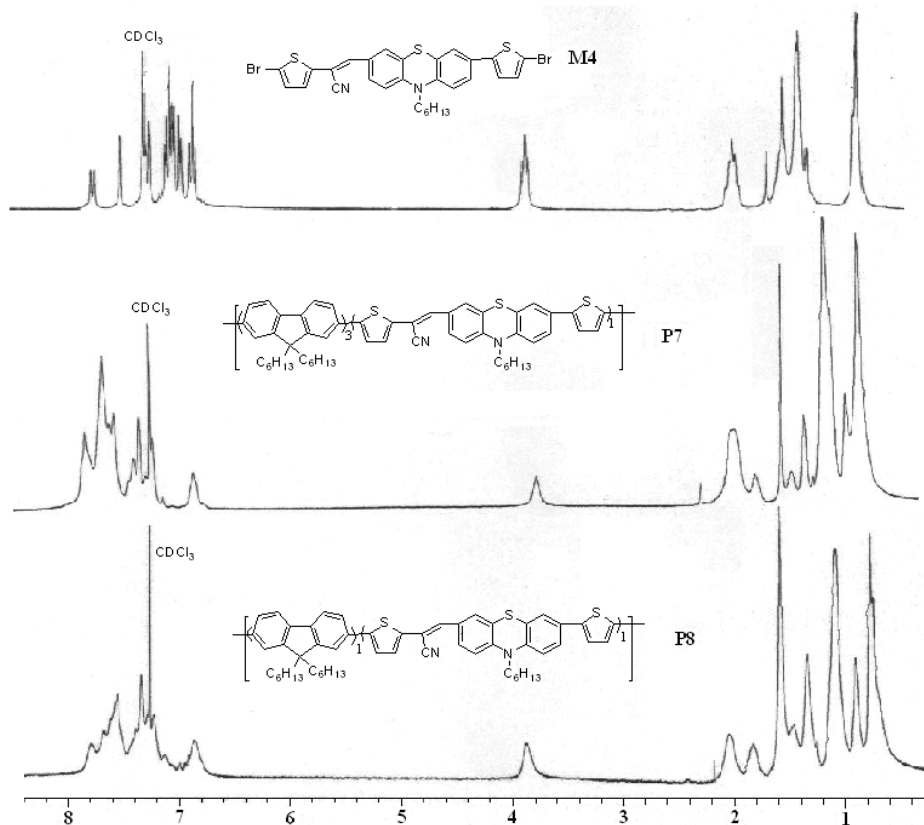
Figure 2.5 ^{1}H NMR spectra of monomer **M4** and polymers **P7-P8** in CDCl$_3$.

2.3.2 Optical Properties

The photophysical characteristics of polymers **P1-P12** were investigated by UV-vis absorption spectra in dilute THF solutions as well as in solid films, as revealed in Figures 2.6 and 2.7, respectively. The UV-vis absorption properties of the D-A copolymers based on 9,9-dihexylfluorene and phenothiazine units are presented in Table 2.2. As shown in Figure 2.6, most of the fluorene-phenothiazine-based (**FO-PT**) copolymers (except **P4** and **P12** in THF solutions) exhibit two distinct peaks, and one of the peaks ca. 375 nm is consistent with that reported for poly(9,9-dihexylfluorene) homopolymer,[82] which can be attributed to the fluorene segments in the copolymers. The other peak with an extra long wavelength absorption band appeared between 439 and 500 nm, with tailing of the absorption to around 610 nm can be attributed to the PT units incorporated into the main-chains of the copolymers. For all copolymers, the higher PT contents in the random copolymers, the larger absorbance ratios of PT to

fluorene units. However, a gradual blue shift of the short wavelength absorption accompanying with a small red shift of the long wavelength absorption were commonly observed in these polymers as the PT contents increased. This result can be explained by that as more PT segments were incorporated into the main-chains of the copolymers (with higher PT contents), more efficient conjugation or higher extents of aggregation occurred between PT units but less sufficient conjugation or lower extents of aggregation arose between fluorene units.[83-84] Two distinguished absorption features revealed that the electronic states of the two contents in random **FO-PT** copolymers were not well overlapped. Compared with the other random copolymers, **P4** and **P12** possessed completely different absorption spectra, where the absorption band ca. 375 nm attributed to the fluorene segments disappeared and only a broad and strong absorption band showed ca. 500 nm. The single UV-vis absorption spectra of polymers **P4** and **P12** were quite different from the two separated absorptions of the other random copolymers derived from fluorene and low band-gap PT aromatic heterocyclics.[85-86] This phenomenum suggested that the electronic configurations of both segments, i.e., fluorene and PT units, were somehow related to each other in the random copolymers **P4** and **P12**.

(a)   (b)

(c)
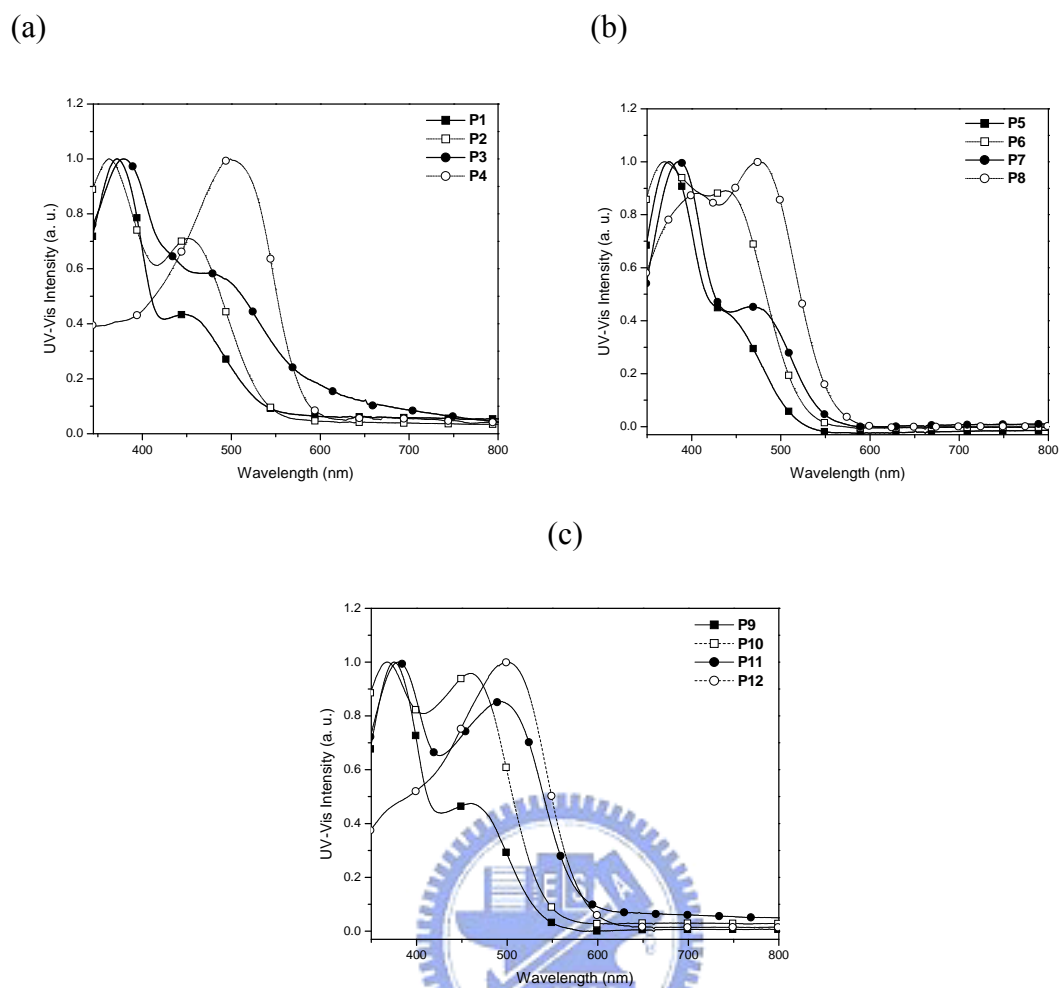
Figure 2.6 Normalized UV-vis absorption spectra of D-A copolymers in THF solutions (~10^{-6} M): (a) **P1-P4**, (b) **P5-P8**, and (c) **P9-P12.**

The UV-vis absorption spectra of the copolymers in solid films are presented in Figure 2.7. The solid films showed similar absorption patterns as THF solutions (see Figure 2.6). However, compared with solutions, the polymer films generally had 8~63 nm of red shifts due to the interchain association and aggregation in the solid state, and the spectral red-shifts were generally more significant when higher PT contents (**FO$_1$-PT** series in comparison with **FO$_3$-PT** series) and longer PT units (e.g., **P9-P12** containing **PT5** and **PT6** units) were incorporated into the polymers (Table 2.2). According to UV absorptions of **FO-PT** copolymers in solid films, **FO$_1$-PT** polymer derivatives (FO:PT=1:1) possessed broader spectral absorption ranges (between 400 and 800 nm) than their **FO$_3$-PT** polymer analogues (FO:PT=3:1) to make them

40

suitable candidates to harvest more photons.
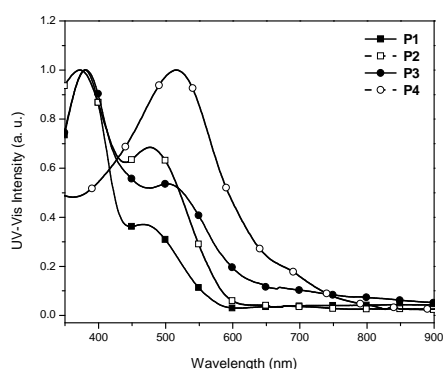
(a)   (b)
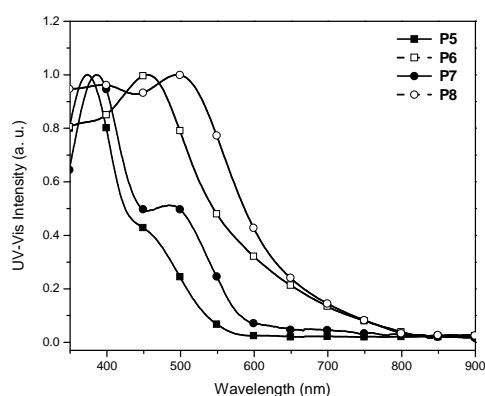
(c)
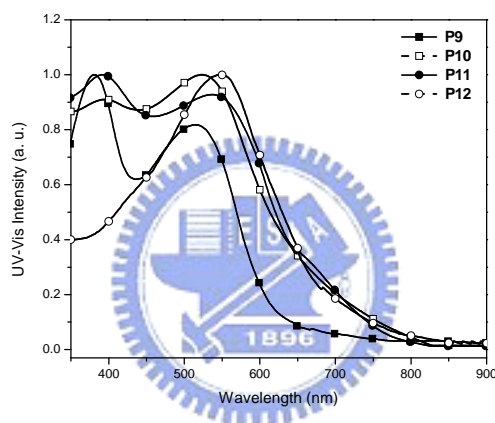
Figure 2.7 Normalized UV-vis absorption spectra of D-A copolymers in solid films (spin-coating from chlorobenzene solutions): (a) **P1-P4**, (b) **P5-P8**, and (c) **P9-P12.**

As mentioned earlier in the reference,[59] the UV-vis absorption result of **P2** in solid films was similar to the reported data. Although some phenothiazine-based conjugated polymers have been developed, longer conjugation relationship of phenothiazine-based conjugated polymers with aromatic (or heterocyclic) structures still need to be further explored. Therefore, our results can be compared with those reported ones and realize the effect of adding different numbers of aromatic rings (i.e., benzene and thiophene groups).[59,80] Among these related literatures, Jenekhe et al.[80] reported that the absorption maxima of the phenothiazine-fluorene alternating copolymer (PPTF) was located ca. 384 nm in solid films. In our copolymers

containing PT units, the donor (D) and acceptor (A) groups, such as thiophene and cyano groups, respectively, were incorporated into these polymers. Hence, the absorption maxima of **FO-PT** copolymers in solid films were around 450 to 548 nm, which were further red-shifted ca. 66-164 nm compared with the corresponding spectrum of PPTF. The differences of the spectra between **FO-PT** and PPTF copolymer can be explained by the push-pull effect of D and A groups within the molecules and the increase of the effective conjugation lengths in the polymers. The optical band gaps of the copolymers in solid films, which were determined by the cutoff wavelengths of optical absorptions, are listed in Table 2.2. For all copolymers, the optical band gaps decreased with increasing PT contents and the push-pull (D-A) effect resulted in narrower optical band gaps of copolymers by our approach, which induced broader visible absorption ranges (between 400 and 800 nm) than PPTF.

Table 2.2 Optical Data of P1-P12 in THF Solutions (~10^{-6} M) and Solid Films[a]

Polymer	UV-vis (λ_a) nm					E_g^{opt} [b] eV	
	Solution	λ_{edge}[c]	Film	λ_{edge}[c]	$\Delta\lambda$[d]	Solution	Film
P1 (FO$_3$-PT1)	373, 450	560	375, 472	600	22	2.21	2.06
P2 (FO$_1$-PT1)	363, 453	569	365, 478	630	25	2.18	1.96
P3 (FO$_3$-PT2)	378, 480	592	381, 510	700	30	2.09	1.77
P4 (FO$_1$-PT2)	491	600	516	830	25	2.07	1.49
P5 (FO$_3$-PT3)	375, 442	550	374, 450	590	8	2.25	2.10
P6 (FO$_1$-PT3)	370, 446	555	457	800	11	2.23	1.55
P7 (FO$_3$-PT4)	380, 475	570	388, 490	690	15	2.18	1.79
P8 (FO$_1$-PT4)	477	585	501	800	23	2.12	1.55
P9 (FO$_3$-PT5)	376, 460	560	380, 518	715	58	2.21	1.73
P10 (FO$_1$-PT5)	366, 462	568	525	800	63	2.18	1.55
P11 (FO$_3$-PT6)	380, 493	608	390, 540	800	47	2.04	1.55
P12 (FO$_1$-PT6)	500	613	548	800	48	2.02	1.55

[a]Spin-coated from THF solution. [b]The optical band gap was obtained from the equation $E_g^{opt} = 1240/\lambda_{edge}$. [c]The onset value of absorption spectrum in long wavelength direction. [d]$\Delta\lambda = \lambda_{max,fiim} - \lambda_{max,solution}$ (nm).

2.3.3 Electrochemical Characterization

The electronic states, i.e. highest occupied molecular orbital (HOMO) and lowest unoccupied molecular orbital (LUMO) levels, of the **FO-PT** copolymers were

investigated by cyclic voltammetry (CV) in order to understand the charge injection processes in these new narrow-band-gap polymers and their PVC devices. The oxidation and reduction cyclic voltammograms of polymers **P1-P12** in solid films are displayed in Figure 2.8. The electrochemical measurements of the formal potentials, onset potentials, band gaps, and the estimated positions of the upper edges of the valence band (HOMO) and the lower edges of the conduction band (LUMO) are summarized in Table 2.3. Ag/AgCl was served as a reference electrode, and it was calibrated by ferrocene ($E^{1/2}_{ferrocene}$ = 0.45 mV vs Ag/AgCl). The HOMO and LUMO energy levels were estimated by the oxidation and reduction potentials from the reference energy level of ferrocene (4.8 eV below the vacuum level) according to the following equation:[87] $E_{HOMO/LUMO}$ = [− (E_{onset} − 0.45) − 4.8] eV. For all copolymers, two p-doping processes and one n-doping process could be recorded, and partial reversibilities in both p-doping and n-doping processes were evidenced from the areas and close proximity of the anodic and cathodic scans. The formal oxidation and reduction potentials of **P1-P12** were in the range of (0.87-1.15) eV and -(1.08-1.36) eV, respectively. The band-gap values directly measured by CV (E_g^{ec} between 1.57 and 2.12 eV) and the optical band-gap values observed from UV-vis spectra (E_g^{opt} between 1.55 and 2.10 eV) were close to each other.

Two different onsets of oxidation processes occurred between ca. 0.74-1.05 eV and 1.28-1.35 eV, which were originated from the PT and FO[88] segments, respectively, in **FO-PT** copolymers. The onsets of the reduction processes of all copolymers were observed at -(0.81-1.07) eV, except the data of copolymer **P2**, which is different from the earlier reported result.[59] Since the reduction potential of polyfluorene homopolymer was observed typically at -2.28 eV,[88] the moderate reduction wave at -(0.81-1.07) eV should be attributed to the electron withdrawing effect of the PT

moiety in the reduction process. The second reduction wave corresponding to the fluorene segment was unable to record. It could be probably because the reduced states of the copolymers at higher negative voltages were unstable.
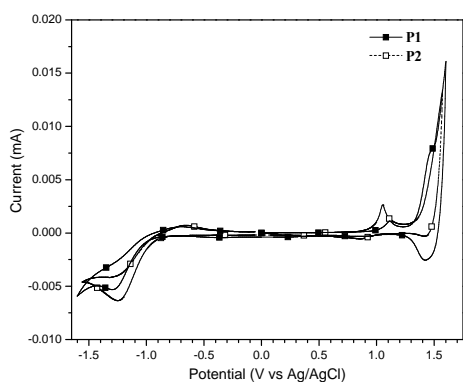
(a)   (b)
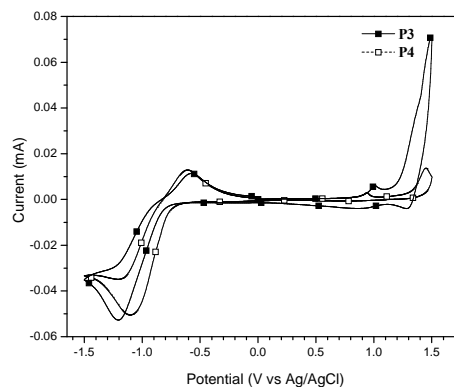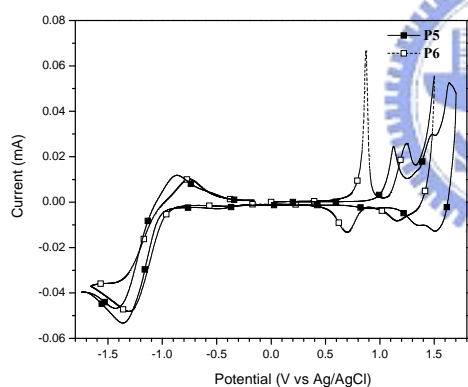
(c)   (d)
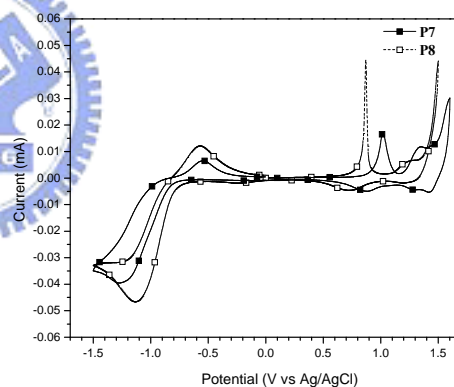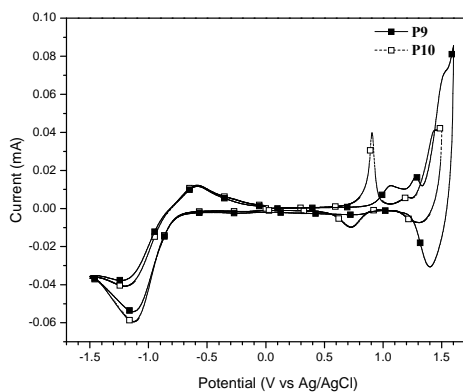
(e)   (f)
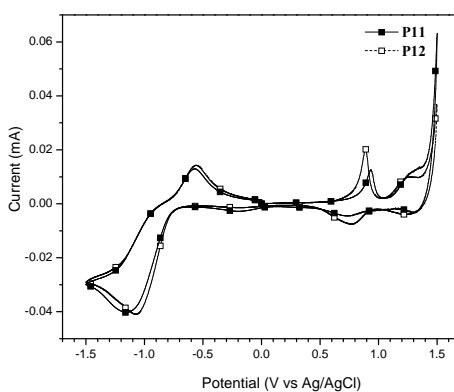
Figure 2.8 Cyclic voltammograms of fluorene-phenothiazine polymers **P1-P12.**

44

Table 2.3 Electrochemical Potentials and Energy Levels of Copolymers P1-P12[a]

Polymer	Oxidation potential V vs Ag/Ag$^+$		Reduction potential V vs Ag/Ag$^+$		Energy level[d] eV		Bandgap eV	
	$E_{ox/onset}$[b]	$E_{ox/o}$[c]	$E_{red/onset}$[b]	$E_{red/o}$[c]	E_{HOMO}	E_{LUMO}	E_g^{ec}	E_g^{opt}
P1	1.03	1.15	-1.07	-1.28	-5.38	-3.28	2.1	2.06
P2	1.00	1.06	-0.99	-1.19	-5.35	-3.36	1.99	1.96
P3	0.94	1.02	-0.88	-1.20	-5.29	-3.47	1.82	1.77
P4	0.83	0.94	-0.86	-1.10	-5.18	-3.49	1.69	1.49
P5	1.05	1.13	-1.07	-1.36	-5.40	-3.28	2.12	2.10
P6	0.80	0.87	-1.04	-1.31	-5.15	-3.31	1.84	1.55
P7	0.96	1.02	-0.91	-1.26	-5.31	-3.44	1.87	1.79
P8	0.75	0.87	-0.89	-1.13	-5.10	-3.46	1.64	1.55
P9	0.97	1.07	-0.84	-1.13	-5.32	-3.51	1.81	1.73
P10	0.74	0.91	-0.83	-1.13	-5.09	-3.52	1.57	1.55
P11	0.81	0.94	-0.81	-1.15	-5.16	-3.54	1.62	1.55
P12	0.78	0.89	-0.81	-1.08	-5.13	-3.54	1.59	1.55

[a]Reduction and oxidation potentials measured by cyclic voltammetry in solid films.
[b]Onset oxidation and reduction potentials. [c] Formal oxidation and reduction potentials.
[d]E_{HOMO}/E_{LUMO} = [-(E_{onset}-0.45)-4.8] eV where 0.45 V is the value for ferrocene vs. Ag/Ag$^+$ and 4.8 eV is the energy level of ferrocene below the vacuum.

According to the previous equation, the copolymers were relatively stable up to oxidation with low HOMO levels varying 5.09-5.40 eV. Owing to the results of low HOMO levels, the copolymers were easily handled in air without encountering undesired oxidation. The copolymers possessing LUMO levels ca. 3.28-3.54 eV were also good donors for charge transfer to PCBM acceptors (with 0.66-0.92 eV LUMO offsets regarding LUMO level of PCBM being at 4.2 eV). These characters are valuable properties to make use of these materials into optoelectronics.

Among the reports of phenothiazine homopolymer (PHPT) and PPTF copolymer, it is clear that HOMO levels of the polymers were dominated by the contribution from the phenothiazine moiety, but no reduction wave of either polymer was observed for LUMO levels.[80] Interestingly, there are clear differences of n-doping processes between the previous phenothiazine copolymers without any functional groups and our PT copolymers (with detectable reduction waves). Furthermore, the presence of different numbers of electron-donating thiophenes and electron-withdrawing cyano groups in both sides of our phenothiazine moieties changed the electrical properties of

PT copolymers so that they possessed both p-type and n-type properties. Therefore, it is clear that the HOMO/LUMO levels of **FO-PT** copolymers have been significantly varied relative to those of PFO and PHPT due to the modulated push-pull strengths of thiophene and cyano groups. Another important feature was also observed that as the PT contents of the copolymers were equivalent to 25% and 50%, the first onset potentials of p-doping and n-doping waves decreased with increasing PT contents. This result eventually induced narrower band-gaps of **FO-PT** copolymers owing to the increase of their HOMO levels and the reduction of their LUMO levels. The characters of reversible electrochemical oxidation and reduction processes in the copolymers suggested promising prospects for superior electrochemical stabilities in the applications of organic electronic devices.

2.3.4 Polymeric Photovoltaic Cell Properties

In the fabrication of bulk-heterojunction photovoltaic cell (PVC) devices, copolymers **P2**, **P6**, **P8**, **P10**, and **P12** were used as the donor phase to blend with different ratios of methanofullerene [6,6]-phenyl C_{61} butyric acid methyl ester (PCBM) as the typical acceptor phase. As described by UV absorptions of **FO-PT** copolymers in solid films, **FO$_1$-PT** polymer derivatives (FO:PT=1:1) possessed broader spectral absorption coverages than their **FO$_3$-PT** polymer analogues (FO:PT=3:1) in the visible ranges between 400 and 800 nm. Due to the benefits of narrower band-gaps and broader visible absorption ranges in **FO$_1$-PT** polymers with higher PT contents, **FO$_1$-PT** polymer derivatives were chosen to survey their potentials for PVC applications. In Figure 2.9(a), the HOMO and LUMO levels of **FO$_1$-PT** polymer derivatives also match those of good hole-transporting materials for PVC devices with an electron-transporting material PCBM. Thus, **FO$_1$-PT** polymer derivatives were appropriate for the fabrication of PVC devices with a configuration of

ITO/PEDOT:PSS/**FO$_1$-PT**:PCBM/LiF/Al as shown in Figure 2.9(b). To evaluate the PVC properties of **FO-PT** copolymers, a composite thin film of **FO$_1$-PT**:PCBM was prepared by spin-coating a solution of **P12** and PCBM (1:4 w/w) in the mixture solution of chlorobenzene and chloroform (1:1 vol.) onto a quartz plate, and its PL spectrum was recorded, as shown in Figure 2.10. Compared with the PL spectrum of pure **P12**, complete PL quenching was observed as a result of blending **P12** with PCBM, which could be attributed to the different kinetics of charge transfer (~10^{-14} s) and recombination (~10^{-3} s).[76] The PL quenching property indicates that **FO-PT** copolymers can be used as proper electron donors in PVC devices.

The *I-V* characteristics of photovoltaic cell devices with different weight ratios of **P12**:PCBM = 1:1, 1:2, and 1:4 as an active layer are presented in Figure 2.11, which were measured under AM 1.5 illumination for a calibrated solar simulator with an intensity of 100 mW/cm^2. The photovoltaic properties obtained from the *I-V* curves are listed in Table 2.4. The open circuit voltage (V_{oc}), short circuit current (I_{sc}), and fill factor (FF) of the PVC device based on the ratio of **P12**:PCBM = 1:4 (w/w) were 0.64 V, 2.7 mA/cm^2, and 29%, respectively, which were all higher than those of PVC devices based on the ratios of **P12**:PCBM = 1:1 and 1:2 (w/w). Generally, the values of energy conversion efficiency (ECE) in PVC devices are sensitive to the weight ratios of acceptors to donors. In the case of **P12**/PCBM blends, the best efficiency observed was **P12**:PCBM = 1:4 (w/w), which was a similar dependence on donor/acceptor weight ratio in some earlier publications.[85,89] In addition, according to the photovoltaic results of these copolymers in Table 2.4, the highest ECE value of 0.51% was obtained from a solar cell device with **P12** as an electron donor. Apparently, comparing the molecular structures of copolymers **P2**, **P6**, **P8**, **P10**, and **P12**, the longest conjugation length and the heterocyclic structures (thiophene units)

of **P12** could lead to the highest photovoltaic efficiency among these synthesized copolymers. This result indicates that the incorporation of longer conjugation lengths and heterocyclic moieties into conjugated copolymers could make favorable contribution to photovoltaic properties.

Several parameters are suspected to responsible for the low efficiencies in the PVCs, such as the thickness of the film, the disorder of the film morphology, and the large difference of charge-carrier mobility, etc. The lower molecular weights of **FO$_1$-PT** polymer derivatives resulted in the solid films with thinner thicknesses and the fewer harvested photons from the solar energy. Therefore, the I_{sc} values of the copolymers (listed in Table 2.4) were only 1.30~2.70 mA/cm^2. For example, the V_{oc}, I_{sc}, FF, and ECE values of **P2** were 0.43 V, 1.86 mA/cm^2, 27%, and 0.22%, respectively, which were not as high as the same polymer published earlier by Cho et al,[85-86] which might be due to the lower molecular weight or the lower fill factor of **P2**. In comparison with the photovoltaic results of **P2**, **P6**, **P8**, and **P10**, the PVC based on **P12** showed a much higher V_{oc} value of 0.64 V in Table 2.4, except **P4** due to its poor solubility. Generally, the V_{oc} value is related to the difference between the oxidation potential of the donor and the reduction potential of the acceptor (PCBM).[90] However, compared with the other polymers with lower HOMO levels, the PVC based on **P12** possessing the highest V_{oc} value did not follow the previous general regulation in this work. In addition to the above-mentioned influences on PVCs, the deficits of the ECE values in our polymers were mainly caused by low fill factors which indicate lacks of ordered continuity in the polymer/PCBM blends.[91] The disorder of the film morphology also severely affects the charge carrier mobility, which is believed to be the bottleneck for the I_{sc} values.

Although the photovoltaic properties of the copolymers in this work were not the

best results compared with the other low bandgap polymers, the preliminary results of PVC devices made of the newly synthesized polymers were still not optimized. Further improvements are underway to optimize the PVC devices by the modification of the film morphology, layer thicknesses, postproduction treatment conditions, and the other electron acceptors.

(a)
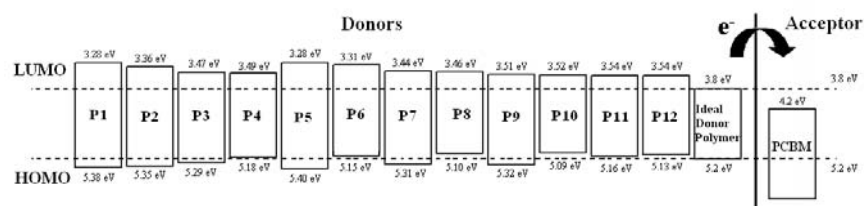
(b)
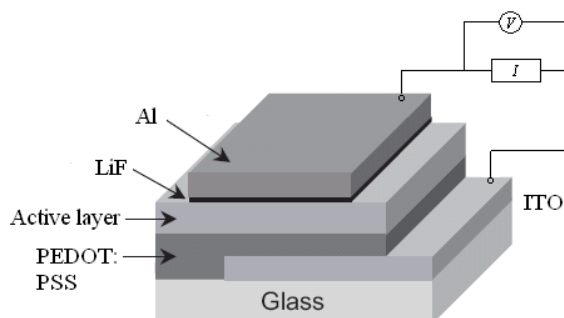
Figure 2.9 (a) Energy levels for an ideal donor polymer for PCBM along with donors **P1-P12**. Dashed lines display the HOMO and LUMO thresholds of an ideal donor polymer between 5.2-3.8 eV for air stability (5.2 eV) and effective charge transfer to PCBM (3.8 eV). (b) Device structure consisting of an 100 nm thick blending active layer (copolymers:PCBM), which was sandwiched between PEDOT:PSS and an aluminum top electrode.
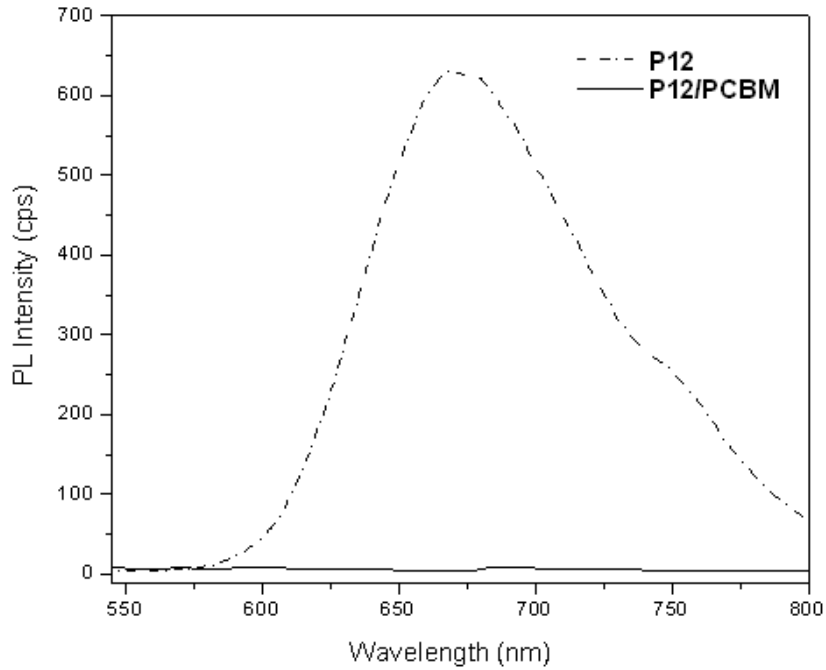
Figure 2.10 PL spectra of **P12** film and a blending film of **P12**/PCBM (1:4 w/w).
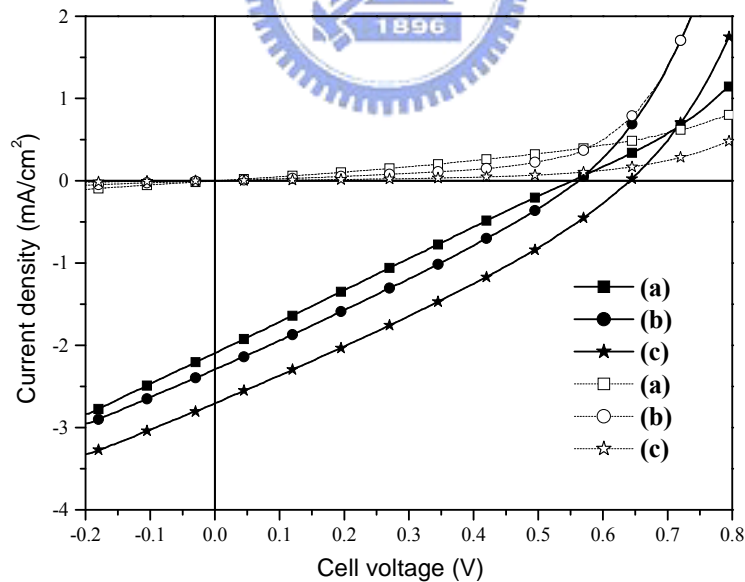
Figure 2.11 *I-V* curves of the polymer solar cells with different compositions of **P12**/PCBM (a) 1:1 w/w (square symbols), (b) 1:2 w/w (circle symbols), and (c) 1:4 w/w (star symbols) measured in the dark (dash lines) and under the illumination of AM 1.5, $100mW/cm^2$ (solid lines).

Table 2.4 Photovoltaic Properties of Copolymers with a Solar Cell Device Configuration of ITO/PEDOT:PSS/Copolymer:PCBM/LiF/Al[a]

Active layer	V_{oc} (V)	I_{sc} (mA/cm^2)	FF (%)	ECE (%)
P2/PCBM(1:4)	0.43	1.86	27	0.22
P6/PCBM(1:4)	0.52	1.46	22	0.17
P8/PCBM(1:4)	0.27	2.21	27	0.16
P10/PCBM(1:4)	0.53	1.30	26	0.18
P12/PCBM(1:1)	0.55	2.10	25	0.29
P12/PCBM(1:2)	0.56	2.30	28	0.36
P12/PCBM(1:4)	0.64	2.70	29	0.51

[a]Measured under AM 1.5 irradiation, 100mW/cm.

2.4 Conclusions

Souble conjugated donor-acceptor low-band-gap copolymers derived from 9,9-dihexylfluorene (FO) and phenothiazine-arylcyanovinyl units were synthesized by palladium (0)-catalyzed Suzuki coupling reactions and characterized by NMR, FTIR, and elemental analyses. The more heterocyclic units and cyano-groups incorporated into phenothiazine derivatives, the stronger strength of intramolecular charge-transfer interaction. Thus, the optical and electrochemical properties of the copolymers were induced to visible and even further to near infrared absorption with narrow band gaps, which the lowest result were 1.55 eV. Photoluminescence quenching measurements indicated that **FO-PT** was functioning as a photo-excited donor in case of blending with PCBM. Bulk heterojunction PVC devices fabricated from a thin film composed of a blend of **FO$_1$-PT** polymer derivatives and PCBM, with the configuration of ITO/PEDOT:PSS/(**FO$_1$-PT**:PCBM = 1:4)/LiF/Al, showed the preliminary results of the PVC devices, and their optoelectronic performance can also be much improved in the future.

Chapter 3 Soluble Narrow-Band-Gap Copolymers Containing Novel Cyclopentadithiophene Derivative for Organic Photovoltaic Cell Applications

3.1 Introduction

The developments of new materials to be used in organic optoelectronic devices such as polymeric solar cells (PSCs) have become dramatically attractive because they represent a green and renewable energy alternative to fossil energy and nuclear power. In particular, the so-called bulk heterojunction (BHJ) concept[72] has been established in thin films of organic solar cell devices utilizing electron-donating conjugated polymers blended with electron-accepting species, such as fullerenes,[20] dicyano-based polymers,[92-93] or n-type nanoparticles.[94-95] For these purposes, several novel polymeric materials have been extensively studied over the past decade. For example, the regio-regular poly(3-hexylthiophene) (P3HT)[51-52] and poly[2-methoxy-5-(3',7'-dimethyloctyloxy)-*p*-phenylenevinylene] (MDMO-PPV)[91] possessed a highest power conversion efficiency (PCE) approaching 5.0% in PSCs. However, several groups proposed new polymeric structures as substitutes for these polymers, since the disadvantages on the PSC performance were somehow restricted by their relatively large band gaps,[96] which only absorbed part of the visible light and limited the utility of the sunlight.

To further improve the absorption properties of the conjugated polymers, the intramolecular charge transfer (ICT) interactions between electron-donor (D) and electron-acceptor (A) moieties have been extensively applied to the developments of novel narrow band-gap conjugated polymers with better PSC performance, especially in the band-gap region of 1.4-1.8 eV.[22,25-26,58,60,97-98] Among them, the derivatives of polyfluorene,[97] thiophene-based,[60] and arylamine-based[98] represent promising features

having PCE values. However, besides band gaps, several characteristics of conjugated polymers, including HOMO/LUMO levels and carrier mobilities, need to be simultaneously optimized in order to achieve higher photovoltaic performance.[22,25,26]

Recently, in order to obtain longer conjugation lengths, more planar molecular geometries, and more rigid structures in π-conjugated polymers,[58] novel heteroaromatic fused-ring derivatives, including cyclopentadithiophene (CPDT) units, have been widely investigated in PSCs. Kraak *et al.* first reported the structural unit of CPDT in 1968,[62] and the later prepared CPDT-based polymers[63-65] showed relatively high conductivities due to more extensive π-conjugation lengths as compared with polythiophene and polyfluorene derivatives. Due to the high planarities, long conjugation lengths, narrow band gaps, and strong intermolecular π-π interactions of the CPDT units, CPDT-based polymers possessing good conductive properties were found to be a powerful approach to optimize the PSC performance. Recently, the derivatives of CPDT copolymers showed very promising PCE results (1.14-5.5%)[66-67,99-101] and high carrier mobilities (10^{-2}-10^{-1} cm^2/Vs),[66,102-103] which demonstrated that the synthesized ICT polymers possess both prominent properties of narrow band gaps and high carrier mobilities.

Up to now, very few investigations of CPDT-based polymers have been reported for the applications of PSC performance. Although the band gaps of the reported derivatives of CPDT homopolymers and copolymers were relatively low,[62-67,99-103] their HOMO energy levels were apparently not low enough to produce air-stable polymers with relatively high open circuit potential (V_{oc}) values in the ultimate PSC devices, where the highest V_{oc} values of the CPDT-based polymers were still not over 0.65 V.[66-67,99-103] It is noticeable that a well-known design to tune the HOMO and LUMO levels of conjugated polymers would be the introduction of

electron-withdrawing units, such as nitro, carboxy, and cyano groups, to the conjugated systems.[57,74] In 1991, Ferraris and Lambert reported that CPDT-based polymers, bearing electron-withdrawing keto groups at the bridging carbons, showed relatively low band gap values around 1.20 eV.[104] On the other hand, another important observation was found that the electron-withdrawing cyano groups could decrease the HOMO level and thus to stabilize the neutral state of the conjugated system.[57]

Based on this concept, two different moieties of CPDT derivatives, i.e., 2,6-diarylene-cyanovinylene-CPDT (**M1**, as shown in Figure 3.1) and CPDT-4-one (**M2**, as shown in Figure 3.1), were utilized as acceptor monomers to synthesize CPDT-based copolymers **P1**-**P5**. Besides, in order to increase the solubility without causing any additional twisting of the repeating units in the resulting copolymers, 4-carbon position of compound **2** could be favorably functionalized by diethylhexyl substitutions to produce CPDT unit (**3**) as the donor monomer. Therefore, our donor-acceptor approaches utilized in these CPDT-based copolymers (**P1**-**P5**, as shown in Figure 3.2) achieve the absorption spectra in the visible range of 400-850 nm (with tailing up to around 1000 nm) in solid films and finely tuned HOMO and LUMO levels with narrow electrochemical band gaps of 1.30-1.66 eV. In addition, after thermal annealing, the molecular configurations of the π-conjugated CPDT-based copolymers could clearly ensure that highly organized π-π stackings could be easily formed in these fused-heteroaromatic molecular frameworks, which were confirmed by the powder X-ray diffraction (XRD) analyses. Compared with those reported CPDT-based polymers, our copolymers in this report showed much improved V_{oc} values with a highest open-circuit voltage up to 0.84 V as well as suitable electronic energy levels and good processabilities for PSC applications. So far,

the preliminary PSC performance of these structurally related copolymers showed the best PCE efficiency up to 0.77% while blended with [6,6]-phenyl C_{61} butyric acid methyl ester (PCBM), with a short circuit current density (I_{sc}) of 2.36 mA/cm^2, an open circuit voltage (V_{oc}) of 0.84 V, and a fill factor (FF) of 0.38 under AM 1.5 (100 mW/cm^2). Although the results for the PCE efficiencies of these un-optimized PSCs are not sufficiently high enough, this research affords a new concept to enhance the V_{oc} properties *via* the electron donor-acceptor (D-A) design to offset the low V_{oc} drawbacks, which encountered in narrow band-gap CPDT-based conjugated polymers.

3.2 Experimental Section

3.2.1 Materials

All chemicals and solvents were used as received. Compounds **1** (cyclopenta[2,1-b:3,4-*b'*]dithiophen-4-one)[105] and **2** (4*H*-cyclopenta [2,1-b:3,4-*b'*]dithiophene)[64] were synthesized according to the literature procedures. The synthetic routes of monomers **1**-**2** and polymers **P1**-**P5** are shown in Schemes 1 and 2, and the synthetic procedures of their intermediates were described.

3.2.2 Synthesis

4,4-Bis(2-ethylhexyl)-4H-cyclopenta[2,1-b:3,4-b']dithiophene **(3)**

Compound **2** (2.0 g, 11.2 mmol) was dissolved in DMSO (50 mL), and then 2-ethylhexyl bromide (4.3 g, 22.4 mmol) was added and followed by potassium iodide (50 mg). The mixture was purged with nitrogen and cooled in an ice bath, and ground KOH (2.0 g) was added in portions. The resulting green mixture was vigorously stirred overnight at room temperature. Water was added after reaction, and the reaction mixture was extracted with dichloromethane. Solvent was removed under vacuum, and the crude product was purified by chromatography using hexane as eluent. Subsequently, the pure compound was obtained as colorless oil. Yield: 3.60 g

(80%). ^{1}H NMR (ppm, CDCl$_3$): δ 7.13 (m, 2H), 6.91 (m, 2H), 1.86 (m, 4H), 0.93 (m, 18H), 0.73 (t, J = 6.4 Hz, 6H), 0.59 (m, J = 7.2 Hz, 6H).

2,6-Dibromo-4,4-bis(2-ethylhexyl)-4H-cyclopenta[2,1-b:3,4-b']   dithiophene (4) Compound **3** (3.5 g, 8.7 mmol) and NBS (3.1 g, 17.4 mmol) were dissolved in 50 mL of DMF. The resulting solution was stirred to react at room temperature under nitrogen over night. Water (50 mL) was then added, and the organic phase was extracted with dichloromethane (100 mL) twice, washed with water. After that, the solvent was removed under reduced pressure to obtain the product. The crude product was purified by column chromatography with hexane to obtain pale yellow oil (4.10 g). Yield: 83%. ^{1}H NMR (ppm, CDCl$_3$): δ 6.92 (s, 2H), 1.80 (m, 4H), 0.94 (m, 18H), 0.76 (m, 6H), 0.60 (m, J = 7.2 Hz, 6H).

4,4-Bis(2-ethylhexyl)-4H-cyclopenta[2,1-b:3,4-b']dithiophene-2,6-dicarbalde hyde (5) To a solution of compound **4** (4.4 g, 7.8 mmol) in THF (80 mL), n-BuLi (2.5 M solution in hexane, 7.0 mL, 17.9 mmol) was added at -78 °C. After stirring for 1h, a solution of N-formylmorpholine (1.9 g, 16.4 mmol) in THF (20 mL) was added. After additional stirring for 1h at -78 °C, the mixture was allowed to warm up to room temperature. Next, the mixture was hydrolyzed by 1 N HCl, and the final solution was extracted with dichloromethane. The organic layer was evaporated and the crude product was purified by column chromatography (silica gel, EA/hexane 1:10) to yield a yellow solid. Yield: 83%. ^{1}H NMR (ppm, CDCl$_3$): δ 9.88 (s, 2H), 7.61 (s, 2H), 1.94 (m, 4H), 0.96-0.86 (m, 18H), 0.71 (m, 6H), 0.55 (m, J = 7.2 Hz, 6H).

2,6-Bis(4,4,5,5-tetramethyl-1,3,2-dioxaborolan-2-yl)-4,4-Bis(2-ethylhexyl)-4 H-cyclopenta[2,1-b:3,4-b']dithiophene (8) A solution of compound **4** (6.5 g, 11.6 mmol) in 150 mL of dry THF was stirred in a two-necked flask and cooled at -78 °C while n-butyllithium (2.5 M solution in hexane, 29.0 mmol) was added dropwisely

under nitrogen atmosphere. After reaction for 2 hours at -78 °C, compound **7** (6.0 ml, 29.0 mmol) was added carefully to the mixture solution at -78 °C and then the mixture was allowed to warm up to react at room temperature overnight. The final solution was acidified with 100 mL of 10 % HCl solution and stirred for 45 mins at room temperature. The solution was extracted by dichloromethane and the organic layer was dried over magnesium sulfate. After removing the solvent by rotavapor, the crude product was purified by column chromatography (silica gel, CH_2Cl_2/hexane 1:2) to afford compound **8** (4.93 g). Yield: 65%. ^{1}H NMR (ppm, $CDCl_3$): δ 7.43 (s, 2H), 1.84 (m, 4H), 1.35 (m, 24H), 0.95-0.56 (m, 30H). ^{13}C NMR (ppm, $CDCl_3$): δ 160.95, 144.06, 131.86, 126.34, 83.89, 52.64, 43.17, 35.11, 33.84, 28.30, 27.42, 24.74, 22.75, 14.06, 10.55. MS (FAB): *m/z* [M[+]] 655; calcd *m/z* [M[+]] 654.4. Anal. Calcd for $C_{37}H_{60}B_2O_4S_2$: C, 67.89; H, 9.24; S, 9.80. Found: C, 67.92; H, 9.52; S, 10.29.

M1 A mixture of compound **5** (2.6 g, 5.6 mmol), compound **6** (i.e., 1-bromophenylacetonitrile, 5.5 g, 28 mmol), and methanol (300 mL) were mixed in a 500 mL two-neck round-bottom flask at room temperature. A catalytic amount of potassium *tert*-butoxide in methanol was added into this mixture. After reaction for 24 h, the product was filtered and dried. Chromatography on silica gel eluted with CH_2Cl_2/hexane 1:4 afforded **M1** as a red solid (4.1 g). Yield: 90%. ^{1}H NMR (ppm, $CDCl_3$): δ 7.62-7.48 (m, 12H), 1.95 (m, 4H), 0.97-0.90 (m, 16H), 0.75-0.59 (m, 14H). ^{13}C NMR (ppm, $CDCl_3$): δ 160.42, 140.25, 134.38, 134.25, 133.02, 132.25, 126.93, 126.67, 122.87, 118.23, 105.34, 54.21, 43.07, 35.29, 34.09, 28.43, 27.30, 22.73, 14.01, 10.62. MS (FAB): *m/z* [M[+]] 815; calcd *m/z* [M[+]] 814.1. Anal. Calcd for $C_{43}H_{46}Br_2N_2S_2$: C, 63.39; H, 5.69; N, 3.44; S, 7.87. Found: C, 63.58; H, 5.39; N, 3.55; S, 8.22.

2,6-Dibromocyclopenta[2,1-b:3,4-b']dithiophen-4-one (M2) The synthesis of

compound **M2** was also followed by the similar procedure of compound **4**. Compound **1** (2.0 g, 10.4 mmol) was dissolved in 50 mL of dimethylformamide under nitrogen in the dark, and NBS (3.8 g, 20.8 mmol) was added gradually. The crude product was purified by column chromatography with CH_2Cl_2/hexane (1:1) to get a purple solid (3.1 g). Yield: 85%. ^{1}H NMR (ppm, $CDCl_3$): δ 6.98 (s, 2H). ^{13}C NMR (ppm, $CDCl_3$): δ 182.56, 150.07, 143.54, 124.41, 113.95. MS (EI): m/z [M[+]] 350; calcd m/z [M[+]] 349.8. Anal. Calcd for $C_9H_2Br_2OS_2$: C, 30.88; H, 0.58; S, 18.32. Found: C, 31.10; H, 0.71; S, 18.42.

General Procedure for the Syntheses of copolymers P1-P5[78]

The synthetic routes of polymers are shown in Scheme 3.2. All of the polymerization procedures were carried out through the palladium(0)-catalyzed Suzuki coupling reactions. In a 50 mL two-neck flask, 1 equiv of dibromo compounds (**M1** and **M2** with various molar ratios, **M1**:**M2** = m:0, 2:1, 1:1, 1:2, and 0:n, respectively) and 1 equiv of 2,6-bis(4,4,5,5-tetramethyl-1,3,2-dioxaborolan-2-yl)-4,4-Bis(2-ethylhexyl)-4H-cyclopenta[2,1-b:3,4-b']dithiophene (**8**) were added into 10 mL of anhydrous toluene. The Pd(0) complex, tetrakis(triphenylphosphine)palladium (1 mol %), was transferred into the mixture in a dry environment. Then, 2M aqueous potassium carbonate and a phase transfer catalyst, i.e., aliquat 336 (several drops), were subsequently transferred via dropping funnel the previous mixture under nitrogen. The reaction mixture was stirred at 85 °C for 2 days, and then both excess amounts of iodobenzene and phenylboronic acid, the end-cappers, dissolved in 1mL of anhydrous toluene were added and stirred for 4 h, respectively. The reaction mixture was cooled to 50 °C and added slowly into a vigorously stirred mixture of methanol/water (10:1). The polymers were collected by filtration and reprecipitation from methanol. The crude polymers were further

purified by washing with acetone for 3 days in a Soxhlet apparatus to remove oligomers and catalyst residues. The chloroform fractions (350-400 mL) were reduced to 40-50 mL under reduced pressure, and were precipitated in acetone and finally air-dried overnight.

P1 Following the general polymerization procedure, compound **8** (1.0 equiv) and **M1** (1.0 equiv) were used in this polymerization to acquire a black powder. Yield: 50%. ^{1}H NMR (ppm, CDCl$_3$): δ 7.67 (br, m, 14H), 1.99 (br, m, 8H), 1.02-0.67 (br, m, ~60H). Elemental Anal. Calcd: C, 77.37; H, 7.83; N, 2.65; S, 12.15. Anal. Found: C, 77.89; H, 7.35; N, 2.77; S, 12.17.

P2 Following the general polymerization procedure, compound **8** (1.0 equiv), **M1** (0.67 equiv), and **M2** (0.33 equiv) were used in this polymerization to attain a black powder. Yield: 80%. ^{1}H NMR (ppm, CDCl$_3$): δ 7.67 (broad), 7.05 (s), 1.98 (broad), 1.02-0.68 (broad). Elemental Anal. Found: C, 74.97; H, 7.06; N, 2.65; S, 13.87; O, 0.96.

P3 Following the general polymerization procedure, compound **8** (1.0 equiv), **M1** (0.5 equiv), and **M2** (0.5 equiv) were used in this polymerization to obtain a black powder. Yield: 67%. ^{1}H NMR (ppm, CDCl$_3$): δ 7.65 (broad), 7.04 (s), 1.96 (broad), 1.00-0.66 (broad). Elemental Anal. Found: C, 73.43; H, 6.97; N, 2.33; S, 15.01; O, 1.53.

P4 Following the general polymerization procedure, compound **8** (1.0 equiv), **M1** (0.33 equiv), and **M2** (0.67 equiv) were used in this polymerization to gain a black powder. Yield: 81%. ^{1}H NMR (ppm, CDCl$_3$): δ 7.66 (broad), 7.02 (s), 1.96 (broad), 1.25-0.69 (broad). Elemental Anal. Found: C, 72.13; H, 7.59; N, 1.67; S, 16.30; O, 1.79.

P5 Following the general polymerization procedure, compound **8** (1.0 equiv) and **M2**

(1.0 equiv) were used in this polymerization to get a black powder. Yield: 56%. ^{1}H NMR (ppm, $CDCl_3$): δ 7.01 (br, s, 4H), 1.93 (br, m, 4H), 1.25-0.67 (br, m, ~30H). Elemental Anal. Calcd: C, 69.11; H, 6.48; S, 21.70; O, 2.71. Anal. Found: C, 69.73; H, 6.09; S, 21.04; O, 3.18.

3.2.3 Measurements and Characterization

^{1}H NMR spectra were recorded on a Varian Unity 300 MHz spectrometer using $CDCl_3$ solvents. Elemental analyses were performed on a HERAEUS CHN-OS RAPID elemental analyzer. Transition temperatures were determined by differential scanning calorimetry (DSC, Perkin-Elmer Pyris 7) with a heating and cooling rate of 10 °C/min. Thermogravimetric analyses (TGA) were conducted with a TA instrument Q500 at a heating rate of 20 °C/min under nitrogen. Gel permeation chromatography (GPC) analyses were conducted on a Waters 1515 separation module using polystyrene as a standard and THF as an eluent. UV-visible absorption and photoluminescence (PL) spectra were recorded in dilute chloroform solutions (10^{-6} M) on a HP G1103A and Hitachi F-4500 spectrophotometer, respectively. Solid films of UV-vis and PL measurements were spin-coated on a quartz substrate from chlorobenzene solutions with a concentration of 10 mg/mL. Cyclic voltammetry (CV) measurements were performed using a BAS 100 electrochemical analyzer with a standard three-electrode electrochemical cell in a 0.1 M tetrabutylammonium hexafluorophosphate (TBAPF6) solution (in acetonitrile) at room temperature with a scanning rate of 50 mV/s. In each case, a carbon working electrode coated with a thin layer of these copolymers, a platinum wire as the counter electrode, and a silver wire as the quasi-reference electrode were used. Ag/AgCl (3M KCl) electrode was served as a reference electrode for all potentials quoted herein. During the CV measurements, the solutions were purged with nitrogen for 30s, and the redox couple

ferrocene/ferrocenium ion (Fc/Fc$^+$) was used as an external standard. The corresponding HOMO and LUMO levels in copolymer films of **P1**-**P5** were calculated from $E_{ox/onset}$ and $E_{red/onset}$ values of the electrochemical experiments. The LUMO value of PCBM was in accordance with the literature data.[106] Each onset potential in the CV measurements was defined by the intersection of two tangents drawn at the rising current and background current.

X-ray Diffraction Characterization

Synchrotron powder X-ray diffraction (XRD) measurements were performed at beamline BL17A of the National Synchrotron Radiation Research Center (NSRRC), Taiwan, where the wavelength of X-ray was 1.33361 Å. The XRD data were collected using Mar345 image plate detector mounted orthogonal to the beam with sample-to-detector distance of 250 mm, and the diffraction signals were accumulated for 3 min. The powder samples were packed into a capillary tube and heated by a heat gun, whose temperature controller is programmable by a PC with a PID feedback system. The scattering angle theta was calibrated by a mixture of silver behenate and silicon.

Fabrication of Hole- and Electron-Only Devices

The hole- and electron-only devices in this study containing copolymers **P1**-**P5**: PCBM (1:4) blend film sandwiched between transparent ITO anode and cathode. The ITO glasses were first ultrasonically cleaned in detergent, de-ionized water, acetone and isopropyl alcohol before the deposition. After routine solvent cleaning, the substrates were treated with UV ozone for 3 min. In the hole-only device, the modified ITO surface was obtained by spin-coating a layer of poly(ethylene dioxythiophene): polystyrenesulfonate (PEDOT:PSS) (~50 nm). After baking at 100 ^{o}C for 1h, the substrates were then transferred into a nitrogen-filled glove box. The

active layer was spin coated (spin rate = 500 rpm; spin time = 40 s) on top of PEDOT:PSS and then dried in covered glass Petri dishes. The film thicknesses of the active layer were measured to be 370, 320, 260, 420, and 290 nm, for **P1**, **P2**, **P3, P4**, and **P5**, respectively. Subsequently, a 15 and 120 nm thick of MoO_3 and aluminum was thermally evaporated under vacuum at a pressure below 2.5×10^{-5} torr through a shadow mask. The active area of the device was 0.0314 cm^2. In the electron-only device, the PEDOT:PSS layer was replaced with Cs_2CO_3, which has been used as an efficient electron injection layer. The modified ITO surface was obtained by spin-coating a layer of Cs_2CO_3 (~2 nm). The film thicknesses of the active layer were measured to be 340, 240, 280, 260 and 460 nm, for **P1**, **P2**, **P3, P4**, and **P5**, respectively. Subsequently, a 40 and 70 nm thick of Ca and aluminum was thermally evaporated under vacuum at a pressure below 2.5×10^{-5} torr through a shadow mask. The active area of the device was 0.0314 cm^2.

3.2.4 Device Fabrication of Polymer Photovotaic Cells

The photovoltaic cell (PVC) device structure used in this study was a sandwich configuration of ITO/PEDOT:PSS/active layer/LiF/Al, where the active layer was made of electron donor polymers **P1-P5** mixed with electron acceptor [6,6]-phenyl C_{61} butyric acid methyl ester (PCBM) in the weight ratio of 1:4 (w/w). The PVC devices were fabricated according to the procedures similar to those of EL devices. An ITO coated glass substrate was pre-cleaned and treated with oxygen plasma prior to use. A thin layer (~50 nm) of PEDOT:PSS was spin-coated on an ITO substrate and heated at 130 °C for 1h. Subsequently, the preliminary active layer was prepared by spin coating from composite solutions of **P1-P5**/PCBM (1:4 w/w) in chlorobenzene (10 mg/mL) on the top of the PEDOT:PSS layer. The spin rate was about 800 rpm, and the thickness of the active layer was typically ranged between 100

and 160 nm, unless the detailed thickness is specified. The PVC devices were completed by deposition with 1 nm of LiF and 120 nm of Al. The film thicknesses were measured by a profilometer (Dektak3, Veeco/Sloan Instruments Inc., USA). For PVC measurements, I-V curves were recorded under a solar simulator with AM 1.5 irradiation (at 100 mW/cm^2). A 300 W xenon lamp (Oriel, #6258) with AM 1.5 filter (Oriel, #81080 kit) was used as the white light source, and the optical power at the sample was 100 mW/cm^2 detected by Oriel thermopile 71964. The I-V characteristics were measured using a CHI 650B potentiostat/galvanostat. The external quantum efficiency (EQE) was measured using a CHI 650B coupled with Oriel Cornerstone 260 monochromator. All PVC devices were prepared and measured under ambient conditions.

3.3 Results and Discussion

3.3.1 Synthesis and Characterization

As outlined in Figure 3.1, two electron-accepting monomers **M1** and **M2** based on cyclopentadithiophene (CPDT) moieties were prepared from cyclopenta[2,1-b:3,4-b']dithiophen-4-one (**1**)[105] using a reduction procedure and followed by dibromination, which were described by Turner et al.[64] The electron-donating unit of CPDT (**8**) was prepared by dilithiation of **4** with n-buthyllithium and followed by reaction with compound **7** to afford 4,4-dialkyl-2,6-bis(4,4,5,5-tetramethyl-1,3,2-dioxaborolan-2-yl)-4H-cyclopenta[2,1-b:3,4-b']dithiophene **8** (see Figure 3.1). Monomers **M1**-**M2** and compound **8** were satisfactorily characterized by ^{1}H NMR, ^{13}C NMR, MS spectroscopies, and elemental analyses. Three-component random copolymers **P2**-**P4** were prepared successfully via Suzuki coupling of compound **8** with a mixture of various molar ratios of monomers **M1** and **M2**. Two-component copolymers **P1** and **P5** were produced by compound **8**

copolymerized with monomers **M1** and **M2**, respectively. The synthetic procedures towards copolymers **P1**-**P5** are outlined in Figure 3.2. Most copolymers are partly soluble in organic solvents such as chloroform, THF, and chlorobenzene at room temperature and completely soluble in high boiling point solvents (e.g., chlorobenzene) at high temperature. The yields and molecular weights of polymers **P1**-**P5** determined by gel permeation chromatography (GPC) against polystyrene standards in THF are summarized in Table 3.1. These results show that considerable molecular weights with high yields (50-81% after Soxhlet extractions) were obtained in these copolymers, where the weight-average molecular weights (M_w) ranging 9700-60800 with polydispersity indices (PDI = M_w/M_n) of 1.41-2.65 were obtained.

The molecular structures of copolymers **P1**-**P5** were identified by ^{1}H NMR and FT-IR. The output ratios of copolymers **P2**-**P4** were calculated from the elemental analyses, which are all reasonably close to the feeding ratios of copolymers **P2**-**P4**. Proton NMR spectra of monomers **M1**-**M2** and copolymers **P1**-**P5** in CDCl$_3$ are illustrated in Figure 3.3. The characteristic resonances at 7.67 and 7.01 ppm in the spectra of **P1**-**P5** are assigned to two different protons of monomers **M1** and **M2**, respectively. In addition, the peak area ratios of output copolymers between the two resonances at 7.67 ppm (**M1**) and 7.01 ppm (**M2**) in the NMR spectra fitted well with the designed molecular structures of copolymers **P1**-**P5**, where a larger integrated signal of δ = 7.01 ppm could be observed in the copolymers with a higher molar ratio of **M2**.
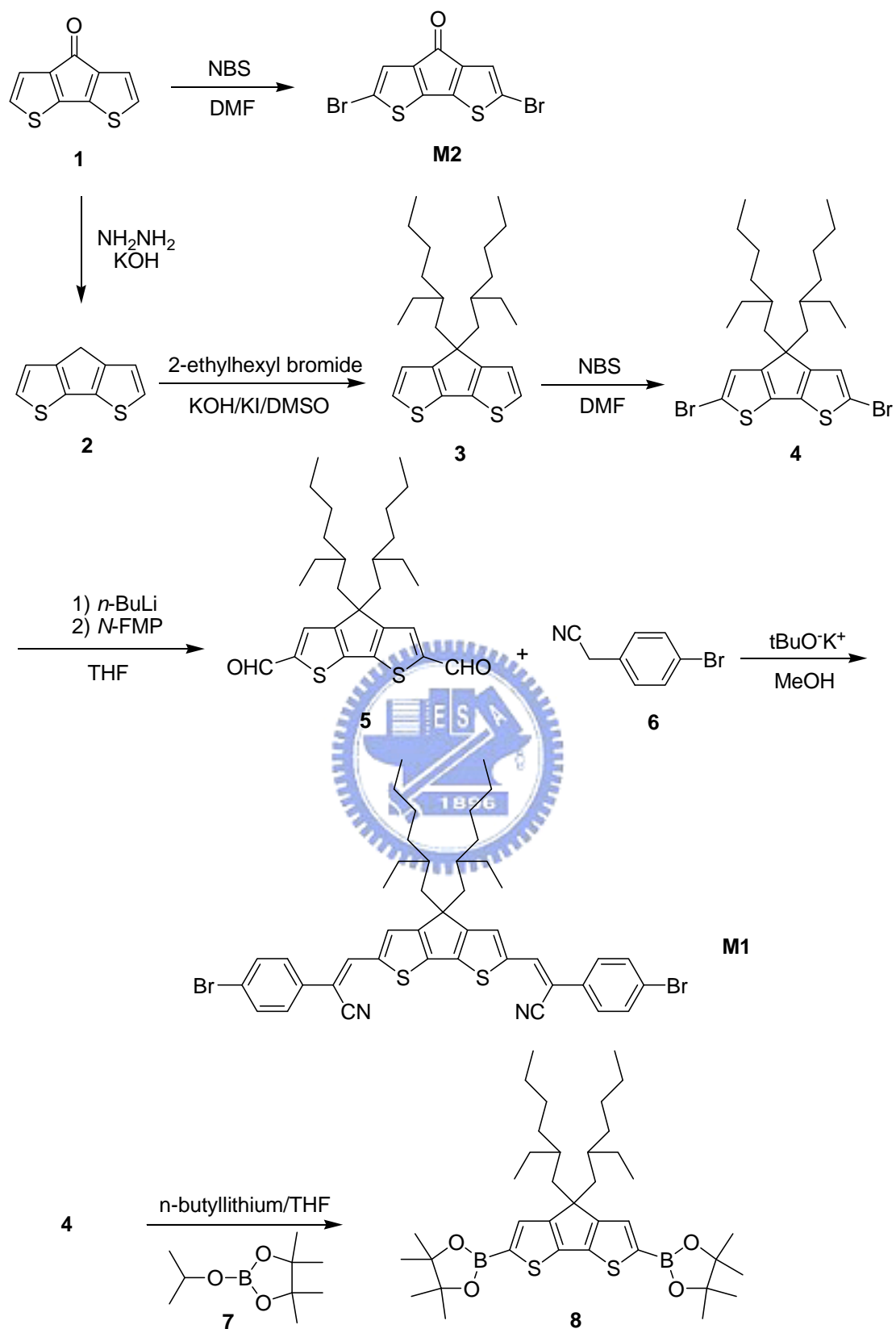
Figure 3.1 Synthetic Routes of Monomers **M1-M2**.
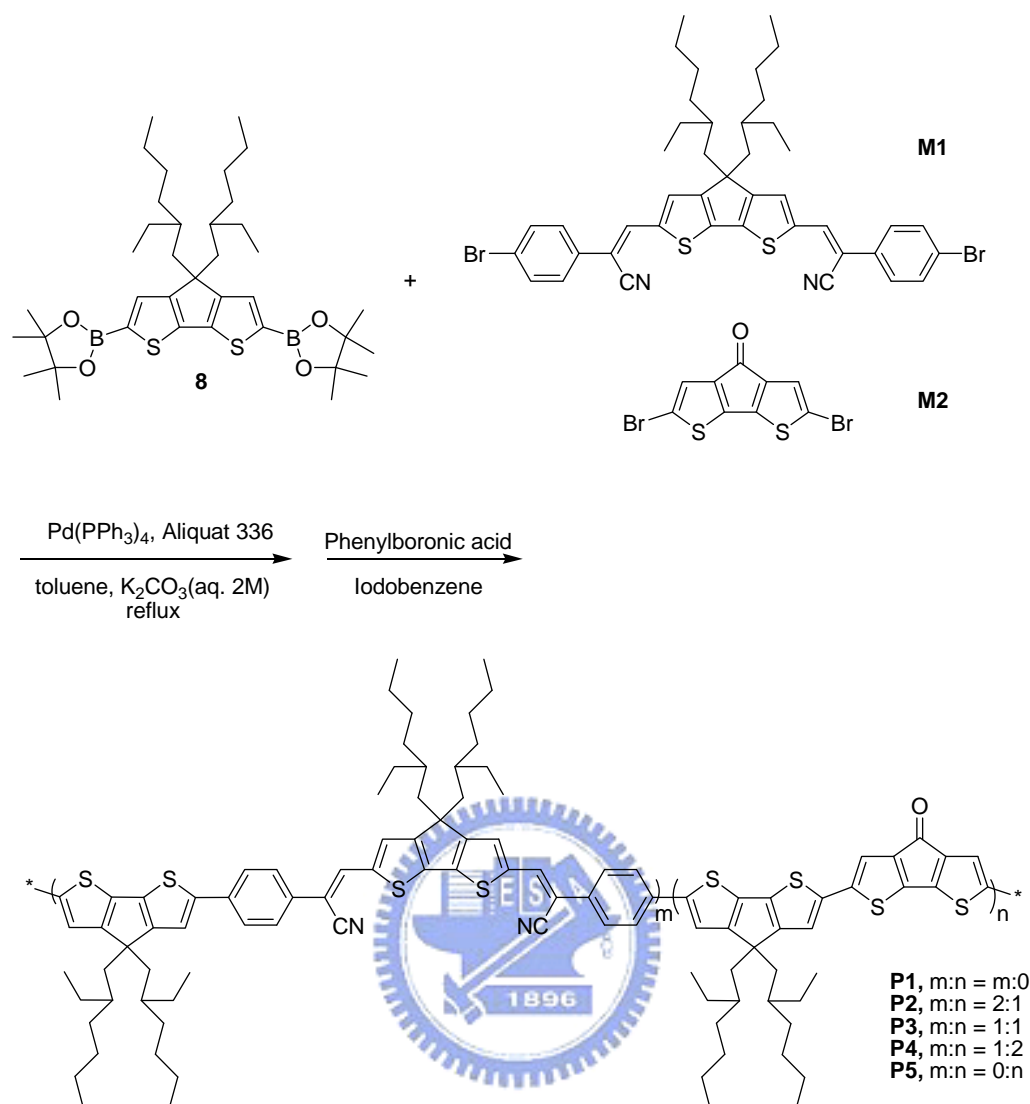
Figure 3.2 Synthetic Routes of Copolymers **P1-P5**.

Table 3.1 Molecular Weights, Yields, and Thermal Data of Polymers 1-5

Polymer	Feeding ratio (m:n)	Output ratio (m:n)[a]	M_n[b]	M_w[b]	PDI	Yield (%)	T_m[c] (°C)	T_d[d] (°C)
P1	m:0	m:0	15000	28800	1.92	50	n.d.[e]	388
P2	2:1	1.58:1	22900	60800	2.65	80	229	360
P3	1:1	0.87:1	14500	26300	1.81	67	192	355
P4	1:2	1:1.87	10200	17400	1.71	81	200	320
P5	0:n	0:n	6900	9700	1.41	56	200	311

[a] Output molar ratios of m:n in copolymers **P2-P4** were calculated from the elemental analyses. [b] Molecular weights (M_n: number average molecular weight; M_w: weight average molecular weight) and polydispersity indexes (PDI) values were measured by GPC, using THF as an eluent, polystyrene as a standard. [c] Melting transition temperatures (°C) were measured by DSC at a heating rate of 10 °C/min. [d] Decomposition temperatures (°C) at 5% weight loss (T_d) were measured by TGA at a heating rate of 20 °C/min under nitrogen. [e] No noticeable T_m was observed.
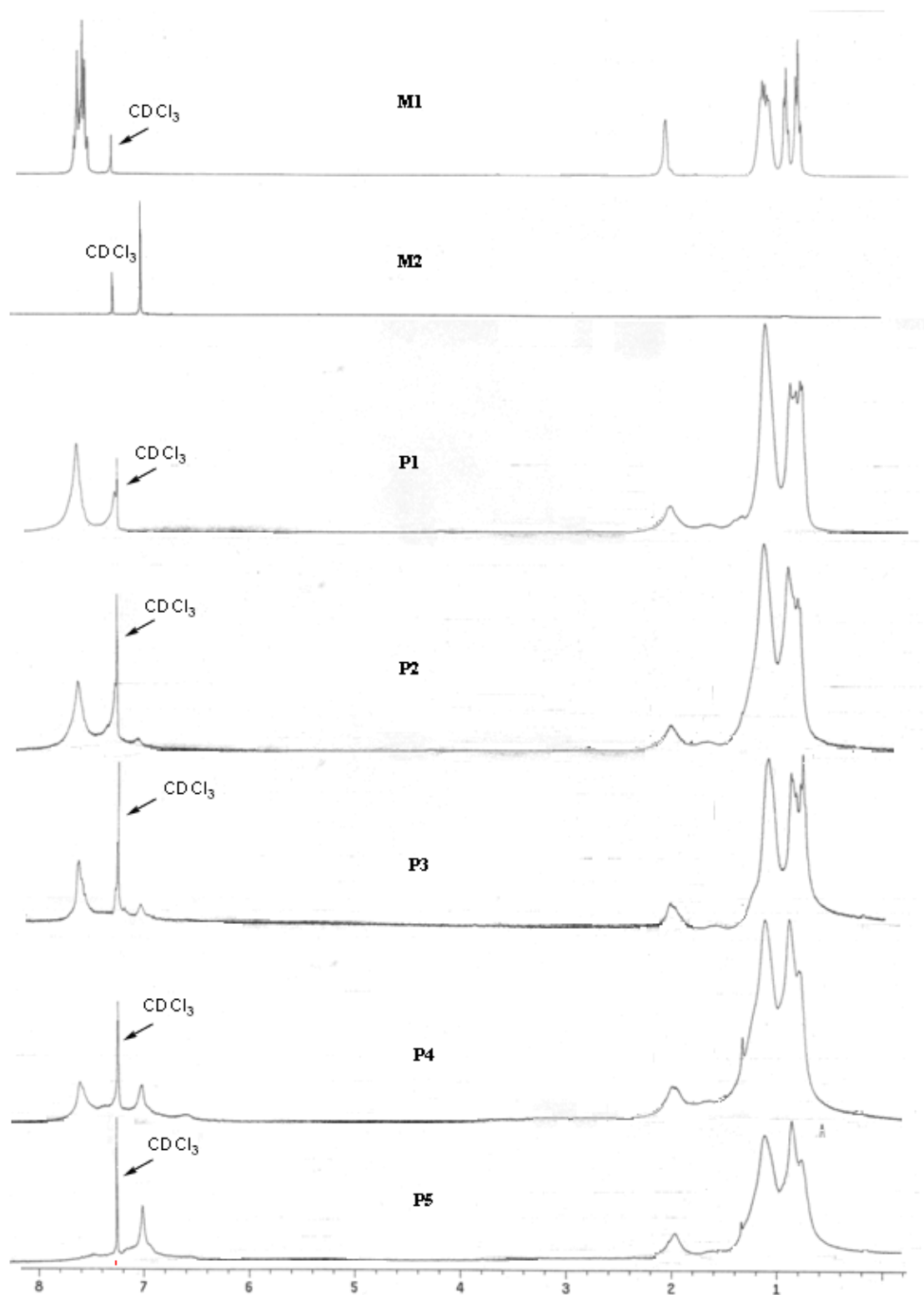
Figure 3.3 ^{1}H NMR spectra of monomers **M1**, **M2** and polymers **P1-P5** in CDCl$_3$.

.   The thermal stabilities and phase transition properties of copolymers **P1-P5**
were characterized by thermogravimetric analyses (TGA) and differential scanning

calorimetry (DSC) measurements under nitrogen atmosphere, and the thermal decomposition temperatures (T_d) and melting points (T_m) are summarized in Table 3.1. It is apparent that all copolymers exhibited good thermal stabilities, which showed less than 5% weight loss upon heating to 311-388 °C. Regarding DSC experiments, there were no distinct glass transition temperatures (T_g) for all copolymers. Except for **P1**, these copolymers showed relatively sharp transitions appearing around 192-229 °C, which were attributed to the melting of the polymer backbones. The absence of sharp transition in **P1** was probably originated from four 2-ethylhexyl irregular side chains belonging to monomers **8** and **M1**.

3.3.2 Optical Properties

The optical absorption spectra of D-A copolymers **P1**-**P5** in chloroform solutions (10^{-6} M) and solid films are shown in Figure 3.4, and their photophysical properties are demonstrated in Table 3.2. As can be seen, the absorption energy band gaps of CPDT-based copolymers **P1**-**P5** could be finely tuned by the molar ratios of electron-accepting units **M1** and **M2** (**M1**:**M2** = m:0, 2:1, 1:1, 1:2, and 0:n), and their absorption spectra covered broad wavelength ranges for both solutions and solid films. The longer maximum absorption wavelengths of **P1** (584 nm) and **P5** (705 nm) in chloroform solutions of Figure 3.4 (a) were about 88 nm and 192 nm red-shifted from the corresponding absorption wavelength of monomers **M1** (496 nm) and **M2** (513 nm), respectively, reflecting much longer effective conjugation lengths of the extended coplanar CPDT-based polymer backbones. However, it is noted that **P1** exhibited one maximum absorption wavelength λ_{max} at 584 nm, which was significantly longer (and had a longer conjugation length) than that of the related homopolymer poly(4,4-dialkyl-4H-cyclopenta[2,1-b:3,4-b']dithiophen) (**PCPDT** with λ_{max} = 565 nm and alkyl = 2-ethylhexyl).[107] Similar trends of UV-vis spectra were

observed in rigid conjugated polymers with strong intramolecular charge transfer (ICT) interactions between electron donor and acceptor moieties.[108] Surprisingly, the UV-vis spectrum of **P5** displayed two well-separated peaks at 484 nm and 705 nm, which were originated from two individual UV-vis absorption peaks of **3** and **M2** at 312 nm[58] and 513 nm, respectively, before copolymerization. The shorter wavelength absorption in the region of 350-550 nm (ca. 484 nm) resulted from the incorporated donor unit (**3**) in copolymer **P5**, which was hypsochromically shifted compared with the corresponding band of homopolymer **PCPDT** (λ_{max} = 565 nm). Besides, the longer wavelength absorption shoulder between 600 and 800 nm (ca. 705 nm) with tailing around 900 nm could be attributed to the acceptor unit (**M2**) incorporated with the main chain of copolymer **P5**, which agreed well with those observed in the CPDT polymer derivatives containing the acceptor unit (**M2**).[104] The main attribution of this effect can be explained by that the introduction of electron-deficient carbonyl moieties into the CPDT-based main-chain could also reduce the effective conjugation length of the polymer backbone, and thus to induce a hypsochromic shift of the absorption spectrum. This phenomena is also suggestive by the *meta* conjugation effect observed from aminostilbenes[109] and similar results with fluorene-CPDT-based copolymers[110]. In other words, the electronic interaction between the carbonyl groups and the π-conjugated polymer backbones corresponds to the condition of *meta*-phenylene-bridged moieties.[110] Therefore, copolymer **P5** exhibits a more blue-shifted absorption maximum (ca. 484 nm) than that of homopolymer **PCPDT** (ca. 565 nm) due to the *meta* conjugation effect to prevent the π-electron delocalization by carbonyl groups. Interestingly, reducing **M1** contents and increasing **M2** contents sequentially in copolymers **P2**, **P3**, and **P4**, gradual hypsochromic shifts of the short wavelength absorption (ca. 560 nm) accompanying with slight increases of the longer

shoulder absorption (ca. 700 nm) were observed in these copolymers. Hence, the introduction of electron-deficient carbonyl group in copolymer **P5** may reduce the effective conjugation length along the CPDT-based main chain due to the out of plane arrangements by the carbonyl groups of **M2**.

Figure 3.4(b) represents the UV-vis absorption spectra of solid films in the CPDT-based copolymers (**P1**-**P5**). The absorption spectra in solid films were generally similar to those in dilute solutions, where one maximum band in **P1** was centered at 620 nm and two characteristic bands in **P2**-**P5** were centered at 520-611 nm (for the shorter wavelength absorption) and 746-750 nm (for the longer wavelength shoulder absorption), respectively. Due to the interchain association and π-π stacking of these copolymers in solids, the maxima of the π-π* transitions generally had longer absorption maxima (36-46 nm of red shifts) in solid films than those in corresponding solutions. All copolymers (**P2**-**P5**) containing acceptor unit **M2** had broad absorption bands that extended to the near-infrared region with a maximum absorption shoulder λ_{max} at ca. 750 nm, especially in **P5**. The long tailing around 900 nm in the absorption spectra of **P2**-**P5** could be observed in both solutions and solid films, which were attributed to their intrinsic properties rather than a reflection of poor film qualities. The optical band gaps ($E_{g,opt}$) of the copolymers in solid films, which were determined by the cutoff absorption wavelengths of the absorption spectra, are in the range of 1.38-1.70 eV (as shown in Table 3.2). As expected, the optical band gaps of all copolymers were not only much smaller than those of homopolymer **PCPDT**[107] and copolymers of poly(3-alkylthiophene)s,[69] but also comparable to those of similar low band-gap copolymers, i.e., poly(CPDT).[66,108] Therefore, the idea of ICT interactions between electron donor and acceptor units in donor-acceptor (D-A) copolymers is further supported by an efficient method to

narrow down the band gaps of the conjugated polymers,[56,99] which suggests that these copolymers can be useful materials for future photovoltaic applications.

The photoluminescence (PL) spectra of copolymers **P1-P5** in chloroform solutions and solid films excited at incident wavelengths of 500 nm and 550 nm, respectively, are shown in Figure 3.5. The PL emission spectra of the CPDT-based copolymers in solutions were dramatically quenched, which were enhanced by increasing the contents of **M2** moieties in the D-A copolymers (**P1-P5**) as shown in Figure 3.5(a). Interestingly, the PL spectra of copolymers **P2-P5** containing **M2** moieties in Figure 3.5(b) were completely quenched in solid films. The PL quenching phenomena of these polymers might stem from the intersystem crossing from the photo-excited singlet state to the triplet one was induced by the carbonyl group, where intramolecular (in solution) and intermolecular (in film) energy transfer along the conjugated main chain occurs. Additionally, the red shift of PL spectra of **P1** from solution to film state might be due to the film morphology of highly crystallinity in **P1** as supported by XRD analysis, which will be described in the XRD section later. The corresponding optical properties of these copolymers in solid films, including the broad and strong optical absorptions, propose their potential applications in photovoltaic cells described below.

Table 3.2 Photophysical Data in Chloroform Solutions and Solid Films and Optical Band Gaps of Polymers P1-P5

Polymer	λ_{max}, UV (nm)		λ_{max}, PL (nm)		$\Delta\lambda$ (nm)[d]	$E_{g,opt}$ (eV)[e]
	Solution	Solid film[b]	Solution	Solid film		
P1	584	495, 620	653	724	36	1.70
P2	574	611	654	-[c]	37	1.59
P3	563 (704)[a]	609	654	-[c]	46	1.55
P4	544 (703)	582 (746)	-[c]	-[c]	38	1.73 (1.46)
P5	484 (705)	520 (750)	-[c]	-[c]	36	1.95 (1.38)

[a] Obtained from the wavelengths of shoulders (values in parentheses). [b] Spin-coated from chlorobenzene solution. [c] PL peaks were not detectable due to the PL quenching behavior. [d] $\Delta\lambda_{absorption} = \lambda_{max,film} - \lambda_{max,solution}$ (nm). [e] Estimated from the onset wavelength of UV-vis spectra of the thin solid film.

(a)
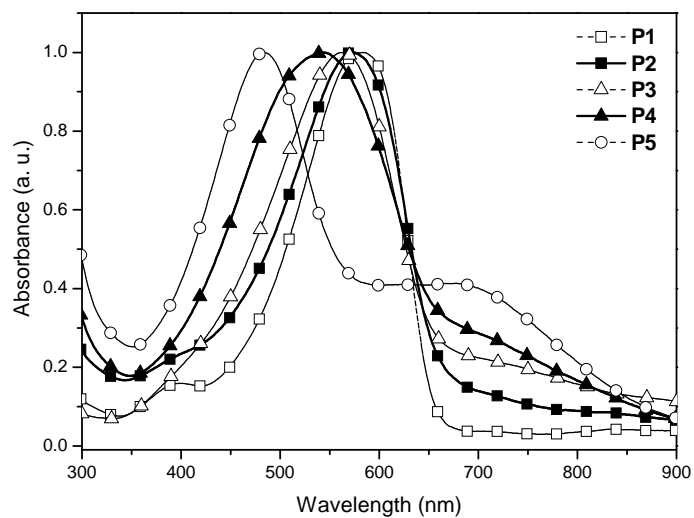
(b)
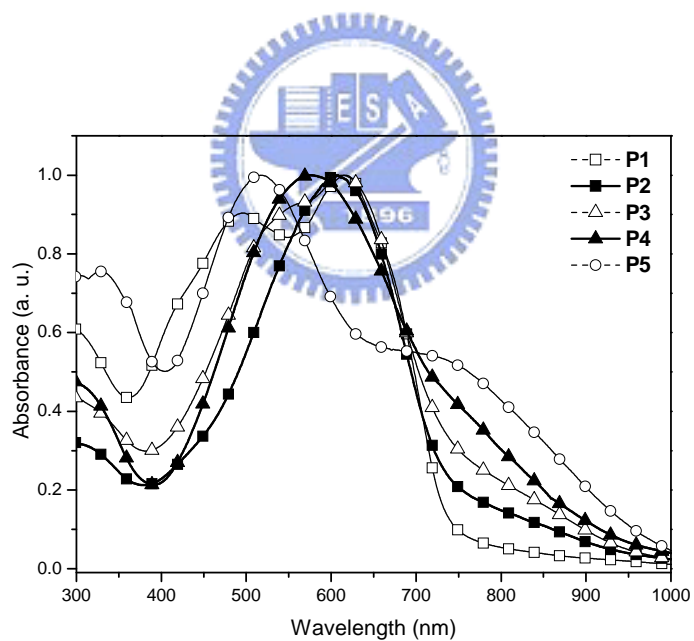
Figure 3.4 Normalized optical absorption spectra of D-A copolymers **P1**-**P5** in (a) solutions (in chloroform), and (b) solid films (spin-coating from chlorobenzene solutions).

(a)
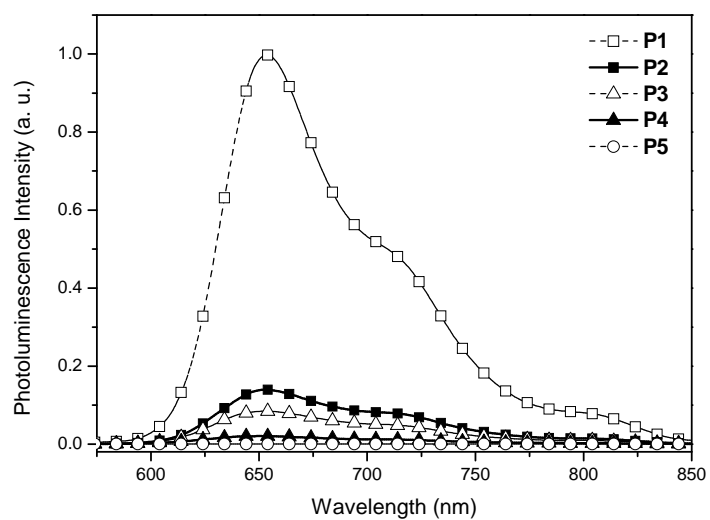
(b)
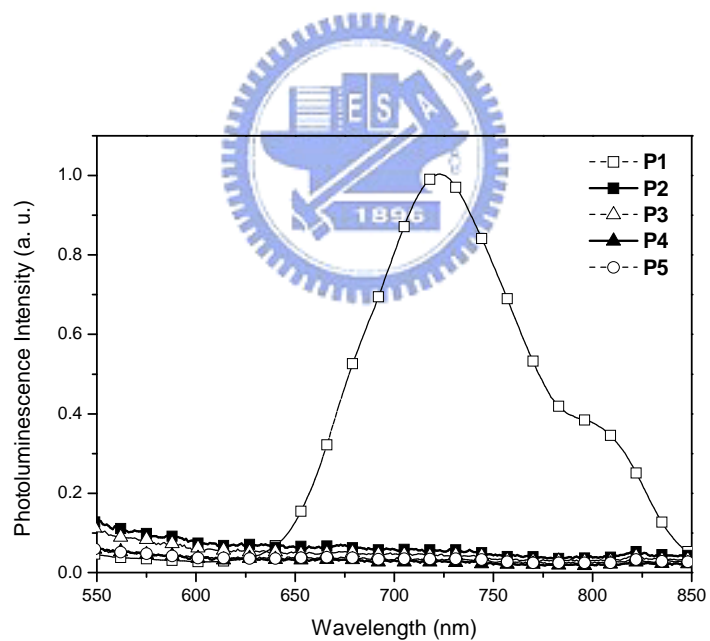
Figure 3.5 Normalized photoluminescence (PL) spectra of D-A copolymers **P1-P5** in (a) solutions (in chloroform), and (b) solid films (spin-coating from chlorobenzene solutions).

3.3.3 Electrochemical Characterization

The electronic states, i.e. highest occupied molecular orbital (HOMO) and lowest unoccupied molecular orbital (LUMO) levels, of the copolymers were investigated by cyclic voltammetry (CV) in order to understand the charge injection processes in these new narrow-band-gap polymers and their PSC devices. The oxidation and reduction cyclic voltammograms of homopolymer **PCPDT** and copolymers **P1-P5** in solid films are displayed in Figure 3.6. In order to obtain solid films of an equal thickness, the concentration in the THF solutions and film forming conditions were kept constant (ca. 5 mg/mL). The electrochemical measurements of the formal potentials, onset potentials, and band gaps, along with the estimated positions of the upper edges of the valence band (HOMO) and the lower edges of the conduction band (LUMO) are summarized in Table 3.3. As shown in Figure 3.6(a), the homopolymer **PCPDT** showed one reversible oxidation but no detectable reduction behavior, implying that the electrons are difficult to inject into this polymer. On the contrary, all copolymers **P1-P5** exhibited one reversible oxidation and two reversible or quasi-reversible reduction peaks as evident from the areas and close proximity of the anodic and cathodic scans in Figure 3.6(b), which are a good sign for high structural stability in the charged state. As illustrated in Table 3.3, the formal oxidation potentials of these polymers were in the range of 0.74-1.05 V, and their formal reduction potentials were in the ranges of (-0.94)-(-0.99) V and (-1.16)-(-1.95) V, respectively.

The moderate onset oxidation potentials and onset reduction potentials of copolymers **P1-P5** occurred between 0.5-0.85 V and ca. -0.81 V, respectively, fromwhich the estimated HOMO levels of (-4.90)-(-5.25) eV and LUMO levels of ca. -3.59 eV were acquired according to the following equation:[106] $E_{\text{HOMO/LUMO}} = [-(E_{\text{onset (vs Ag/AgCl)}} - E_{\text{onset (Fc/Fc+ vs Ag/AgCl)}}) - 4.8]$ eV, where 4.8 eV is the energy level of

ferrocene below the vacuum level and $E_{onset\ (Fc/Fc+\ vs\ Ag/AgCl)}$ = 0.4 eV. In addition, the onset oxidation potential of homopolymer **PCPDT** was observed at ca. 0.55 V, from which the HOMO level of -4.95 eV was estimated. It is worthwhile to note that the HOMO energy levels of copolymers **P1**-**P5** were significantly varied relative to that of homopolymer **PCPDT** as measured under the same condition. Compared with **PCPDT**, the HOMO energy levels of copolymers **P4** to **P1** were reduced gradually by ca. 0.1-0.3 eV *via* the incorporation of the increasing amounts of electron-withdrawing cyano groups into the polymer backbones. Therefore, based on the oxidation potential data, the higher contents of electron-withdrawing cyano groups in copolymers **P1**-**P5** can induce the decreases of HOMO levels[57] and show good air stabilities, especially for **P1**.[111] However, the HOMO energy level of copolymer **P5** was slightly higher than that of **PCPDT** (with a difference of ca. 0.05 eV). It is probably that the electron-withdrawing effect of the ketone groups and the contribution of the primary resonance form might decrease the aromaticity of the system and hence to increase the quinoid character of the polymer backbones.[76,104] In contrast, the electrochemical reductions of copolymers **P1**-**P5** showed similar LUMO energy levels at ca. (-3.59)-(-3.60) eV, which represent to possess high electron affinities and also make these copolymers suitable donors for electron injection and transporting to PCBM acceptors (with 0.70-0.71 eV offsets in LUMO levels regarding PCBM with a LUMO level of -4.3 eV[106]) for the polymeric bulk heterojunction solar cell devices.[112] Interestingly, the energy band gaps $E_{g,ec}$ ($E_{g,ec}$ = $E_{ox/onset}$ - $E_{red/onse}$, where $E_{g,ec}$ values are between 1.30 and 1.66 eV) measured directly from CV are close to the optical band gaps ($E_{g,opt}$ between 1.38 and 1.70 eV) acquired from the absorption spectra.

Table 3.3 Electrochemical Potentials, Energy Levels and Band Gap Energies of Polymers P1-P5[a]

Polymer	Oxidation potential V vs Ag/Ag$^+$		Reduction potential V vs Ag/Ag$^+$		Energy level[d] eV		Band gap eV
	$E_{ox/onset}$[b]	$E_{ox/o}$[c]	$E_{red/onset}$[b]	$E_{red/o}$[c]	E_{HOMO}	E_{LUMO}	$E_{g,ec}$[e]
PCPDT	0.55	0.74	N. A.[e]	N. A.[e]	-4.95	N. A.[e]	N. A.[f]
P1	0.85	1.05	-0.81	-0.95 -1.95	-5.25	-3.59	1.66
P2	0.74	1.04	-0.81	-0.97 -1.28	-5.14	-3.59	1.55
P3	0.70	1.02	-0.81	-0.95 -1.24	-5.10	-3.59	1.51
P4	0.65	0.84	-0.81	-0.94 -1.24	-5.05	-3.59	1.46
P5	0.50	0.83	-0.80	-0.99 -1.16	-4.90	-3.60	1.30

[a] Reduction and oxidation potentials measured by cyclic voltammetry in solid films.
[b] Onset oxidation and reduction potentials. [c] Formal oxidation and reduction potentials.
[d] Estimated from the onset potentials using empirical equations: E_{HOMO}/E_{LUMO} = $[-(E_{onset\ (vs\ Ag/AgCl)} - E_{onset\ (Fc/Fc+\ vs\ Ag/AgCl)})-4.8]$ eV where 4.8 eV is the energy level of ferrocene below the vacuum level and $E_{onset\ (Fc/Fc+\ vs\ Ag/AgCl)}$ = 0.4 eV. [e] $E_{g,ec} = E_{ox/onset} - E_{red/onse}$. [f] No properties of cathodic reduction potentials were available.
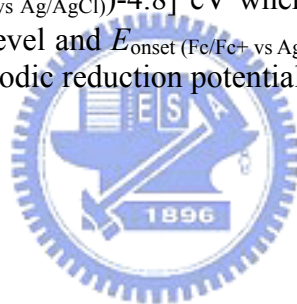
(a)
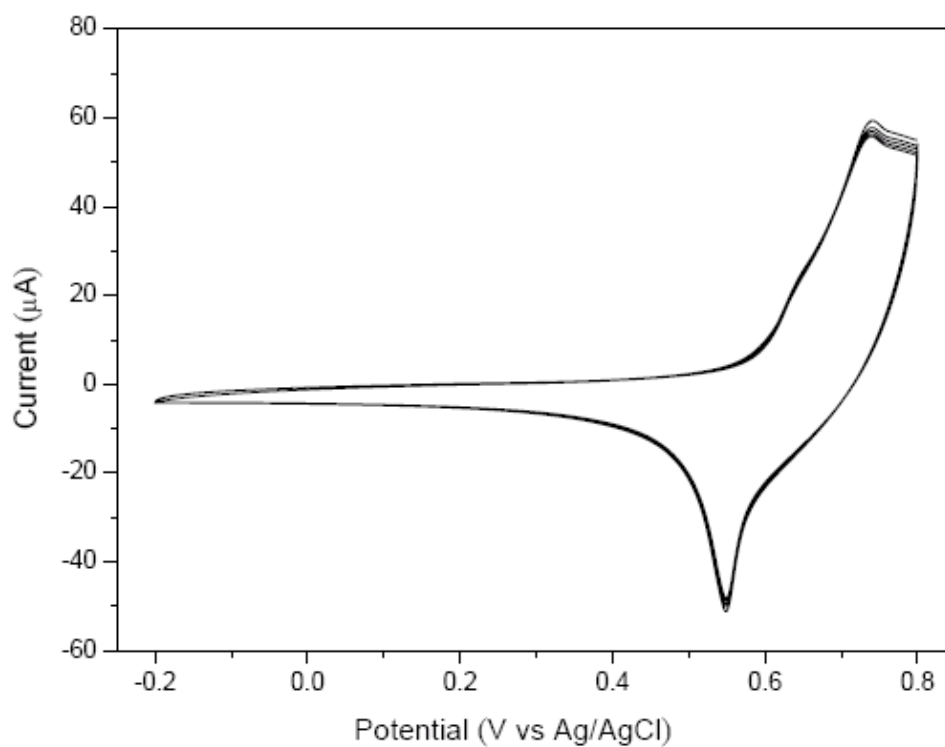
(b)
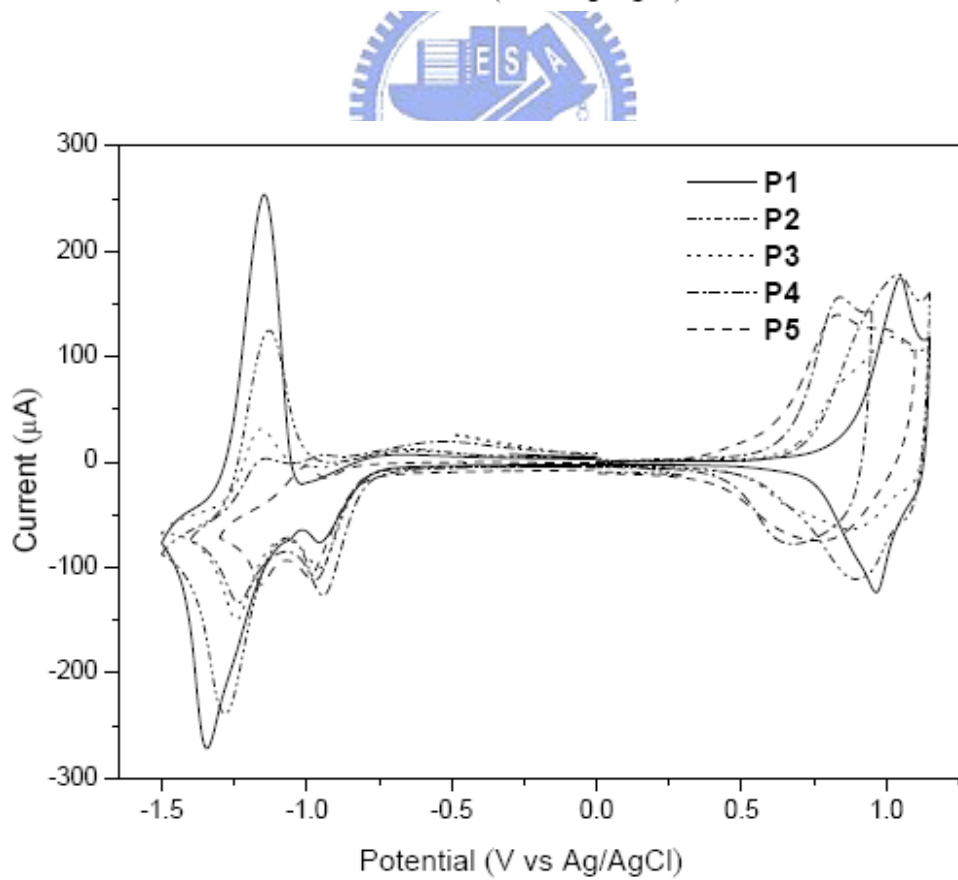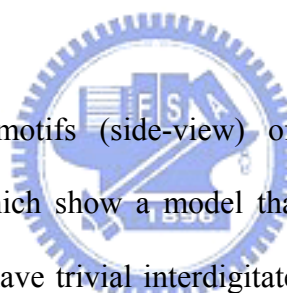
Figure 3.6 Cyclic voltammograms of (a) homopolymer **PCPDT** and (b) copolymers **P1**-**P5** (thin solid films) at a scan rate of 100 mV/s.

3.3.4 X-ray Diffraction (XRD) Analyses

In order to investigate the microstructural orders and molecular arrangements of thermal annealed CPDT-based copolymers in solids, X-ray diffraction (XRD) measurements were performed on powder samples before and after the thermal treatment at 150 °C. As shown in Figure 3.7, the annealed copolymers **P1** and **P5** both exhibited well crystalline patterns, which indicate highly order arrangements in solids. Distinct primary diffraction peaks, including one peak at $2\theta = 5.1°$ associated with a d-spacing value of 15.0 Å, were observed in copolymer **P1** after thermal annealing. Compared with **P1**, copolymer **P5** exhibited substantially a primary diffraction feature with a wider angle at $2\theta = 5.36°$ (corresponding to a smaller d-spacing value of 14.26 Å), which was assigned to a distance between the conjugated backbones separated bythe long side chains as reported for other similar π-conjugated polymers with long pendants.[113-114] The XRD diffraction patterns at $2\theta = 10.2°$ and 10.7°, related to the d-spacing values of 7.51 and 7.15 Å for copolymers **P1** and **P5**, respectively, were the second-order peaks of the diffractions at 15.0 and 14.26 Å. Furthermore, copolymer **P1** showed a higher crystalline characteristic with a diffraction peak up to the third-order at $2\theta = 15.3°$, correlated to a d-spacing value of 5.0 Å. Since the effective cross section (S) of polymer pendent alkyl chains is equal to 20 Å, the hexagonal-like aggregations of the alkyl chains showed a characteristic side-to-side distance between alkyl chains with $d = 4.2$ Å.[115] The value observed for the diffraction feature at the d-spacing value of 4.22 Å in copolymer **P1** is in agreement with the result as previously reported.[115] However, the hexagonal-like aggregation ca. $d = 4.2$ Å was not observed in **P5**, which means that the alkyl side-chains in copolymer **P5** have less crystalline behavior (only amorphous halo observed ca. $2\theta = 18°$) and the hexagonal-like aggregations of alkyl side-chains did not exist. Compared with

copolymer **P1**, this lower packing order of the alkyl side-chains in **P5** might be due to the lower packing density of alkyl pendants from **M2** moieties in **P5** than that from **M1** moieties in **P1**. For the CPDT-based copolymers **P1** and **P5**, the diffraction features at $2\theta = 20.2°$ and $21.5°$, corresponding to the d-spacing values of 3.80 and 3.52 Å, respectively, are close to the layer-to-layer π-π stacking distances between the coplanar backbones of the reported π-conjugated polymers[103,113-118] and being somewhat larger than the sheet-to-sheet distance of graphite (3.35 Å).[115] The diffraction features of both copolymers **P1** and **P5** were often observed in the XRD patterns of the π-conjugated polymers.[103,113-118] Based on the observation, it can be assumed that copolymers **P1** and **P5** form good π-π stackings consisting of π-conjugated coplanar backbones, but **P1** has a better crystalline form in alkyl side chains than **P5**.

The possible packing motifs (side-view) of copolymers **P1** and **P5** are represented in Figure 3.8, which show a model that the alkyl side chains stack as bilayered packings and may have trivial interdigitated arrangements. It is interesting to note that the primary diffraction interchain distance of copolymer **P1** was somewhat (ca. 0.74 Å) larger than that of **P5** from XRD data. As possible side-view packing motifs in Figure 3.8, the cyanovinylene and phenylene segments in the polymer backbones of copolymer **P1** result in a more kinked molecular configuration with a wider π-π stacking region (5.59 Å in Figure 3.8(a)). Comparatively, owing to the only simple CPDT-based moieties in copolymer **P5**, the comparatively linear backbones of copolymer **P5** stack more compactly with a narrower rigid-core width (4.57 Å in Figure 3.8(b)). Since copolymers **P1** and **P5** have the same length of flexible tails, both copolymers might prefer the bilayered lamellar stacking in the soft regions with thesame thickness of 5.2 Å x $2 = 10.4$ Å. Therefore, the total lamellar

thickness difference of 0.74 Å in the diffraction interchain distance of copolymers **P1** and **P5** from XRD data (15.0 and 14.26 Å for copolymers **P1** and **P5**, respectively) was induced from the variation of their backbones' widths in π-π stacking rigid-core regions, i.e., 5.59 - 4.57 = 1.02 Å, where 5.59 Å and 4.57 Å are the rigid-core regions of copolymers **P1** and **P5**, correspondingly. Moreover, the interchain lamellar *d*-spacing values of **P1** and **P5** (15.0 and 14.26 Å, respectively) from XRD are roughly equal to the total sum of the twice length of 2-ethylhexyl group plus the individual widths of their respective polymer backbones in the Chem3D ultra 8.0 calculations (ca. 15.99 and 14.97 Å, correspondingly) from the side-view of Figure 3.8. This result suggests that the side chains of the copolymers likely stack as bilayered structures in the lamellar sheets, though the precise orientation of the alkyl side chains can not be determined with the present XRD information alone. The *d*-spacing values of 3.80 and 3.52 Å (obtained from XRD patterns at $2\theta = 20.2°$ and 21.5°) for copolymers **P1** and **P5** are correspondent to the (top-view) layer-to-layer π-π stacking distances between the top layer and bottom layer of the coplanar backbones in Figure 3.8(a) and 3.8(b), respectively. According to the XRD results, copolymer **P1** has more and sharper XRD peaks to possess a better crystallinity than **P5**, especially for wide angles of (top-view) alkyl side-chain arrangements, where the hexagonal-like aggregation (ca. $d = 4.2$ Å) was only observed in **P1**. Overall, the proposed model can explain the possible structural arrangements of the copolymer chains in copolymers **P1** and **P5**.
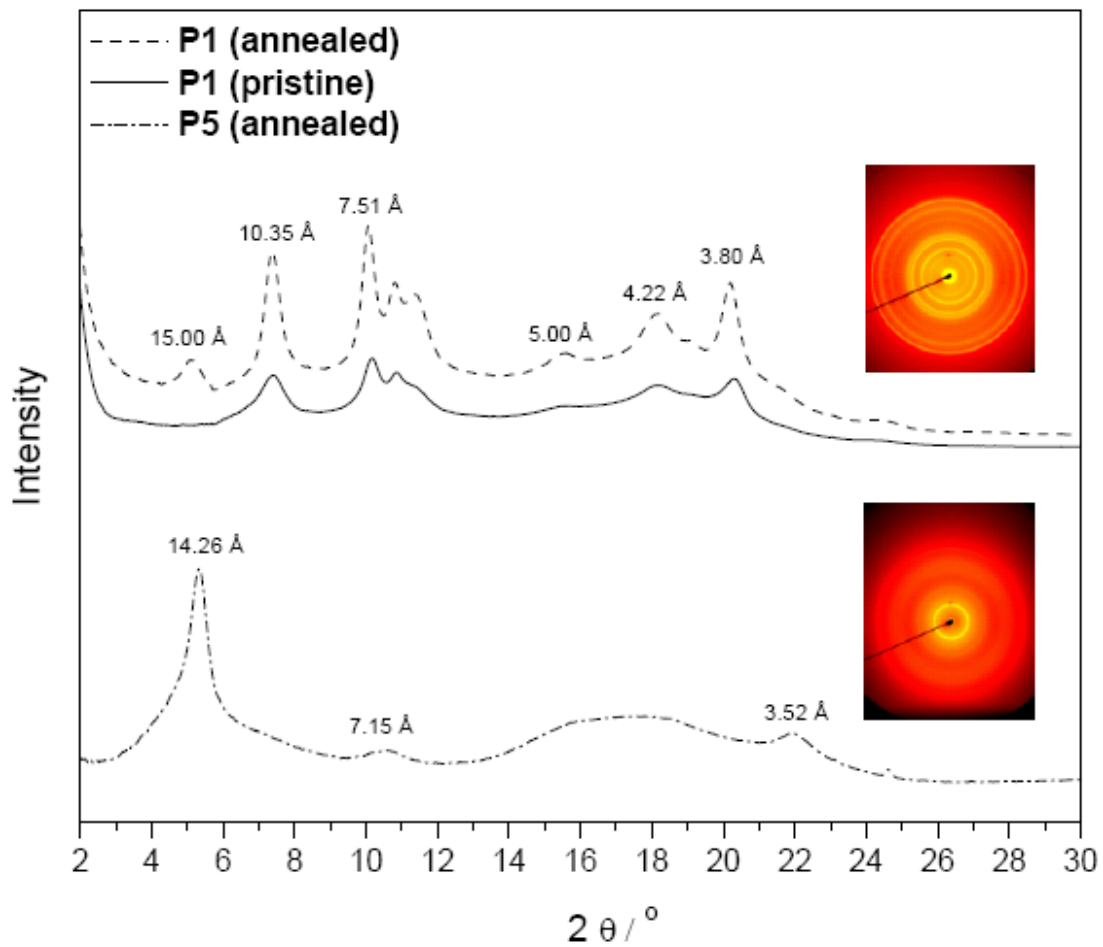
Figure 3.7 Powder X-ray diffraction patterns of copolymers **P1** (pristine and annealed samples) and **P5** (annealed sample). The sharp diffraction peaks indicated that the polymers formed an order structure in the solid state.

(a)
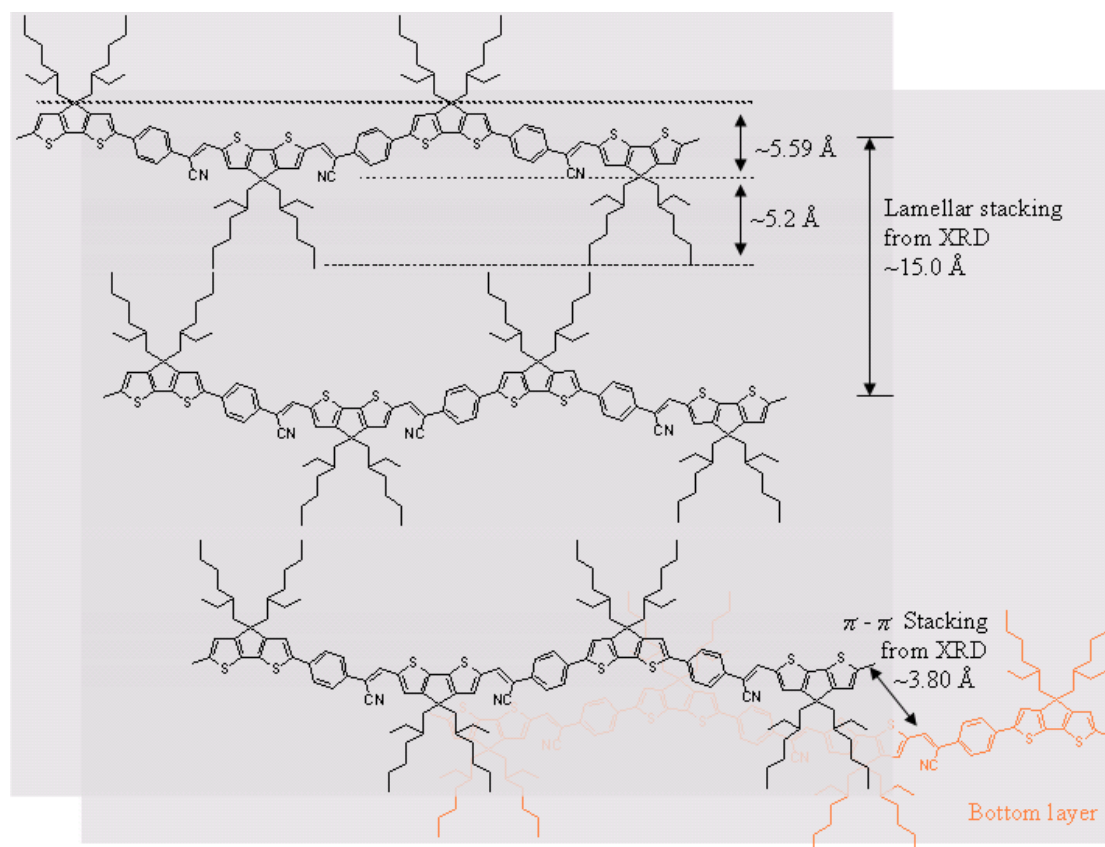
(b)
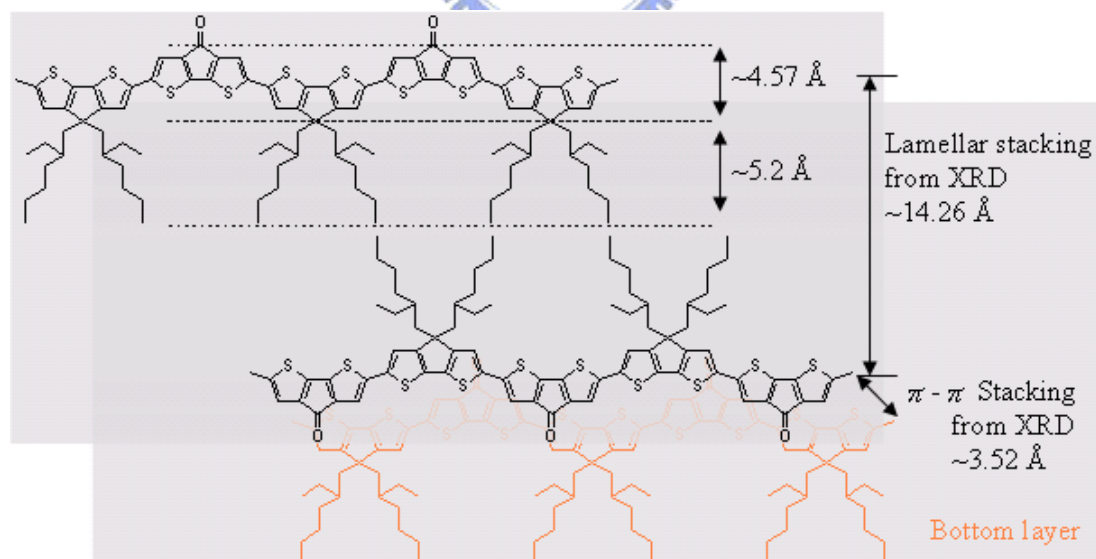
Figure 3.8 Schematic representation of a proposed layered and π-π stacked copolymer structure in the Chem3D ultra 8.0 calculations of (a) **P1** and (b) **P5** in solid state.

3.3.5 Polymeric Photovoltaic Cell Properties

The motivation for the design and syntheses of the conjugated CPDT-based copolymers is to look for new narrow band-gap polymers for the application of PSCs. To investigate the potential use of copolymers **P1**-**P5** in PSCs, bulk heterojunction devices were fabricated from an active layer in which copolymers **P1**-**P5** were blended with the complementary fullerene-based electron acceptor, PCBM, in a weight ratio of 1:4 (w/w). PSC devices with a configuration of ITO/PEDOT:PSS/**P1**-**P5**:PCBM(1:4 w/w)/LiF/Al were fabricated by depositing a thin layer (ca. 50 nm) of PEDOT:PSS onto patterned ITO slides. The active layer (ca. 100-160 nm) consisting of **P1**-**P5** and PCBM (1:4 w/w) was then deposited from a solution (10 mg/mL in chlorobenzene) by a spin rate of 800 rpm on the PEDOT:PSS film, and followed by the deposition of a LiF (ca. 1 nm) and aluminum (120 nm) back electrode. The PSC devices were measured under AM 1.5 illumination for a calibrated solar simulator with an intensity of 100 mW/cm^2. The preliminarily obtained properties are summarized in Tables 3.4 and 3.5, and the typical *I-V* characteristics and external quantum efficiency (EQE) wavelength dependencies of all PSC devices are shown in Figure 3.9. Under the white-light illumination, the current density (I_{sc}), open circuit voltage (V_{oc}), and fill factor (FF) of the PSC devices composed of copolymers **P1**-**P5** were in the range of 0.09-2.36 mA/cm^2, 0.36-0.84 V, and 17-38%, respectively, with the power conversion efficiency (PCE) values between 0.01% and 0.77%.

The photovoltaic properties of the PSC devices containing CPDT-based copolymers **P1**-**P5** were dependent on the solubility and film-forming quality of the copolymers. Among these PSC devices containing **P1**-**P5**, copolymer **P1** gave the best performance in Figure 3.9(b) with I_{sc} = 2.36 mA/cm^2, V_{oc} = 0.84 V, FF = 38%, and

PCE = 0.77%, respectively. Interestingly, the I_{sc} value of the PSC device containing **P1** was strongly enhanced relative to those containing **P2-P5** (by a factor of ca. 26 times higher than that of the worst **P3**), which might be due to the promoted solubility and the better film-forming capability by adding a higher molar ratio of **M1** units with alkyl side chains to **P1**. Ideally, the I_{sc} values were determined by the product of the photoinduced charge carrier densities and the charge carrier mobilities within the organic semiconductors.[22] Thus, it can be recognized that the better results of I_{sc} and FF in the PSC device containing **P1** were obtained likely due to the well-balanced charge flow and less significant recombination loss[52,119] originated from the highly order structural packing of alkyl side chains, as previously proved by the XRD patterns in the wide angle region of **P1**. However, the relatively low I_{sc} and FF values in the PSC device containing **P3** is poorly understood at this time, but it might be related to geminate charge recombination at the interface due to stable charge-transfer states, which limited the values of the photocurrents.[120] Therefore, to further explore the dependence of charge transfer properties on the PSC devices, we have performed current measurements on hole-only and electron-only devices. The electron and hole mobilities can be determined precisely by fitting the plot of the current versus the voltage *(I–V)* curves for single carrier devices to the SCLC model.[121-122] These devices in this study containing copolymers **P1-P5**: PCBM (1:4) blend film sandwiched between transparent ITO anode and cathode. The current is given by $J = 9\varepsilon_0\varepsilon_r\mu V^2/8L^3$, where $\varepsilon_0\varepsilon_r$ is the permittivity of the polymer, μ is the carrier mobility, L is the device thickness. The best result of hole mobility was found to be 9.74×10^{-6} cm^{2}V^{-1}s^{-1} for copolymer **P1**, and the others copolymers **P2-P5** were found to be below 1.41×10^{-6} cm^{2}V^{-1}s^{-1}. Reasonably, copolymer **P1** gave the best performance efficiency and highest photocurrent property in the PSC devices.

Additionally, the electron mobilities of copolymers **P1**-**P5** were found to be a range near ca. 4.78×10^{-5} $cm^2V^{-1}s^{-1}$. In comparison with the hole- and electron-mobilities of these copolymers in the blend system (polymers:PCBM = 1:4), the electron-mobilities showed relatively fast charge transporting rates than that hole-mobilities due to larger PCBM amounts blended in the system. Therefore, it revels that the electron is the dominant charge carrier in the PSC devices, which results in the unbalanced charge transport obtained in this study.

The V_{oc} values were noticeably varied among the PSC devices containing copolymers **P1**-**P5**, which were related to the differences between the HOMO energy levels of the polymers and the LUMO energy levels of the acceptors.[22,25-26] Therefore, the HOMO energy levels of the donor polymers in PSC devices are very important to be finely tuned for PSC devices with high efficiencies. As discussed previously for the oxidation potentials of all copolymers, copolymer **P1** incorporated with the electron-withdrawing cyano groups has the lowest HOMO level among copolymers **P1**-**P5**. Thus, the highest V_{oc} value (0.84 V) is satisfactorily reached in **P1**, which has the highest V_{oc} value for any reported CPDT-based materials so far. Surprisingly, followed by the decrease of the HOMO levels, the V_{oc} values did not comply with the previous general regulation in the results of PSC devices for **P2**-**P5**. However, the photovoltaic parameters could be also influenced to some extent by the thickness of the active layer.[123] Especially for **P3**, although the copolymer had a medium HOMO level, its PSC device had the worst V_{oc} value owing to a worse film with a thinner thickness of ca. 100 nm induced by the poor solubility of copolymer **P3**.

To investigate the explanation for different efficiencies of the PSC devices, the external quantum efficiency (EQE) spectra of the PSC devices containing copolymers **P1**, **P2**, and **P5** blended with PCBM (1:4 w/w) as the photovoltaic layer are compared

in Figure 3.10(b). The broad EQE curves of **P1**, **P2**, and **P5** covered almost the entire visible spectrum from 350 to 700 nm with maximum EQE values of 23%, 5%, and 8% for **P1**, **P2**, and **P5**, respectively. In a detailed comparison, the PSC devices containing **P1** and **P2** exhibited photovoltaic responses at both 380 and 600 nm, but with a shoulder at 470 nm only for **P1**. However, the PSC device containing **P5** merely showed the maximum EQE values at 360 and 440 nm, but the longer wavelength shoulder absorption of 700-750 nm (as shown in Figure 3.4) was not observed in the EQE spectra. The result shows that the unit of monomer **M2** incorporated into the polymer backbone can not participate in the generation of photocurrents and thus to result in a feature of absorption limitation, which can be explained by the I_{sc} value of **P5** was relatively lower than that of **P1**. Comparing the PSC devices containing **P2** and **P5**, the measured current and EQE properties in the region of **P1** absorption comprised a wider wavelength range and a higher efficiency (with a maximal 4.6 times larger), which propose that **P1** somehow contributed significantly to the overall current generated by the (**P1**:PCBM)-based PSC device under illumination presumably owing to a more efficient intermolecular charge transfer.

Finally, the effect of varying the thickness of the active layer on the photovoltaic performance of **P1**-based PSC devices is explored as shown in Figure 3.10 and Table 3.5. The thicknesses of the active layers were varied in the range of 120 to 310 nm by changing the spin concentrations (5, 10, and 20 mg/mL) of **P1** in chlorobenzene under the same spin rate. Quite surprisingly, decreasing the active layer thickness to 120 nm or increasing to 310 nm did not result in higher PCE efficiencies, because there were simultaneous decreases in both FF and I_{sc} values as revealed in Figure 3.10(a). In contrast to the medium 160 nm thickness in the PSC device, both thicker (310 nm)

and thinner (120 nm) devices showed slightly lower V_{oc} values but significantly reduced FF and I_{sc} values, where the thicker active layer had a combined influence on the hindered charge carrier transport or recombination[124-125] and the thinner active layer reduces the absorption of the irradiated light. As shown in Figure 3.10 (b), a similar tendency was also conceived in EQE spectra, where the PSC device with the medium thickness of 160 nm possessed a maximal external quantum efficiency (EQE) of 23% at the irradiation wavelength of 350-400 nm. The higher EQE values covering the broad absorption wavelength region further explain the improved PSC performance of the medium thickness device (160 nm) over the other two devices with thicker and thinner thicknesses (310 nm and 120 nm). Additional improvements are underway to optimize the PSC devices by the modification of the film morphology, the process of thermal annealing treatments, and the replacement of some other electron acceptors, which can augment the formation of phase-separated structures and the charge mobilities.

Table 3.4 Photovoltaic Properties of PSC Devices Containing an Active Layer of P1-P5:PCBM = 1:4 (w/w) with a Device Configuration of ITO/PEDOT:PSS/Polymer:PCBM/LiF/Al[a]

Active layer[b] Polymer:PCBM	Thickness (nm)[b]	V_{oc} (V)	I_{sc} (mA/cm^2)	FF (%)	PCE (%)
P1	160	0.84	2.36	38	0.77
P2	140	0.48	0.77	23	0.08
P3	100	0.36	0.09	17	0.01
P4	140	0.49	0.67	25	0.08
P5	140	0.51	0.81	26	0.11

[a] Measured under AM 1.5 irradiation, 100 mW/cm^2. [b] **P1-P5**:PCBM = with the fixed weight ratio of 1:4 (w/w).

(a)
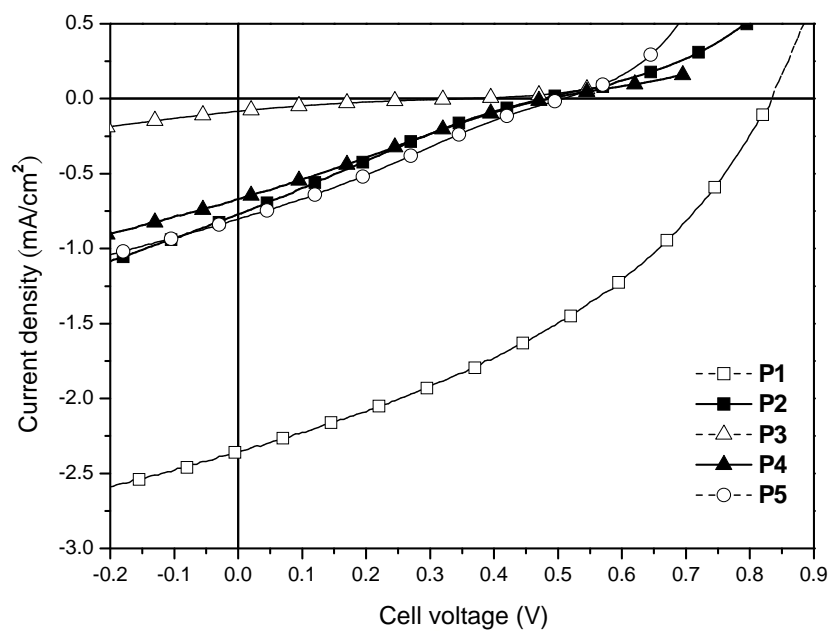
(b)
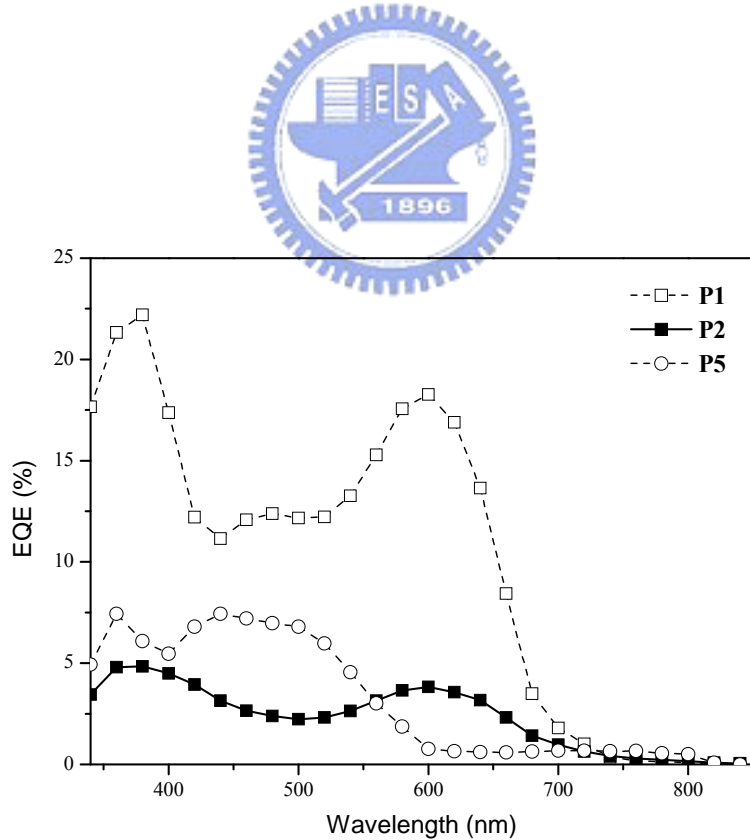
Figure 3.9 (a) *I*-V curves of solar cells with active layers **P1-P5**:PCBM (1:4 w/w) under simulated AM 1.5 solar irradiation. (b) EQE wavelength dependencies of solar cell devices based on active layers **P1**:PCBM, **P2**:PCBM, and **P5**:PCBM (1:4 w/w). Inset: representative device configuration.

(a)
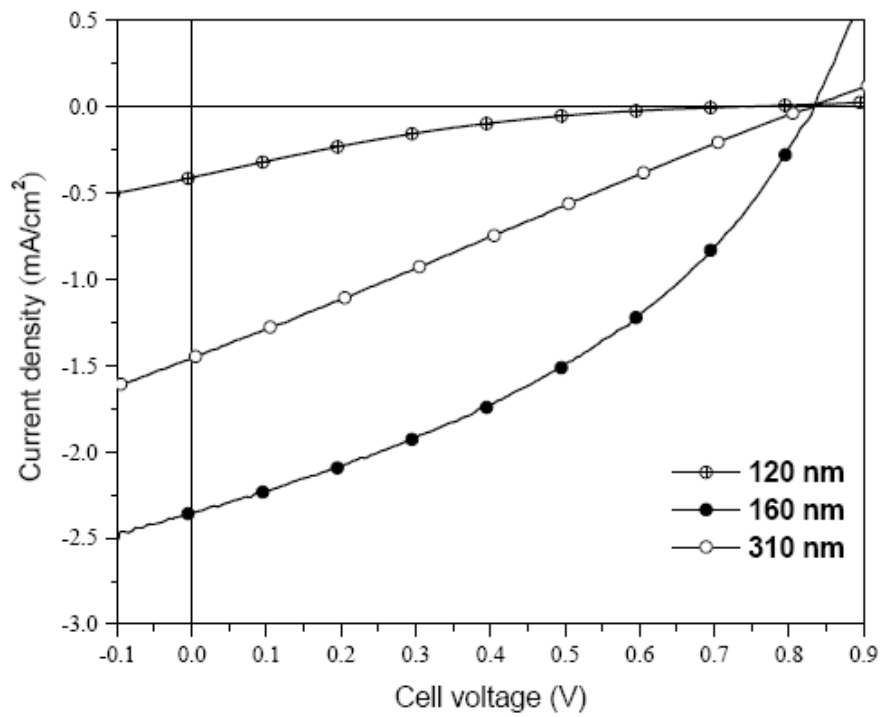
(b)
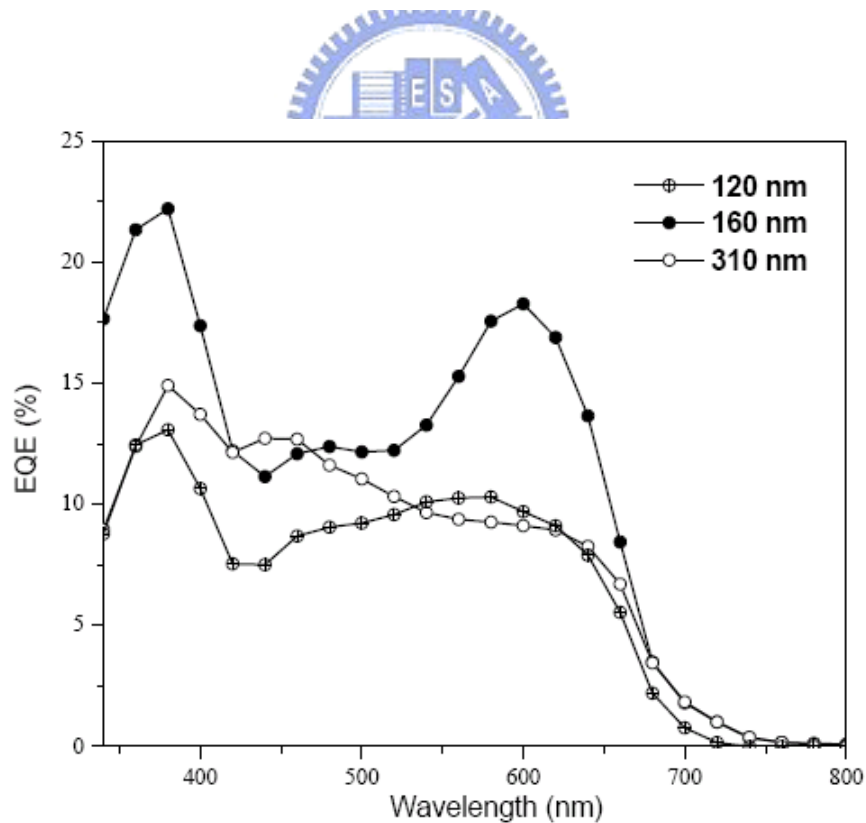
Figure 3.10 (a) *I*-V curves of solar cells under simulated AM 1.5 solar irradiation and (b) EQE spectra for PSC devices containing an active layer of **P1**:PCBM=1:4 (w/w) with three different thicknesses (⊕) 120 nm, (●) 160 nm, and (○) 310 nm.

Table 3.5 Photovoltaic Properties[a] of Bulk-Heterojunction Solar Cells Containing an Active Layer of P1:PCBM = 1:4 (w/w) with Various Thicknesses

Thickness (nm)[b]	Spin Concentrations of active layer (P1) (mg/mL)[c]	V_{oc} (V)	I_{sc} (mA/cm^2)	FF (%)	PCE (%)
120	5/1	0.77	0.42	15	0.05
160	10/1	0.84	2.36	38	0.77
310	20/1	0.83	1.46	25	0.31

[a] Measured under AM 1.5 irradiation, 100 mW/cm^2. [b] The thickness (± 10 nm) was controlled by the solution concentrations of the active layer P1/PCBM (1:4 by wt.), and the spin rate of the active layer (P1/PCBM) was fixed at ca. 800 rpm. [c] The active layer (P1/PCBM) was prepared from spin-coating of different solution concentrations (in chlorobenzene), but the weight ratio of P1:PCBM was fixed at 1:4.

3.4 Conclusions

Using the concept of incorporating electron-withdrawing groups in the donor-acceptor conjugated polymers, we have successfully synthesized five cyclopentadithiophene-based copolymers employing arylcyanovinyl and keto groups in different molar ratios by palladium (0)-catalyzed Suzuki coupling reactions. The band gaps and the HOMO/LUMO energy levels of these resulting copolymers can be finely tuned as demonstrated by the investigation of optical absorption properties and electrochemical studies. In powder X-ray diffraction (XRD) measurements, these copolymers exhibited obvious diffraction features indicating a highly ordered π-π stacking in the solid state. Preliminary PSC devices based on these five copolymers blended with PCBM acceptors (1:4 w/w) had the power conversion efficiency up to 0.77%, which gave the best performance with the values of I_{sc} = 2.36 mA/cm^2, FF = 38%, and V_{oc} = 0.84 V. Furthermore, this study provides novel conception that the HOMO energy levels can be reduced via the syntheses of merging with electron-withdrawing functional groups and thus the open-circuit voltage can be considerably enhanced, which will significantly improve the low V_{oc} values mainly possessed by most CPDT-based narrow band-gap polymers.

Chapter 4 Tunable Novel Cyclopentadithiophene-Based Copolymers Containing Various Numbers of Bithiazole and Thienyl Units for Organic Photovoltaic Cell Applications

4.1 Introduction

Extensive researches in the field of electro-optical devices have been focused on soluble π-conjugated semiconducting polymers, especially for the developments of organic photovoltaic (OPV) devices, which offer the advantages of lightweight, high-throughput, and environmentally renewable energy for future applications. Since the pioneering achievements of A. J. Heeger and co-workers in 1995,[72] the so-called bulk heterojunction (BHJ) concept has significantly improved the power conversion efficiency (PCE) values of the OPV devices, where interpenetrating electron donor-acceptor (D-A) networks were formed by blending phase-separated π-conjugated polymers (as electron donors) with soluble fullerenes, strong electron-affinity polymers,[20,92-93] or n-type nanocrystals[94-95] (as electron acceptors). For the electron-donating purpose, an increasing interest for novel polymeric materials with high charge carrier mobility and good processability has recently been found in thiophene-based conducting copolymers, such as derivatives of region-regular poly(3-hexylthiophene)s (P3HTs),[51-52] polythiophenes,[126] and fused heterocyclic conjugated polymers,[102,127] etc, resulting in OPV devices with the highest PCE value approaching 5.0%.

Recently, in order to obtain longer conjugation lengths, more planar molecular geometries, and more rigider structures in π-conjugated polymers,[58] novel heteroaromatic fused-ring derivatives, including cyclopentadithiophene (CPDT) units,

have been widely investigated in PSCs. Kraak *et al.* first reported the structural unit of CPDT in 1968,[62] and the later prepared CPDT-based polymers showed relatively high conductivities[63] due to the more extensive π-conjugation lengths as compared with polythiophene and polyfluorene derivatives.[65,107] These enhanced photovoltaic properties of CPDT-based polymers have been found to be a powerful approach to optimizing the PSC performance, and thus to lower HOMO-LUMO band gaps and enable closer intermolecular interactions, resulting from the increases of coplanarities and longer conjugation lengths. Lately, the derivatives of cyclopentadithiophene-based copolymers have been emerged as very promising materials for OPV devices which possess both prominent properties of high carrier mobility[66,102-103] and improved power conversion efficiency (PCE).[66-67,99-101]

Furthermore, a novel class of π-conjugated polymers composed of five-membered heteroaromatic rings with alkyl side chains, i.e., poly(alkylbithiazole)s, have a strong tendency to self-assemble into stacked solid structures, and exhibit interesting thermochromic and electrochemical behavior.[68-70,115,128] These conjugated polymers containing five-membered rings were considered to possess more coplanar structures and form more highly extended π-conjugated systems owing to their less sterically hindered structures compared with those containing six-membered rings. Thiazole unit is one of the strongest electron-accepting azaheterocycles because it contains one electron-withdrawing nitrogen of imine (–C=N) in place of the carbon atom at the 3-position of thiophene. Therefore, π-conjugated polymers incorporating with bithiazole (BT) moieties have been demonstrated to be as new n-type transporting materials. [68-70,114-115,128-129] However, only a limited number of bithiazole-based polymers have been explored, and their applications of in PSC devices were quite rare.[70]

The band-gaps along with the HOMO and LUMO levels of the conjugated polymers are finely tunable by copolymerization of different monomer units.[57,70b,74,127a] Another important observation was found that the electron-withdrawing cyano groups could decrease the HOMO level and thus to stabilize the neutral state of the conjugated system.[57,74] These results suggest that it is necessary to investigate the effects of copolymerized functional units on the optical, electrochemical, and PSC properties of the π-conjugated polymers.

Based on this electron donor-acceptor (D-A) concept, six different bithiazole-based monomers, i.e., oligo(bithiazole)s **M1**-**M3** (as shown in Figure 4.1), bithiazole-oligo(thiophene)s **M4**-**M5** (as shown in Figure 4.2), and diarylene-cyanovinylene-bithiazole **M6** (as shown in Figure 4.2), were utilized as electron acceptor moieties to synthesize CPDT-BT-based copolymers **P1**-**P6** (as shown in Figure 4.3). Therefore, our donor-acceptor approaches utilized in the solid films of the CPDT-BT-based copolymers (**P1**-**P6**) achieve the absorption spectra in the visible range of 300-800 nm (with tailing up to around 900 nm) possessing narrow electrochemical band gaps of 1.51-1.83 eV. In addition, the molecular configurations of the π-conjugated CPDT-BT-based copolymers could clearly ensured that highly organized π-π stackings could be easily generated in these fused-heteroaromatic molecular frameworks by thermal annealing, which were confirmed by the powder X-ray diffraction (XRD) analyses. They also showed good charge-transporting properties with hole mobilities of 3.3-5.6 × 10^{-4} $cm^2V^{-1}s^{-1}$ and fair processabilities for PSC applications. So far, the preliminary PSC performance of these structurally related copolymers showed the best PCE value up to 3.04% while blended with [6,6]-phenyl C_{61} butyric acid methyl ester (PCBM), with a short circuit current density (I_{sc}) of 8.00 mA/cm^2, an open circuit voltage (V_{oc}) of 0.70 V, and a fill factor

(FF) of 53.7% under AM 1.5 (100 mW/cm^2).

4.2 Experimental Section

4.2.1 Materials

Compounds 4,4′-dihexyl-2,2′-bithiazole (**1**)[70a] and 4*H*-cyclopenta [2,1-b:3,4-*b*′]dithiophene (**12**)[105] were synthesized according to the known literature procedures. The other procedures and monomers **M1-M6** and copolymers **P1-P6** are shown in Figures 4.1-4.2 and 4.3, respectively, and their synthetic procedures are described as follows:

4.2.2 Synthesis

5,5′-Dibromo-4,4′-dihexyl-2,2′-bithiazole (M1) Compound **1** (4.7 g, 14.2 mmol) was dissolved in a mixture of *N,N*-dimethylformamide (30 mL) and glacial acetic acid (30 mL) under nitrogen in the dark, and then NBS (6.3 g, 35.6 mmol) was added dropwise. After 2 h of stirring in the dark, a white crude solid was precipitated in the reaction mixture. The precipitate was filtered, washed with methanol, and then purified by column chromatography with CH$_2$Cl$_2$/hexane (1:3) to obtain the dibromo product (6.5 g). Yield: 92%. ^{1}H NMR (ppm, CDCl$_3$): δ 2.72 (t, *J* = 7.2 Hz, 4H), 1.68 (m, 4H), 1.31 (m, 12H), 0.87 (t, *J* = 7.2 Hz, 6H). ^{13}C NMR (ppm, CDCl$_3$): δ 159.90, 157.35, 106.80, 31.54, 29.47, 28.80, 28.62, 22.57, 14.06. MS (FAB): *m/z* [M$^+$] 495; calcd *m/z* [M$^+$] 494.0. Anal. Calcd for C$_{18}$H$_{26}$Br$_2$N$_2$S$_2$: C, 43.73; H, 5.30; N, 5.67; S, 12.97. Found: C, 43.66; H, 5.36; N, 5.75; S, 13.14.

5-Bromo-4,4′-dihexyl-2,2′-bithiazole (2) The synthesis of compound **2** was followed by the similar procedure as that of monomer **M1**. Compound **1** (4.7 g, 14.2 mmol) was dissolved in a mixture of *N,N*-dimethylformamide (50 mL) under nitrogen in the dark, and then NBS (2.6 g, 14.2 mmol) was added dropwise. The crude product was purified by column chromatography with CH$_2$Cl$_2$/hexane (2:5) to yield a white

solid (3.95 g). Yield: 67%. ^{1}H NMR (ppm, CDCl$_3$): δ 6.95 (s, 1H), 2.77 (m, 4H), 1.70 (m, 4H), 1.33 (m, 12H), 0.89 (m, 6H).

5-Tributylstannyl-4,4′-dihexyl-2,2′-bithiazole (3) In a 250 mL flask, compound **1** (3.1 g, 9.1 mmol) was placed in dry THF (100 mL), to which *n*-BuLi (2.5 M solution in hexane, 4.0 mL, 10.0 mmol) was added at -78 °C under stirring for 1 h. Thereafter, the mixture was warmed up slowly to room temperature in an ambient environment with stirring for 1 h. After the mixture was cooled down to -78 °C again, an amount of Bu$_3$SnCl (3.7 mL, 13.7 mmol) was added slowly. The mixture was then stirred at ambient temperature for 18 h, followed by the addition of water (100 mL). Finally, the aqueous layer was extracted with dichloromethane (200 mL) while the combined organic layer was dried with anhydrous magenesium sulfate and concentrated under a reduced pressure to give a crude product. The crude product was purified by column chromatography with CH$_2$Cl$_2$/hexane (2:5) to get a pale yellow oil (3.50 g). Yield: 62%. ^{1}H NMR (ppm, CDCl$_3$): δ 6.91 (s, 1H), 2.76 (m, 4H), 1.73 (m, 4H), 1.55 (m, 6H), 1.32 (m, 18H), 1.13 (m, 6H), 0.89 (m, 15H).

5,5′-Di(tributylstannyl)-4,4′-dihexyl-2,2′-bithiazole (4) Compound **1** (6.0 g, 17.8 mmol) was dissolved in dry THF (200 mL), and *n*-BuLi (2.5 M solution in hexane, 21.4 mL, 53.4 mmol) as well as Bu$_3$SnCl (23.2 mL, 71.2 mmol) were added, respectively, following a similar procedure as described for compound **3**. The crude product was purified by column chromatography with CH$_2$Cl$_2$/hexane (1:3) to acquire a pale yellow oil (17.80 g). Yield: 98%. ^{1}H NMR (ppm, CDCl$_3$): δ 2.83 (t, *J* = 7.2 Hz, 4H), 1.74 (m, 4H), 1.54 (m, 12H), 1.32 (m, 24H), 1.14 (m, 12H), 0.88 (m, 24H).

2,2′-Di(4-hexylthiazol-5-yl)-4,4′-dihexyl-5,5′-bithiazole (5) A mixture of compound **2** (1.84 g, 4.43 mmol), compound **3** (3.47 g, 4.43 mmol), tetrakis(triphenylphosphine)palladium(0) (0.50 g), and toluene (50 mL) was heated at

120 °C for over night. After cooling to room temperature, a solvent of methanol (200 mL) was added and an orange solid was precipitated in the mixture. The precipitate was filtered, washed with methanol, and then purified by column chromatography with ethyl acetate (EA)/hexane (1:10) to produce the dibromo product (2.0 g).Yield: 67%. ^{1}H NMR (ppm, CDCl$_3$): δ 7.00 (s, 2H), 2.82 (t, J = 7.2 Hz, 4H), 2.71 (t, J = 7.2 Hz, 4H), 1.74 (m, 8H), 1.34 (m, 24 H), 0.87 (m, 12H).

5,5'-Bis{2,2'-di-[2,2'-bi(4-hexylthiazol-5-yl)]4,4'-dihexyl-5,5'-bithiazole}-4,4'-dihexyl-2,2'-bithiazole (6) The synthesis of compound **6** was followed by the similar procedure as that of compound **5**. A mixture of compound **2** (4.8 g, 11.6 mmol), compound **4** (6.0 g, 6.56 mmol), tetrakis(triphenylphosphine)palladium(0) (0.80 g), and toluene (100 mL) was heated at 120 °C for over night. The crude product was purified by column chromatography with CH$_2$Cl$_2$/hexane (1:4) to produce a red solid (5.1 g). Yield: 77%. ^{1}H NMR (ppm, CDCl$_3$): δ 7.01 (s, 2H), 2.82 (t, J = 7.2 Hz, 4H), 2.73 (t, J = 7.2 Hz, 8H), 1.73 (m, 12H), 1.32 (m, 36H), 0.87 (m, 18H).

M2 Compound **5** (1.7 g, 2.6 mmol) was dissolved in a mixture of *N,N*-dimethylformamide (30 mL) and chloroform (30 mL) in the dark. NBS (1.2 g, 6.3 mmol) was added dropwise and the reacted solution was heated at 70 °C for 3 h under nitrogen. After cooling to room temperature, the reaction was stopped under reduced pressure and a red crude solid was precipitated in the mixture. The precipitate was filtered, washed with methanol, and then purified by column chromatography with CH$_2$Cl$_2$/hexane (2:5) to attain the dibromo product (1.7 g).Yield: 82%. ^{1}H NMR (ppm, CDCl$_3$): δ 2.77 (t, J = 7.2 Hz, 4H), 2.69 (t, J = 7.2 Hz, 4H), 1.69 (m, 8H), 1.29 (m, 24H), 0.87 (m, 12H). ^{13}C NMR (ppm, CDCl$_3$): δ 160.43, 160.14, 158.36, 157.55, 121.84, 107.05, 31.55, 29.79, 29.55, 29.37, 28.99, 28.82, 28.71, 22.57, 22.53, 14.06, 14.03. MS (FAB): m/z [M$^+$] 828.0; calcd m/z [M$^+$] 828.1. Anal. Calcd for

C$_{36}$H$_{52}$Br$_2$N$_4$S$_4$: C, 52.16; H, 6.32; N, 6.76; S, 15.47. Found: C, 51.85; H, 6.15; N, 6.61; S, 14.97.

M3 The synthesis of monomer **M3** was followed by the similar procedure as described for monomer **M2**. Compound **6** (3.0 g, 3.0 mmol) was dissolved in a mixture of *N,N*-dimethylformamide (80 mL) and chloroform (80 mL) in the dark. NBS (1.6 g, 9.0 mmol) was added dropwise and the reacting solution was heated at 70 °C for 3 h under nitrogen. The crude product was purified by column chromatography with CH$_2$Cl$_2$/hexane (2:3) to obtain a red solid (3.1 g). Yield: 90%. ^{1}H NMR (ppm, CDCl$_3$): δ 2.74 (t, *J* = 7.2 Hz, 4H), 2.71 (t, *J* = 7.2 Hz, 8H), 1.71 (m, 12H), 1.30 (m, 36H), 0.86 (m, 18H). ^{13}C NMR (ppm, CDCl$_3$): δ 160.67, 160.45, 160.15, 158.55, 158.39, 157.56, 122.13, 121.89, 107.04, 31.56, 29.82, 29.56, 29.45, 29.39, 29.01, 28.82, 28.72, 22.55, 14.07, 14.03. MS (FAB): *m/z* [M$^+$] 1163.0; calcd *m/z* [M$^+$] 1162.3. Anal. Calcd for C$_{54}$H$_{78}$Br$_2$N$_6$S$_6$: C, 55.75; H, 6.76; N, 7.22; S, 16.54. Found: C, 55.94; H, 6.66; N, 6.99; S, 17.04.

5,5′-Di(thiophene-2-yl)-4,4′-dihexyl-2,2′-bithiazole (8) Monomer **M1** (8.9 g, 18.0 mmol), thiophen-2-yl-2-boronic acid (**7**) (5.8 g, 45.0 mmol), and tetrakis(triphenylphosphine)palladium(0) (1.0 g) were reacted in THF (180 mL) for 10 min, and then 100 mL of 2 M aqueous Na$_2$CO$_3$ solution was added. The reaction mixture was refluxed for 48 h. The cooled solution was washed with dilute hydrochloric acid (10%) and water, and dried over magnesium sulfate. The final solution was purified by column chromatography (silica gel, CH$_2$Cl$_2$/hexane 1:6) to yield a yellow solid (8.3 g). Yield: 92%. ^{1}H NMR (ppm, CDCl$_3$): δ 7.37 (d, *J* = 5.1 Hz, 2H), 7.20 (d, *J* = 3.9 Hz, 2H), 7.10 (m, 2H), 2.94 (t, *J* = 7.2 Hz, 4H), 1.79 (m, 4H), 1.44-1.30 (m, 12H), 0.89 (t, *J* = 7.2 Hz, 6H).

5,5′-Bis(bithienyl)-4,4′-dihexyl-2,2'-bithiazole (9) The synthesis of compound

9 was followed by the similar procedure as that of compound **8**. Monomer **M4** (1.5 g, 2.3 mmol), thiophen-2-yl-2-boronic acid (**7**) (0.8 g, 5.7 mmol), and tetrakis(triphenylphosphine)palladium(0) (0.16 g) were reacted in THF (80 mL) for 10 min, and then 60 mL of 2 M aqueous Na_2CO_3 solution was added. The reaction mixture was refluxed for 48 h, and the final solution was purified by column chromatography (silica gel, CH_2Cl_2/hexane 1:3) to yield a red solid (1.23 g). Yield: 80%. ^{1}H NMR (ppm, $CDCl_3$): δ 7.27-7.16 (m, 4H), 7.15-7.03 (m, 6H), 2.96 (t. $J = 7.2$ Hz, 4H), 1.80 (m, 4H), 1.46-1.26 (m, 12H), 0.89 (t. $J = 7.2$ Hz, 6H).

5,5′-Di(5-bromothiophene-2-yl)-4,4′-dihexyl-2,2′-bithiazole (M4) Compound **8** (3.0 g, 6.0 mmol) was dissolved in chloroform (100 mL) under nitrogen, and then *N*-bromosuccinimide (2.2 g, 12.1 mmol) was added finally. After refluxing the reaction mixture for 4 h, the product was poured into water (200 mL). The solution was extracted with dichloromethane (100 mL × 3), and dried over magnesium sulfate. The solvent was removed under reduced pressure, and the crude product was purified by column chromatography (silica gel, CH_2Cl_2/hexane 1:6) to afford **M4** (3.4 g). Yield: 86%. ^{1}H NMR (ppm, $CDCl_3$): δ 7.04 (d, $J = 3.0$ Hz, 2H), 6.93 (d, $J = 3.0$ Hz, 2H), 2.87 (t, $J = 7.2$ Hz, 4H), 1.75 (m, 4H), 1.42-1.31 (m, 12H), 0.89 (t, $J = 7.2$ Hz, 6H). ^{13}C NMR (ppm, $CDCl_3$): δ 157.95, 155.02, 134.36, 130.53, 127.66, 126.66, 113.26, 31.59, 30.28, 29.42, 29.10, 22.59, 14.07. MS (FAB): *m/z* [M[+]] 659; calcd *m/z* [M[+]] 658.0. Anal. Calcd for $C_{26}H_{30}Br_2N_2S_4$: C, 47.42; H, 4.59; N, 4.25; S, 19.47. Found: C, 47.47; H, 4.31; N, 4.39; S, 19.81.

2,2′-Dibromo-5,5′-bis(bithienyl)-4,4′-dihexyl-2,2′-bithiazole (M5) The synthesis of monomer **M5** was followed by the similar procedure as described for monomer **M4**. Compound **9** (1.71 g, 2.57 mmol) was dissolved in chloroform (50 mL) under nitrogen, and then *N*-bromosuccinimide (0.92 g, 5.19 mmol) was added

completely. The final solution was purified by column chromatography (silica gel, CH_2Cl_2/hexane 1:3) to yield a red solid (1.94 g). Yield: 92%. ^{1}H NMR (ppm, $CDCl_3$): δ 7.07 (m, 4H), 7.00-6.98 (d, J = 3.9 Hz, 2H), 6.95-6.93 (d, J = 4.5 Hz, 2H), 2.94 (t. J = 7.2 Hz, 4H), 1.82-1.77 (m, 4H), 1.45-1.31 (m, 12H), 0.91-0.87 (m, 6H). ^{13}C NMR (ppm, $CDCl_3$): δ 157.65, 154.83, 138.09, 137.20, 132.21, 130.77, 128.02, 127.27, 124.44, 124.13, 31.62, 30.49, 29.36, 29.16, 22.61, 14.09. MS (FAB): m/z [M[+]] 822.0; calcd m/z [M[+]] 821.9. Anal. Calcd for $C_{34}H_{34}Br_2N_2S_6$: C, 49.63; H, 4.16; N, 3.40; S, 23.38. Found: C, 49.23; H, 4.31; N, 3.20; S, 23.95.

4,4′-Dihexyl-2,2′-bithiazole-5,5′-dicarbaldehyde (10) To a solution of **M1** (4.9 g, 9.9 mmol) in THF (180 mL), *n*-BuLi (2.5 M solution in hexane, 9.1 mL, 22.7 mmol) was added at -78 °C. After stirring for 1h, a solution of *N*-formylmorpholine (3.4 g, 29.7 mmol) in THF (20 mL) was added. After additional stirring for 1h at -78 °C, the mixture was allowed to warm up to room temperature overnight. The final solution was acidified with 100 mL of 1 N HCl solution and stirred for 45 min at room temperature. The aqueous phase was extracted with dichloromethane, and the organic layer was dried over magnesium sulfate. After evaporation of the solvent, the final crude product was purified by column chromatography (silica gel, EA/hexane 1:3) to yield a yellow solid (2.5 g). Yield: 65%. ^{1}H NMR (ppm, $CDCl_3$): δ 10.11 (s, 2H), 3.09 (t, J = 7.2 Hz, 4H), 1.80 (m, 4H), 1.37-1.29 (m, 12H), 0.89 (t, J = 7.2 Hz, 6H).

4,4-Bis(2-ethylhexyl)-4*H*-cyclopenta[2,1-b:3,4-*b'*]dithiophene (13) Compound **12** (2.0 g, 11.2 mmol) was dissolved in DMSO (50 mL), and then 2-ethylhexyl bromide (4.3 g, 22.4 mmol) was added, followed by potassium iodide (50 mg). The mixture was purged with nitrogen and cooled in an ice bath, and ground KOH (2.0 g) was added in portions. The resulting green mixture was vigorously stirred overnight at room temperature. Water was added, and the reaction was extracted with

dichloromethane. The organic layer was separated and dried with magenesium sulfate. The solvent was removed under vacuum, and the crude product was purified by chromatography using hexane as an eluent. The pure compound was obtained as a colorless oil. Yield: 3.60 g (80%). ^{1}H NMR (ppm, CDCl$_3$): δ 7.13 (m, 2H), 6.91 (m, 2H), 1.86 (m, 4H), 0.93 (m, 18H), 0.73 (t, J = 6.4 Hz, 6H), 0.59 (m, J = 7.2 Hz, 6H).

4,4-Bis(2-ethylhexyl)-2,6-bis(trimethylstannanyl)-4H-cyclopenta[2,1-b:3,4-b']dithiophene (14) Compound **13** (1.5 g, 3.72 mmol) was dissolved in dry THF (30 mL). The solution was cooled to -78 °C and n-butyllithium (2.5 M solution in hexane, 6.0 mL, 14.9 mmol) was added dropwise under nitrogen. The mixture was stirred to react at this temperature for 1 h and allowed to warm to room temperature over 3 h, after which it was stirred for an additional hour. The reaction was then cooled to -78 °C, and Me$_3$SnCl (1M in hexanes, 18.0 mL, 18.0 mmol) was added carefully. The reaction was allowed to warm up to room temperature and stirred overnight. Water was added, and the reaction was extracted with ethyl ether. The organic layer was washed with water and dried over magnesium sulfate. After removing the solvent by rotavapor, the crude product was dissolved in toluene and quickly passed through a plug of Celite pretreated with triethylamine. The solvent was removed, and the residue was dried under vacuum at 80 °C overnight. The distannyl compound was dissolved in hexane and filtered through a plug of densely packed Celite. The solvent was removed, and the monomer was obtained as a light brownish viscous oil (2.60 g). Yield: 96%. ^{1}H NMR (ppm, CDCl$_3$): δ 6.93 (m, 2H), 1.86 (m, 4H), 1.29 (m, 2H), 0.94 (m, 16H), 0.78 (t, J = 6.8 Hz, 6H), 0.62 (t, J = 7.3 Hz, 6H), 0.37 (m, 18H). ^{13}C NMR (ppm, CDCl$_3$): δ 160.12, 143.04, 136.58, 130.44, 52.80, 43.57, 35.66, 34.85, 29.15, 28.04, 23.21, 14.63, 11.25, -7.76. MS (FAB): m/z [M$^+$] 728.0; calcd m/z [M$^+$] 728.2. Anal. Calcd for C$_{31}$H$_{54}$S$_2$Sn$_2$: C, 51.12; H, 7.47. Found: C, 51.47; H, 7.30.

M6 A mixture of compound **10** (2.4 g, 6.1 mmol), compound **11** (6.0 g, 30.5 mmol), and methanol (300 mL) were placed in a 500 mL two-neck round-bottom flask at room temperature. A catalytic amount of potassium *tert*-butoxide in methanol was added into this mixture. After reaction for 24 h, the product was filtered and dried. **M6** was obtained as a red solid (4.1 g) by column chromatography on silica gel eluted with CH_2Cl_2/hexane 1:4. Yield: 90%. ^{1}H NMR (ppm, CDCl$_3$): δ 7.64 (s, 2H), 7.51-7.39 (m, 8H), 2.93 (t. *J* = 7.2 Hz, 4H), 1.80 (m, 4H), 1.35 (m, 12H), 0.89 (t. *J* = 7.2 Hz, 6H). ^{13}C NMR (ppm, CDCl$_3$): δ 164.93, 160.81, 132.46, 132.30, 130.76, 129.34, 127.09, 123.64, 117.24, 109.29, 31.58, 30.21, 29.86, 29.14, 22.59, 14.08. MS (FAB): *m/z* [M$^+$] 749; calcd *m/z* [M$^+$] 748.1. Anal. Calcd for $C_{36}H_{36}Br_2N_4S_2$: C, 57.76; H, 4.85; N, 7.48; S, 8.57. Found: C, 57.62; H, 4.72; N, 7.60; S, 9.04.

General Procedure for the Synthesis of copolymers P1-P6.[65,102,108]

The synthetic route of copolymers is shown in Figure 4.3. All polymerization steps were carried out through the palladium(0)-catalyzed Stille coupling reactions. Into 50 mL of two-neck flask, 1 equiv of dibromo monomers (**M1**-**M6**) and 1 equiv of 4,4-bis(2-ethylhexyl)-2,6-bis(trimethylstannyl)-4*H*-cyclopenta[2,1-b:3,4-b']dithiophene (**14**) were added in anhydrous toluene and deoxygenated with nitrogen for 30 min. The Pd(0) complex, i.e., tetrakis(triphenylphosphine)palladium (1 mol %), was transferred into the mixture in a dry environment. The reaction mixture was stirred at 110 °C for 4-5 days, and then an excess amount of 2-bromothiophene was added to end-cap the trimethylstannyl groups for 4 h. The reaction mixture was cooled to 40 °C and added slowly into a vigorously stirred mixture of methanol/acetone (3:1). The polymers were collected by filtration and reprecipitation from methanol. The crude polymers were further purified by washing with acetone and EA for 2 days in a Soxhlet apparatus to remove oligomers and catalyst residues, respectively.

P1 Following the general polymerization procedure, compound **14** (1.0 mmol), **M1** (1.0 mmol), and toluene (8 mL) were used in this polymerization, and the polymer was obtained as a dark red powder. Yield: 46%. ^{1}H NMR (ppm, CDCl$_3$): δ 7.07 (br, s, 2H), 2.98 (br, s, 4H), 1.83 (br, m, 8H), 1.46-1.02 (br, m, 12H), 0.96-0.91 (br, m, 22H), 0.75-0.61 (br, m, 14H). Anal. Calcd for C$_{43}$H$_{62}$N$_2$S$_4$: C, 70.25; H, 8.50; N, 3.81. Found: C, 68.77; H, 8.25; N, 3.59.

P2 Following the general polymerization procedure, compound **14** (0.96 mmol), **M2** (0.96 mmol), and toluene (8 mL) were used in this polymerization, and the polymer was obtained as a black powder. Yield: 58%. ^{1}H NMR (ppm, CDCl$_3$): δ 7.09 (br, s, 2H), 2.99 (br, s, 4H), 2.74 (br, s, 4H), 1.74 (br, m, 12H), 1.45-1.29 (br, m, 24H), 1.03-0.85 (br, m, 28H), 0.77-0.61 (br, m, 14H). Anal. Calcd for C$_{61}$H$_{88}$N$_4$S$_6$: C, 68.49; H, 8.29; N, 5.24. Found: C, 67.26; H, 7.24; N, 5.10.

P3 Following the general polymerization procedure, compound **14** (0.72 mmol), **M3** (0.72 mmol), and toluene (6 mL) were used in this polymerization, and the polymer was obtained as a dark black powder. Yield: 65%. ^{1}H NMR (ppm, CDCl$_3$): δ 7.09 (br, s, 2H), 2.98 (br, s, 4H), 2.75 (br, 2, 8H), 1.74 (br, m, 16H), 1.29 (br, m, 36H), 1.03-0.87 (br, m, 34H), 0.76-0.62 (br, m, 14H). Anal. Calcd for C$_{79}$H$_{114}$N$_6$S$_8$: C, 67.57; H, 8.18; N, 5.98. Found: C, 65.94; H, 7.77; N, 5.94.

P4 Following the general polymerization procedure, compound **14** (0.68 mmol), **M4** (0.68 mmol), and toluene (6 mL) were used in this polymerization, and the polymer was obtained as a dark black powder. Yield: 61%. ^{1}H NMR (ppm, CDCl$_3$): δ 7.11-7.07 (br, m, 6H), 2.99 (br, s, 4H), 1.83 (br, m, 8H), 1.46-1.37 (br, m, 12H), 1.03-0.92 (br, m, 22H), 0.77-0.61 (br, m, 14H). Anal. Calcd for C$_{51}$H$_{66}$N$_2$S$_6$: C, 68.10; H, 7.40; N, 3.11. Found: C, 67.31; H, 7.21; N, 3.34.

P5 Following the general polymerization procedure, compound **14** (0.74 mmol),

M5 (0.74 mmol), and toluene (6 mL) were used in this polymerization, and the polymer was obtained as a dark black powder. Yield: 58%. ^{1}H NMR (ppm, CDCl$_3$): δ 7.11-6.97 (br, m, 10H), 2.94 (br, s, 4H), 1.79 (br, m, 8H), 1.45-1.37 (br, m, 12H), 0.91-0.87 (br, m, 22H), 0.77-0.61 (br, m, 14H). Anal. Calcd for C$_{59}$H$_{70}$N$_2$S$_8$: C, 66.62; H, 6.63; N, 2.63. Found: C, 65.69; H, 7.04; N, 2.55.

P6 Following the general polymerization procedure, compound **14** (0.96 mmol), **M6** (0.96 mmol), and toluene (12 mL) were used in this polymerization, and the polymer was obtained as a dark black powder. Yield: 15%. ^{1}H NMR (ppm, CDCl$_3$): δ 7.71-7.42 (br, m, 12H), 2.96 (br, s, 4H), 1.90 (br, m, 8H), 1.49-1.35 (br, m, 12H), 1.00-0.92 (br, m, 22H), 0.73-0.60 (br, m, 14H). Anal. Calcd for C$_{61}$H$_{72}$N$_4$S$_4$: C, 74.04; H, 7.33; N, 5.66. Found: C, 72.53; H, 7.79; N, 5.21.

4.2.3 Measurements and Characterization

^{1}H NMR spectra were recorded on a Varian Unity 300 MHz spectrometer using CDCl$_3$ solvents. Elemental analyses were performed on a HERAEUS CHN-OS RAPID elemental analyzer. Transition temperatures were determined by differential scanning calorimetry (DSC, Perkin-Elmer Pyris 7) with a heating and cooling rate of 10 °C/min. Thermogravimetric analyses (TGA) were conducted with a TA instrument Q500 at a heating rate of 20 °C/min under nitrogen. Gel permeation chromatography (GPC) analyses were conducted on a Waters 1515 separation module using polystyrene as a standard and THF as an eluant. UV-visible absorption and photoluminescence (PL) spectra were recorded in dilute chloroform solutions (10^{-6} M) on a HP G1103A and Hitachi F-4500 spectrophotometer, respectively. Solid films of UV-vis and PL measurements were spin-coated on a quartz substrate from chlorobenzene solutions with a concentration of 10 mg/mL. Cyclic voltammetry (CV) measurements were performed using a BAS 100 electrochemical analyzer with a

standard three-electrode electrochemical cell in a 0.1 M tetrabutylammonium hexafluorophosphate (TBAPF6) solution (in acetonitrile) at room temperature with a scanning rate of 50 mV/s. During the CV measurements, the solutions were purged with nitrogen for 30s. In each case, a carbon working electrode coated with a thin layer of copolymers, a platinum wire as the counter electrode, and a silver wire as the quasi-reference electrode were used, and Ag/AgCl (3M KCl) electrode was served as a reference electrode for all potentials quoted herein. The redox couple of ferrocene/ferrocenium ion (Fc/Fc$^+$) was used as an external standard. The corresponding highest occupied molecular orbital (HOMO) and lowest unoccupied molecular orbital (LUMO) levels were calculated using $E_{\text{ox/onset}}$ and $E_{\text{red/onset}}$ for experiments in solid films of copolymers **P1-P6**, which were performed by drop-casting films with the similar thickness from THF solutions (ca. 5 mg/mL). The LUMO level of PCBM employed was in accordance with the literature datum.[19b] The onset potentials were determined from the intersections of two tangents drawn at the rising currents and background currents of the cyclic voltammetry (CV) measurements.

X-ray Diffraction Characterization

Synchrotron powder X-ray diffraction (XRD) measurements were performed at beamline BL17A of the National Synchrotron Radiation Research Center (NSRRC), Taiwan, where the wavelength of X-ray was 1.33361 Å. The XRD data were collected using Mar345 image plate detector mounted orthogonal to the beam with sample-to-detector distance of 250 mm, and the diffraction signals were accumulated for 3 min. The powder samples were packed into a capillary tube and heated by a heat gun, where the temperature controller is programmable by a PC with a PID feedback system. The scattering angle theta was calibrated by a mixture of silver behenate and

silicon.

4.2.4 Device Fabrication of Polymer Photovotaic Cells

The polymer photovoltaic (PV) cells in this study were composed of an active layer of blended copolymers (**P1-P6**:PCBM) in solid films, which was sandwiched between a transparent indium tin oxide (ITO) anode and a metal cathode. Prior to the device fabrication, ITO-coated glass substrates ($1.5 \times 1.5\,cm^2$) were ultrasonically cleaned in detergent, de-ionized water, acetone, and isopropyl alcohol. Afterwards, the substrates were treated with UV ozone for 15 min, and a layer of poly(ethylene dioxythiophene): polystyrenesulfonate (PEDOT:PSS, ~30 nm) was subsequently spin-coated onto the substrates. After baking at 130 °C for one hour, the substrates were transferred to a nitrogen-filled glove box. The PSC devices were fabricated by spin-coating solutions of blended copolymers **P1-P6**:PCBM (with various weight ratios) onto the PEDOT:PSS modified substrates at 600 rpm for 60 s (ca. 200 nm), and placed in a covered glass petri dish. Initially, the blended solutions were prepared by dissolving both copolymers (**P1-P6**) and PCBM (with a 1:1 weight ratio initially and then with various weight ratios for the optimum copolymer) in DCB (20 mg/1 mL), followed by continuous stirring for 12 h at 50 °C. In the slow-growth approach, blended copolymers in solid films were kept in the liquid phase after spin-coating by using the solvent with a high boiling point. Finally, a calcium layer (30 nm) and a subsequent aluminum layer (100 nm) were thermally evaporated through a shadow mask at a pressure below 6×10^{-6} Torr, and the active area of the device was 0.12 cm². All PSC devices were prepared and measured under ambient conditions. In the hole-only devices,[17a] the calcium layer was replaced with a MoO₃ ($\Phi = 5.3 eV$) layer, which has been shown to provide a good hole injection contact in PSC devices containing copolymers **P1-P6**. The MoO₃ layer with a thickness of 20 nm was

thermally evaporated and then capped with 50 nm of Al.

4.3 Results and Discussion

4.3.1 Synthesis and Characterization

Six new donor-acceptor bithiazole-based (BT) monomers **M1**-**M6** were prepared

from 4,4′-dihexyl-2,2′-bithiazole (**1**)[70a] via Stille and Suzuki coupling reactions. By

insertion of phenylene and cyanovinylene functionalities to BT units,

oligo(bithiazole)s **M1**-**M3**, and bithiazole-oligo(thiophene)s **M4**-**M5**, and **M6** were

obtained correspondingly, and their synthetic routes are outlined in Figures 4.1 and

4.2. Monomers **M1**-**M6** and compound **14** were satisfactorily characterized by [1]H

NMR, ^{13}C NMR, MS spectroscopy, and elemental analyses. As shown in Figure 4.3,

further Stille coupling of bis-stannane **14** with monomers **M1**-**M6** successfully

resulted in the well-defined CPDT-BT copolymers **P1**-**P6**.[65,102,108] All the copolymers

were completely soluble in organic solvents such as chloroform, THF, and

chlorobenzene at room temperature, except that copolymers **P5** and **P6** were only

completely soluble in high boiling point solvents (e.g., chlorobenzene). The less

solubilities of copolymers **P5** and **P6** were likely owing to the higher rigidities of the

polymer main chains caused by the larger number of thiophene units and rigid

electron-withdrawing cyano groups.

The yields and molecular weights of copolymers **P1**-**P6** determined by GPC

against polystyrene standards in THF are summarized in Table 4.1. After washing

final products in Soxhlet apparatus, the yields of 15-65% for **P1**-**P6** were obtained.

The copolymers have the number molecular weights (M_n) of 5100 to 42100 with the

polydispersity index (PDI) values ranging 1.08-1.81. The molecular weights of

copolymers **P5**-**P6** were relatively smaller than the other copolymers, which were

likely due to the lower solubilities originated from the rigid thiophene and cyano

groups. The thermal stabilities and phase transition temperatures of copolymers **P1-P6**, including 5% weight loss temperatures (T_d), glass transition temperatures (T_g), melting temperatures (T_m), and crystallization temperatures (T_c) characterized by TGA and DSC are summarized in Table 4.1. All copolymers were thermally stable up to 363-398 °C upon heating and showed T_g values over 120 °C, except that the phase transition temperatures of **P1** and **P6** were not observed by DSC. The detectable melting temperatures (T_m) and crystallization temperatures (T_c) of copolymers **P4** and **P5** suggested the higher ordering capabilities of **P4** and **P5** for their potential applications in organic solar cells, since the formation of phase-separated ordered nanostructures in the photovoltaic layer was desirable for charge transport and separation.[52]

Table 4.1 Molecular Weights, Yields, and Thermal Data of Copolymers P1-P6

Polymer	$M_n{}^a$ ($\times10^3$)	$M_w{}^a$ ($\times10^3$)	PDI	Yield (%)	Transition temperature (°C)			
					$T_g{}^b$	$T_m{}^b$	$T_c{}^b$	$T_d{}^c$
P1	15.1	20.3	1.34	46	n.d.^{d}	n.d.^{d}	n.d.^{d}	363
P2	38.0	52.2	1.37	58	130	n.d.^{d}	n.d.^{d}	395
P3	42.1	70.0	1.66	65	161	n.d.^{d}	n.d.^{d}	398
P4	17.7	32.0	1.81	61	168	237	207	396
P5	9.5	14.0	1.47	58	123	256	244	398
P6	5.1	5.5	1.08	15	n.d.^{d}	n.d.^{d}	n.d.^{d}	377

^{a} Molecular weights and polydispersity were measured by GPC, using THF as an eluent, polystyrene as a standard. M_n, number average molecular weight. M_w, weight average molecular weight. ^{b} Glass transition temperature, melting temperature, and crystalline temperature (°C) were measured by DSC at a heating rate of 10 °C/min. ^{c} Temperature (°C) at 5% weight loss measured by TGA at a heating rate of 20 °C/min under nitrogen. ^{d} No noticeable transition temperature was observed.
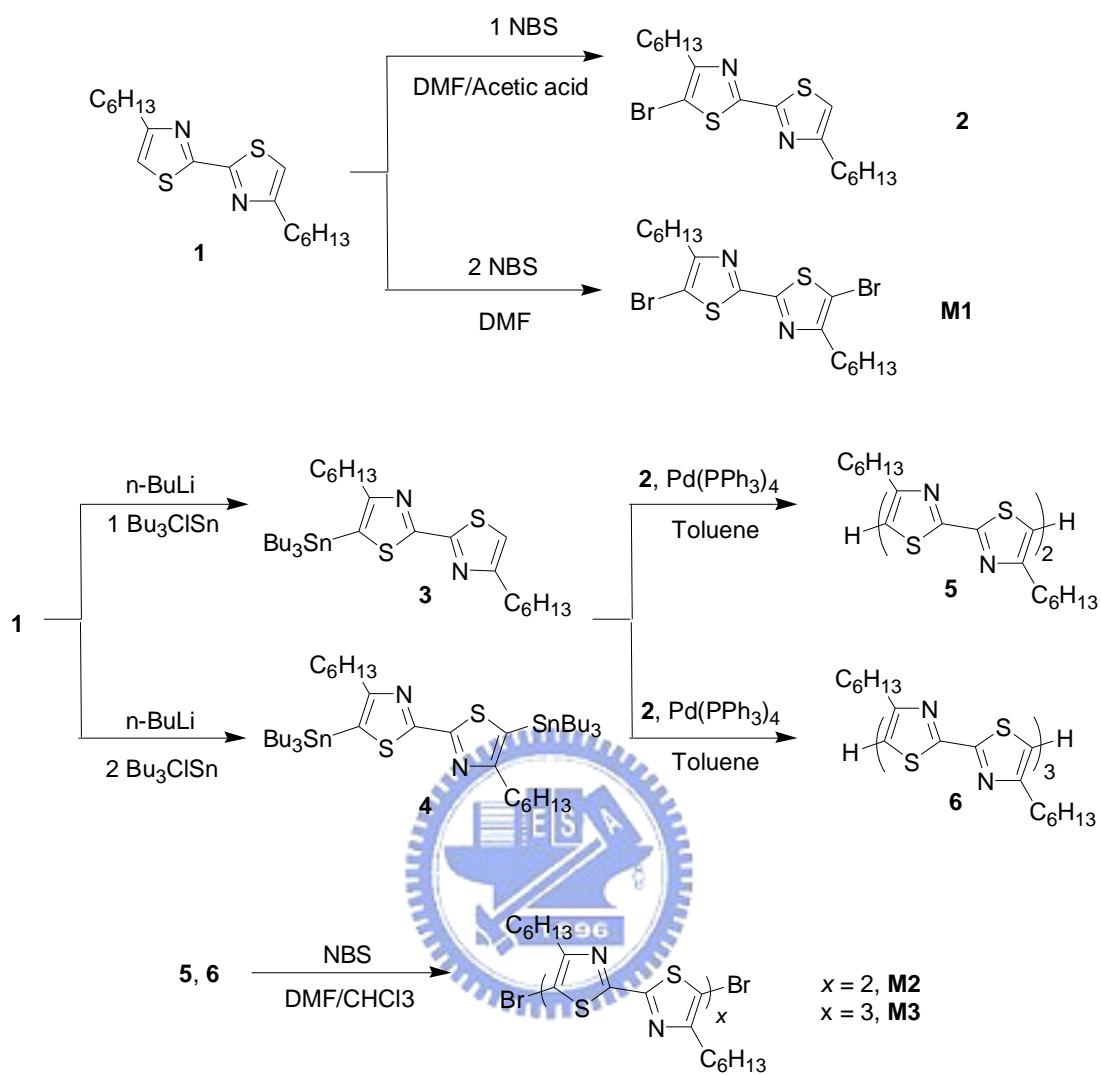
Scheme 4.1 Synthetic Routes of Oligo(bithiazole) Based Monomers **M1-M3**.
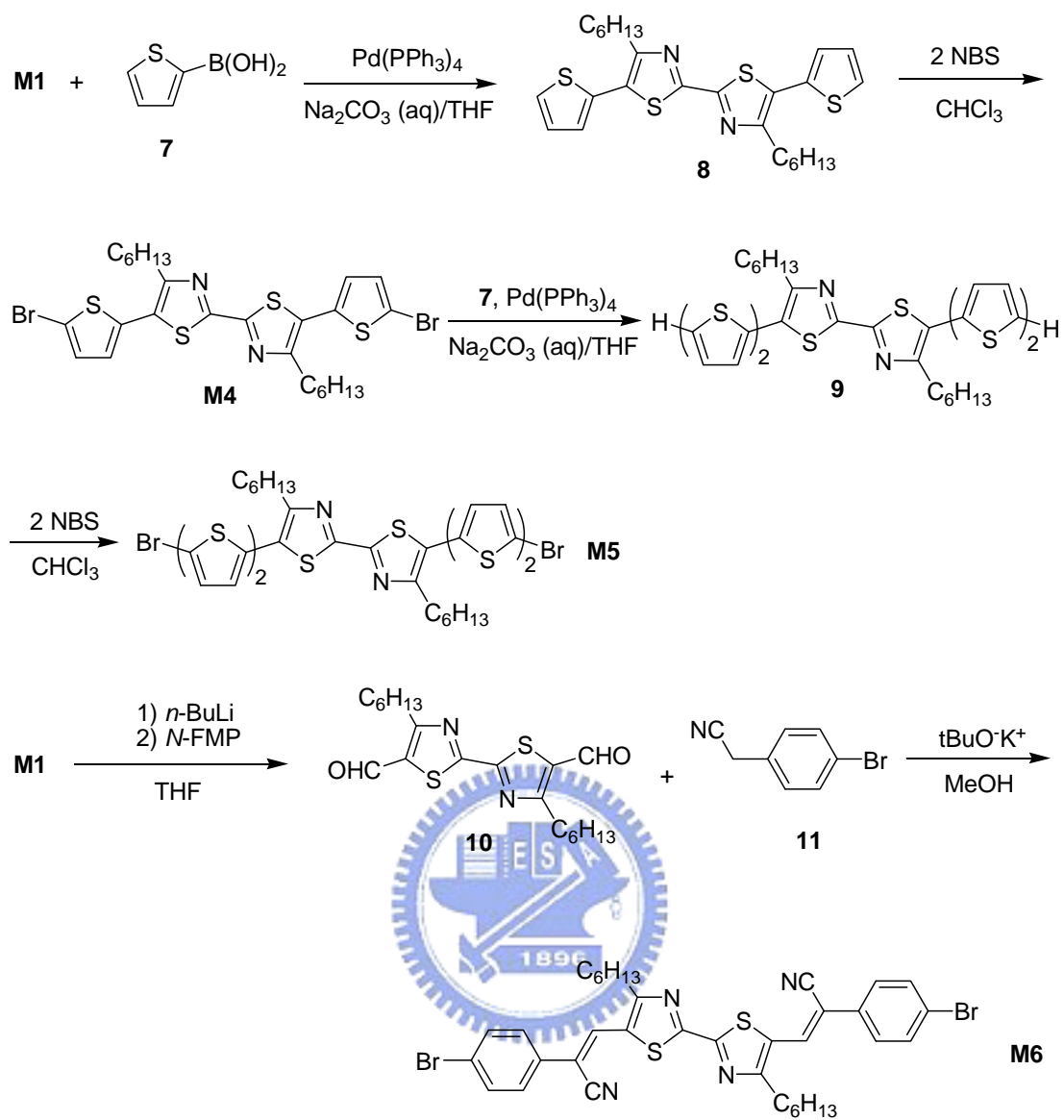
Scheme 4.2 Synthetic Pathways of Bithiazole-based Monomers **M4-M6** and Cyclopentadithiophene.
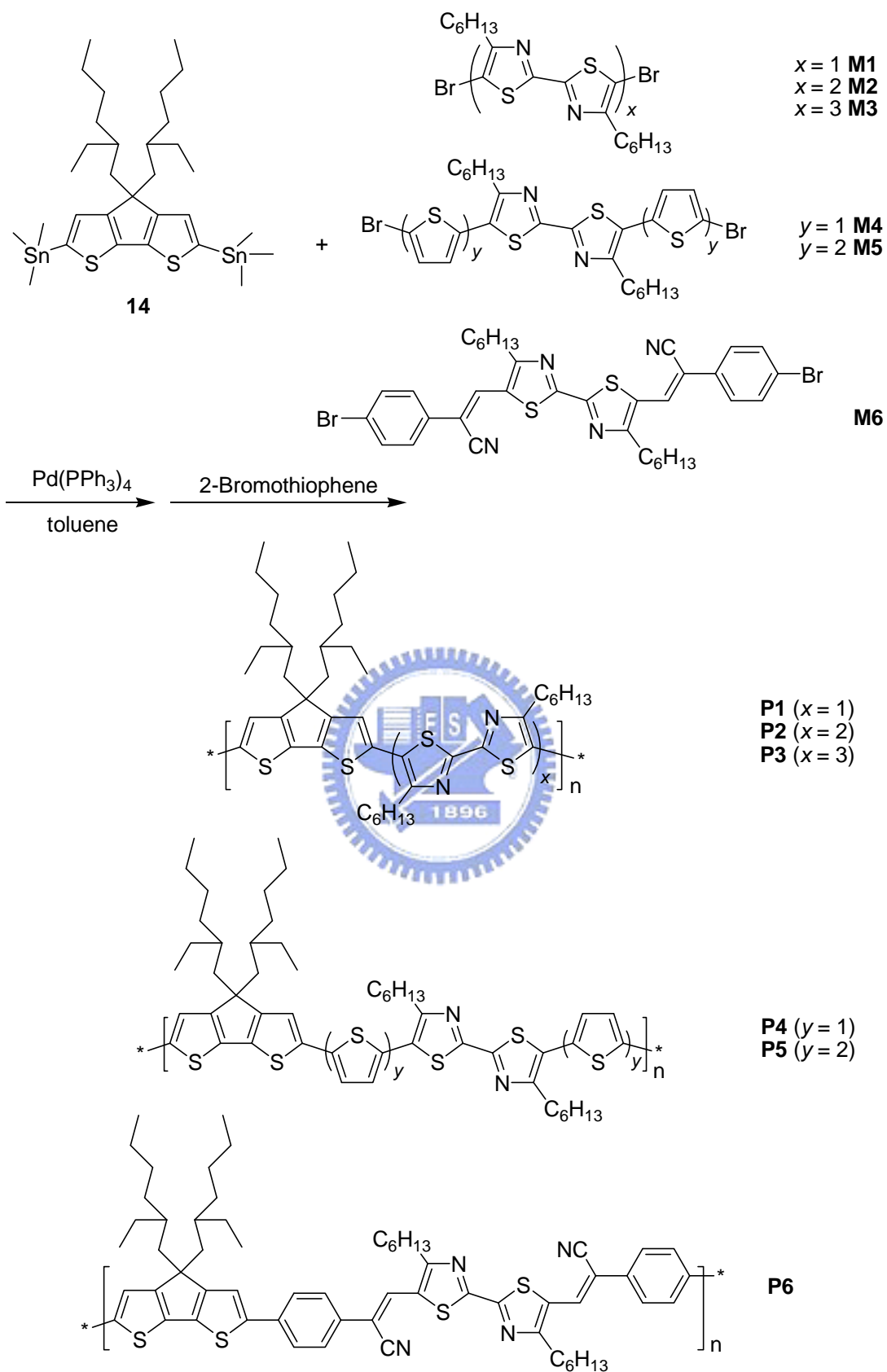
Scheme 4.3 Synthetic Routes of Copolymers **P1-P6**.

4.3.2 Optical Properties

The optical absorption spectra of copolymers **P1-P6** in chlorobenzene solutions (10^{-6} M) and solid films are shown in Figure 4.4. The photophysical properties of the D-A copolymers (**P1-P6**) based on CPDT-BT units are illustrated in Table 4.2. As expected, by tuning the numbers of the conjugated heterocyclic rings and electron donor-acceptor compositions, the effect of conjugation lengths of the copolymers will be affected, which will also influence the absorption spectra of **P1-P6** effectively (in both solutions and solid films). For instance, due to the presence of a more extended and delocalized π-electron system by increasing the number of the donor thiophene (Th) ring, an obvious red-shifted absorption of copolymer **P5** was observed compared with that of copolymer **P4** in both solutions and solid films. Furthermore, copolymer **P6** containing electron-accepting cyano groups showed the longest absorption wavelength among all copolymers in solutions. However, the numbers of BT acceptor units in copolymers **P1-P3** affected the absorption maxima in solutions and solid films by different ways. Surprisingly, a blue-shifted absorption in solutions was observed by increasing the number of BT units in solutions of **P1-P3**, which might be due to the twist of polymer main chains by the BT units with alkyl side-chains. Nevertheless, due to the enlarged full width at half maximum (FWHM) values from **P1** to **P3**, a blue-shifted absorption in solid films of **P1-P3** was observed; but their optical band gaps (in solid films) had been reduced from 1.94 eV of **P1** to 1.83 eV of **P3**. Even though the numbers of the conjugated rings in both **P2** and **P4** or both **P3** and **P5** are the same, the electron donor (Th) and acceptor (BT) units still have some influences on copolymers **P2-P5**. Compared with copolymers **P2** and **P3**, the corresponding **P4** and **P5** had 23 nm (44 nm) and 54 nm (105 nm) of red-shift absorption maxima in solutions (in solid films). Similar changes of UV-vis spectra

were found in rigid π-conjugated polymers with an intramolecular charge transfer (ICT) interaction between electron donor and acceptor moieties.[70b,108]

Interestingly, by increasing the numbers of the conjugated heterocyclic rings in the donor-acceptor systems, the gradually enhanced red-shifted absorption (from solutions to solid films) in **P1-P5** were likely due to their longer conjugated organization, which led to higher aggregation forms of these copolymer chains in solid films in contrast to those in solutions. The optical band gaps (E_g^{opt}) of the copolymers in solid films, which were determined by the cutoff wavelengths of the optical absorptions, were in the range of 1.70-1.94 eV (Table 4.2). As a result, the electron donor Th rings in combination with the electron acceptor BT rings[70b,115,128] or cyano groups[56-57] presented a more extended π-conjugated system through the rigid main-chains and electron D-A chromophores, where the optical band gaps of **P1-P6** were gradually lowered from **P1** with the largest value of 1.94 eV to **P5** with the narrowest value of 1.70 eV (0.24 eV lower than **P1**).

Table 4.2 Photophysical Data and Optical Bandgap of Copolymers P1-P6

Polymer	λ_{max}, UV (FWHM)[a]		E_g^{opt}
	Solution (nm)[b]	Film (nm)[b]	(eV)[c]
P1	525 (130)	527 (150)	1.94
P2	500 (133)	516 (205)	1.90
P3	482 (143)	511 (260)	1.83
P4	523 (130)	560, 607[d]	1.84
P5	536, 613[d]	544,[d] 616	1.70
P6	426,[d] 570, 645[d]	443,[d] 587, 650[d]	1.71

[a] FWHM = Full width at half maximum. [b] Obtained or spin-coated from chlorobenzene solutions. [c] Estimated from the onset wavelengths of UV-vis spectra in solid films. [d] Shoulder peak.

(a)
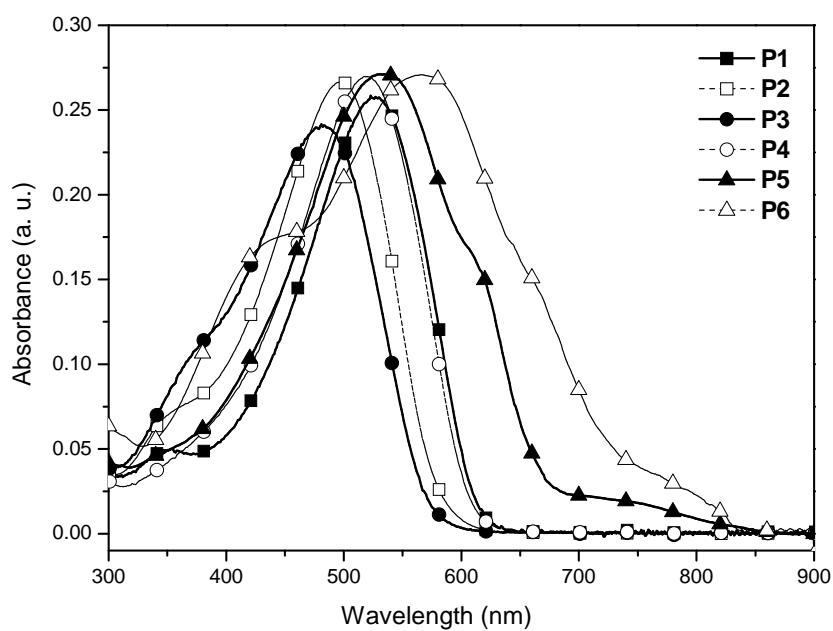
(b)

Figure 4.4 Optical absorption spectra of D-A copolymers **P1-P6** (a) in chlorobenzene solutions, and (b) in solid films (spin-coated from chlorobenzene solutions).

4.3.3 Electrochemical Characterization

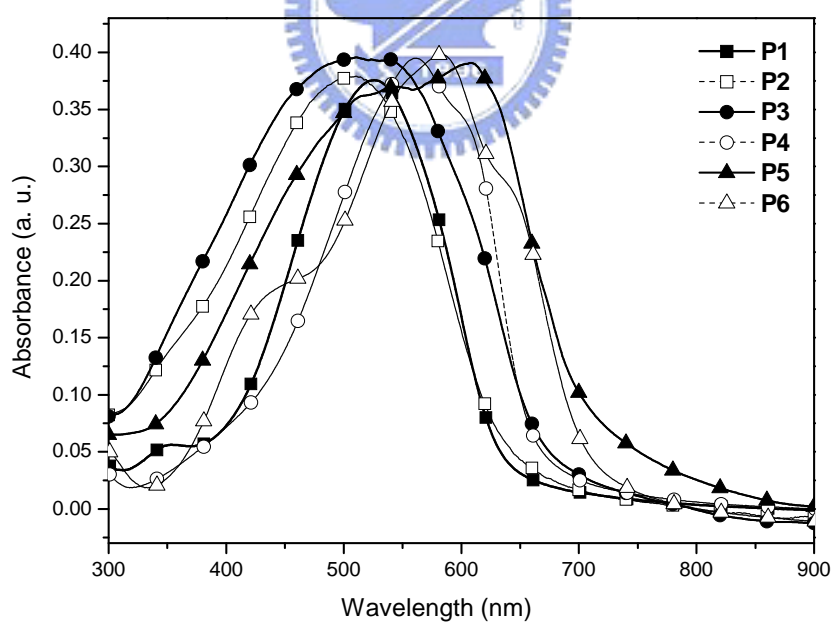The electrochemical results are shown in Figure 4.5 and the data are summarized in Table 4.3. The formal oxidation potentials were in the range of 0.79-1.24 V (the first peaks) for **P1-P6**, 0.98-1.42 V (the second peaks) for **P2-P5**, and 1.34-1.68 V (the third peaks) for **P3-P5**. In addition, the formal reduction potentials were in the range of -(0.88-1.05) V (the first peaks) and -(1.13-1.77) V (the second peaks) for **P1-P6**, respectively. Both reversible oxidation and reduction were found in **P1**, whereas irreversible oxidation and partially reversible reduction were observed in **P2** and **P3**. It suggested that **P1** containing electron-donating CPDT and electron-accepting BT moieties was closer to be both p-type and n-type materials. As the electron-accepting character of BT moieties increased in **P2** and **P3**, they were found to be suitable as n-type materials than p-type materials. Besides, **P4**, **P5**, and **P6** all exhibited partially reversible oxidation and reduction behavior as evident from the areas and close proximity of the anodic and cathodic scans, which were a good sign for high structural stability in the charged state.

The moderate onset oxidation potentials and onset reduction potentials of **P1-P6** were observed between 0.64-1.15 V and –(0.67-0.87) V, respectively, from which the HOMO levels of 5.04-5.55 eV and LUMO levels of 3.53-3.73 eV for all copolymers were calculated according to the following equation:[106] $E_{HOMO}/E_{LUMO} = [-(E_{onset\ (vs\ Ag/AgCl)} - E_{1/2}\ (ferrocene)+4.8)]$ eV, where 4.8 eV was the energy level of ferrocene below the vacuum level. It was worthwhile to note that the oxidation potentials of copolymers **P1-P6** were significantly varied when different numbers of Th donor units and BT/cyano acceptor moieties were incorporated into the molecular structures. Interestingly, the oxidation potentials of **P1-P3** and **P6** were ca. 0.2 V higher than those of **P4-P5**, thus indicating higher oxidation stability for **P1-P3** and **P6**. The

noticeably higher oxidation potentials **P1-P3** and **P6** can be explained by that the resulting conjugated copolymers were more electron-deficient due to the imine group in their planar π-conjugated systems. Oppositely, in contrast to **P4**, the oxidation potential of **P5** was reduced by the extension of Th rings, and thus **P5** showed a lower oxidation potential (0.64 V) due to the longer Th ring. On the other hand, the LUMO energy level of the donor (polymer) has to be positioned above the LUMO energy level of the acceptor (PCBM) by at least 0.3 eV, so the exciton binding energy of polymer could be overcome and result in efficient electron transfer from donor to acceptor.[106] Hence, the electrochemical reduction potentials of copolymers **P1-P6** showed similar LUMO energy levels at ca. 3.53-3.73 eV, which represented high electron affinity to make these copolymers suitable donors to inject and transport electrons to PCBM acceptor (with 0.57-0.77 eV LUMO offsets regarding the LUMO level of PCBM at 4.3 eV[106]) for the bulk heterojunction polymer solar cell devices.[112] The differences between the band-gap values directly measured by CV (E_g^{ec} between 1.51 and 1.83 eV) and the optical band-gap values obtained from UV-vis spectra (E_g^{opt} between 1.70 and 1.94 eV) lied within an acceptable range of errors.
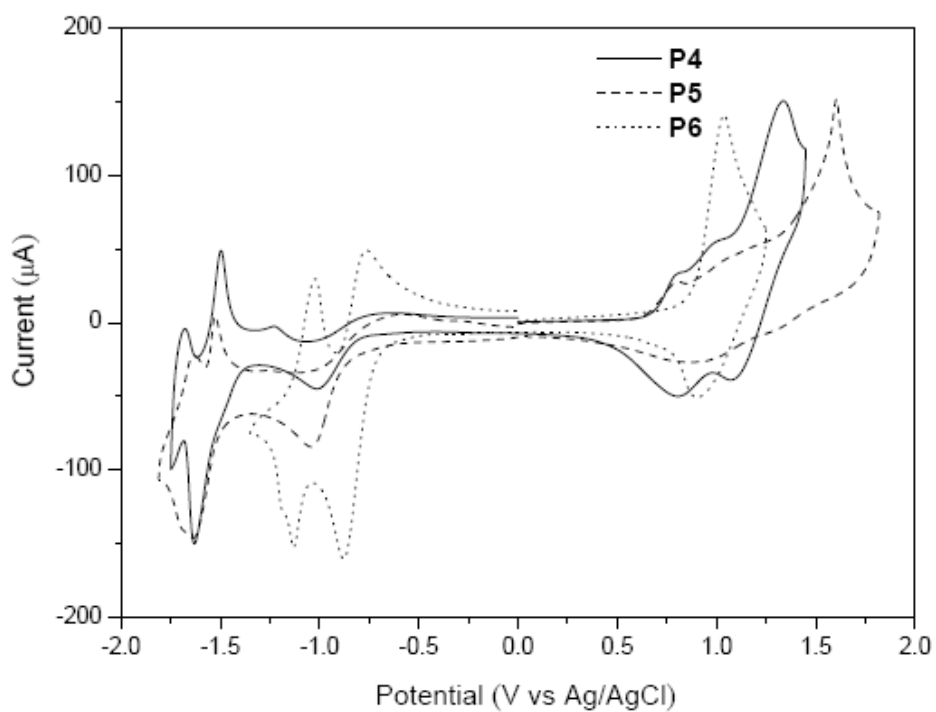
(a)
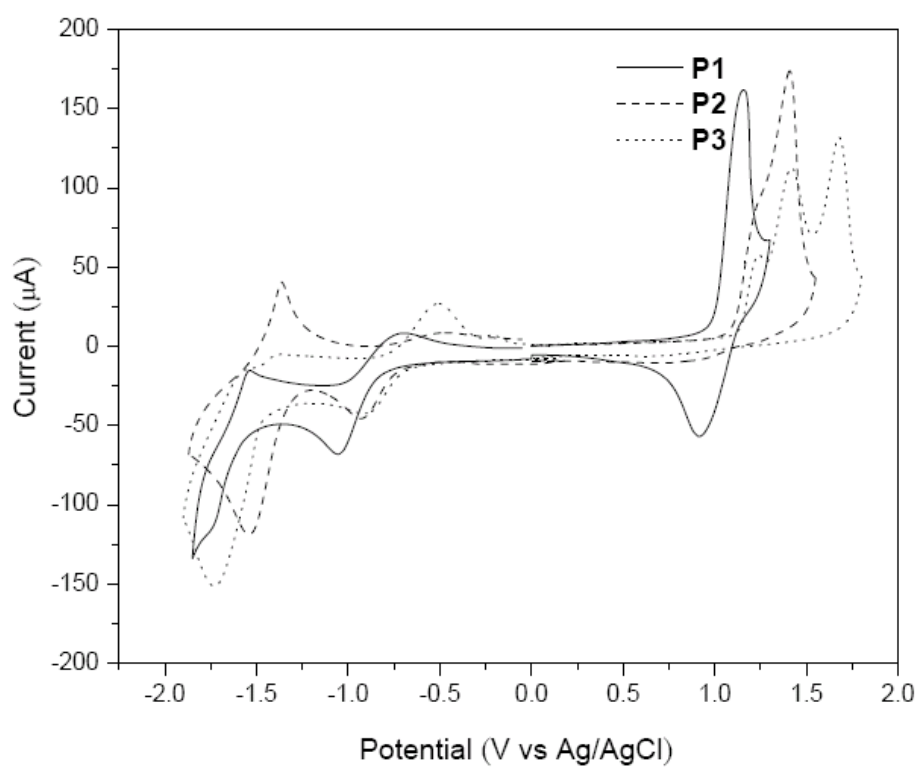
(b)

Figure 4.5 Cyclic voltammograms of D-A copolymers (a) **P1-P3** and (b) **P4-P6** (at a scan rate of 100 mV/s in solid films).

Table 4.3 Electrochemical Potentials, Energy Levels, and Band Gaps of Copolymers P1-P6[a]

Polymer	Oxidation potential[a] V		Reduction potential V		Energy level[d] eV		Band gap[e] eV
	$E_{ox/onset}$[b]	$E_{ox/o}$[c]	$E_{red/onset}$[b]	$E_{red/o}$[c]	E_{HOMO}	E_{LUMO}	E_g
P1	1.00	1.16	-0.83 -1.57	-1.05 -1.77	-5.40	-3.57	1.83
P2	1.11	1.22 1.42	-0.71 -1.36	-0.89 -1.52	-5.51	-3.69	1.82
P3	1.15	1.24 1.42 1.68	-0.67 -1.48	-0.88 -1.73	-5.55	-3.73	1.82
P4	0.67	0.80 0.98 1.34	-0.85 -1.49	-1.01 -1.63	-5.07	-3.55	1.52
P5	0.64	0.79 1.15 1.60	-0.87 -1.51	-1.03 -1.64	-5.04	-3.53	1.51
P6	0.88	1.04	-0.73 -1.09	-0.88 -1.13	-5.28	-3.67	1.61

[a] Reduction and oxidation potentials measured by cyclic voltammetry in solid films. [b] Onset oxidation and reduction potentials. [c] Formal oxidation and reduction potentials. [d] Estimated from the onset potentials using empirical equations: E_{HOMO}/E_{LUMO} = $[-(E_{onset\ (vs\ Ag/AgCl)}- E_{1/2}\ (\text{ferrocene})+4.8)]$ eV where 4.8 eV is the energy level of ferrocene below the vacuum level. [e] Bad gaps measured by cyclic voltammograms.

4.3.4 X-ray Diffraction

As shown in Figure 4.6, powder X-ray diffraction (XRD) patterns of copolymers **P1-P6** were acquired to investigate the molecular organization and morphological change after the thermal treatment of ca. 150 °C for 5 min. Interestingly, except **P2**, the annealed copolymers **P1** and **P3-P6** exhibited several strong diffraction peaks with high crystalline patterns, similar to the thiazole-[114-115,128-129] and thiophene-based polymers.[52b,102,113] Distinct primary diffraction peaks at 2θ = 6.3°, 4.3°, 4.3°, 5.1°, 5.7°, and 5.4° (small-angle region), corresponding to the d_l-spacing values of 11.9, 17.3, 17.3, 15.1, 13.3, and 14.2 Å for copolymers **P1-P6**, were assigned to the interchain spacing between polymer main chains, where the alkyl substituents were segregated as reported for similar π-conjugated polymers with long side chains.[52b,102,113-115,128-129] The second-order diffraction peaks for **P1** and **P3-P6** as well

as the third-order diffraction peaks for **P1**, **P3,** and **P6** were clearly observed at d_1/n Å (n = 2-3), respectively, which implied a highly organized assembly of these π-conjugated copolymers. Planar polymer molecules with side chains might prefer the face-to-face parallel packing.[129a] Some reasonable packing modes of these copolymers in view of van der Waals contacts are depicted in Figure 4.7. The distances between the segregation of the polymer main chains accounted for the interchain d_1 spacings. The distances between top and bottom layers of the backbones accounted for the π-π stacking at wide-angle d spacings. The regioregular π-π stacking distances of the backbones in **P1-P6** were in the range of wide-angle X-ray diffraction (XRD) at 3.55-3.66 Å, which were somewhat smaller than that (ca. 3.80 Å) observed in HT-P3RTh[130] with a similar stacked structure. It suggested that the π-conjugated polymers containing thiazole units had a stronger tendency to form the face-to-face stacking than those containing thiophene units.[114,128a,129b]

In bithiazole-based copolymers **P2** and **P3**, the larger d_1 spacing of 17.3 Å was presumed to adopt the possible end-to-end packing motifs and π-stacking structures, because the number density of the alkyl groups was similar to that of HT-P3RTh (ca. 17.7 Å),[114] as illustrated in Figure 4.7(b). Interestingly, **P1** and **P4-P6** showed smaller d_1 spacing values of 11.9-15.1 Å than **P2** and **P3**, which suggested that the packings of these copolymer chains were likely interdigitated in the lamellar sheets, as shown in Figure 4.7(a). The number densities of the alkyl groups in these copolymers were not as high as those of **P2** and **P3**, and furthermore the nonsubstituted thiophene rings or arylcyanovinyl units provided a sufficient space to facilitate the side-chain interdigitation. Based on the observation, it could be assumed that these characters of **P1-P6** formed highly crystalline diffraction patterns, indicating good π-π stacking of coplanar π-conjugated backbones with very promising electro-optical properties.

Overall, the charge carrier mobilities of PSC devices were substantially improved by

increasing the crystallinities and intermolecular stacking degrees in solid films.

(a)   (b)
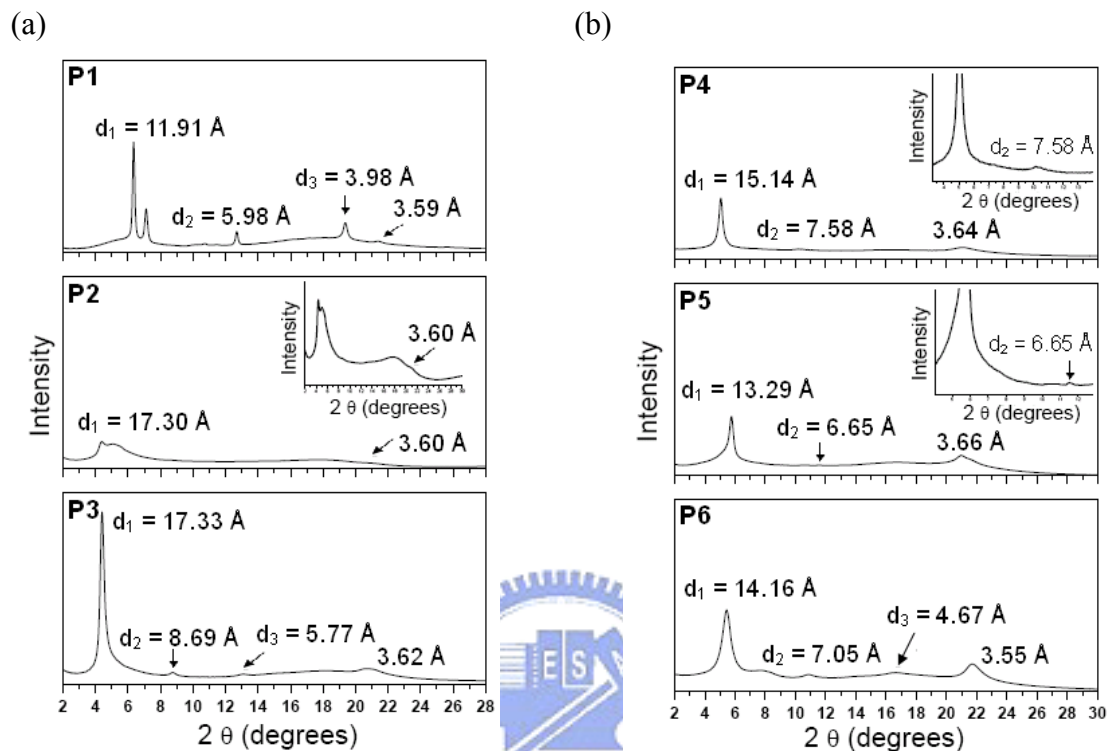
Figure 4.6 X-ray diffraction patterns of copolymers **P1-P6** in powder solids. The sharp diffraction peaks indicated that copolymers formed ordered structures in the solid state.

(a)
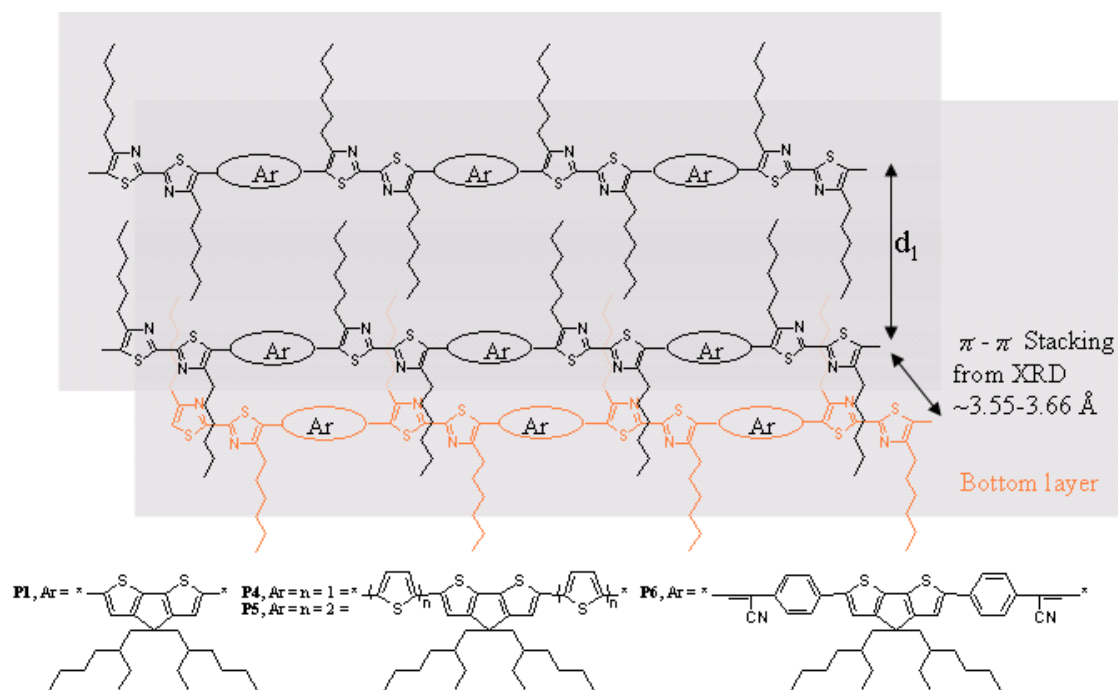
(b)
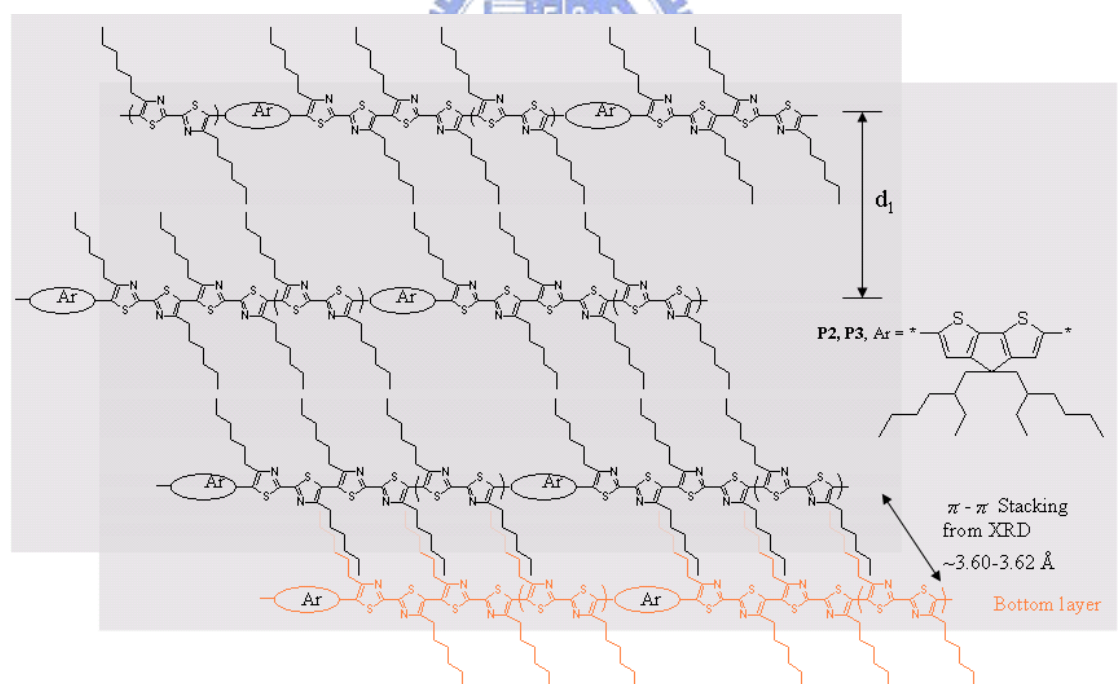
Figure 4.7 Schematic representation of proposed layered and packing models of copolymers (a) **P1**, **P4-P6** and (b) **P2-P3** with long side chains in the solid state. The distances between the segregation of the polymer main chains accounted for the interchain d_1 spacings. The distances between top and bottom layers of the backbones accounted for the π-π stacking at wide-angle d spacings.

4.3.5 Organic Photovoltaic Cell Properties

According to the previously described physical properties of **P1-P6**, these coplanar semiconducting copolymers **P1-P6** are suitable for PSC applications. To investigate the potential use of copolymers **P1-P6** in PSCs, bulk heterojunction PSC devices with a configuration of ITO/PEDOT:PSS/**P1-P6**:PCBM (1:1 w/w)/Ca/Al were fabricated from an active layer where copolymers **P1-P6** were blended with a complementary fullerene-based electron acceptor (PCBM) in a weight ratio of 1:1 (w/w) initially (and later followed with various weight ratios for the optimum copolymer). The photovoltaic properties of PSC devices containing copolymers **P1-P6**:PCBM (1:1 w/w) are listed in Table 4.4. Figures 4.8(a) and 4.8(b) illustrate *I-V* curves and EQE values, respectively, for PSC devices containing copolymers **P1-P6**:PCBM (1:1 w/w) under monochromatic illumination, where EQE is displayed as a function of wavelength. Due to the minor variations in open circuit voltage (V_{oc}) values (0.822-0.630 V) in **P1-P6**, Figure 4.8(a) demonstrates the sequence of the best power conversion efficiency (PCE) values for **P4**, **P1**, and **P2** according to their short circuit current density (I_{sc}) values of 7.70, 6.34, and 5.26 mA/cm^2, respectively. As shown in Figure 4.8(b), broader EQE curves for **P4**, **P1**, and **P2** covered almost the entire visible spectrum from 350 to 650 nm with the maximum EQE values of 60%, 50%, and 40%, respectively, which also explained for their high power conversion efficiency (PCE) values over 2.12%. Among these PSC devices containing copolymers **P1-P6**, the best performance was the PSC device fabricated by **P4**:PCBM (1:1 w/w) which reached an AM 1.5G power conversion efficiency (PCE) of 2.79%, with a short circuit current density (I_{sc}) of 7.70 mA/cm^2, an open circuit voltage (V_{oc}) of 0.683 V, and a fill factor (*FF*) of 0.53.

Due to the requirements of higher charge mobilities and better absorptions of

polymers in PSC devices,[131] the hole mobility values of copolymers **P1-P6** were (see Table 4.4) estimated from Equation 1 via space-charge limit current (SCLC) by fabricating a hole-only device.[132]

$$J = 9\varepsilon_0\varepsilon_r\mu V^2 / 8L^3 \tag{1}$$

where $\varepsilon_0\varepsilon_r$ is the permittivity of the polymer, μ is the carrier mobility, L is the device thickness. Ideally, I_{sc} was determined by the product of the photoinduced charge carrier density and the charge carrier mobility within the organic semiconductors.[22] Surprisingly, the hole mobilities of copolymers **P5-P6** were not as high as those of copolymers **P1-P4**, which was probably due to the lower molecular weights and worse solubilities resulting in inferior film-forming qualities, even though their optical band gaps were smaller than the other copolymers (**P1-P4**). Thus, due to the relatively lower hole mobilities and less light-harvesting capabilities at the longer absorption wavelength ranges of **P3**, **P5**, and **P6**, their PSC devices showed lower photocurrent values of 4.43, 3.03, and 2.68 mA/cm^2, respectively, in comparison with those containing **P1**, **P2**, and **P4**. This phenomenon of lower photocurrents further explained the worse EQE values and narrower absorption wavelength regions in the PSC devices containing copolymers **P3**, **P5**, and **P6**, where the EQE values of the visible spectra from 350 to 600 nm were only below 40%. Thus, not only optical properties but also charge transporting properties could be tuned by changing the lengths of oligothienyl and bithiazole-based main-chains. Comparing the FF values in **P1-P4** (excluding **P5-P6** due to their poor soubilities), the highest values of 53% in PSC devices containing copolymers **P1** and **P4** were obtained likely due to the more densely packed lamellar sheets in **P1** and **P4** (with smaller d_l spacing values of 11.9 and 15.1 Å resulting from highly ordered structural packings) than **P2** and **P3** with a longer d_l spacing value of 17.3 Å), as proven by XRD patterns previously.

The V_{oc} values covered a rather wide range among the PSC devices containing copolymers **P1**-**P6**, which were related to the differences of energy levels between the HOMO levels of the polymers and the LUMO levels of the acceptors.[22,25-26] Therefore, the PSC devices containing copolymers **P1**, **P2**, and **P3** (with HOMO energy levels of -5.40, -5.51, and -5.55 eV, respectively) showed slight increases of V_{oc} values (0.730, 0.777, and 0.822 V, respectively), which indicated that the insertion of more bithiazole units had some influence on the relationship between the HOMO levels of copolymers and the V_{oc} values of PSC devices. Moreover, followed by increasing the HOMO level of copolymer **P4** (from -5.40 to -5.07 V), the V_{oc} value of the PSC device containing **P4** was ca. 0.05 V lower than that containing **P1**, which was due to the insertion of the strong electron-donating thiophene moieties in the molecular structure of **P4**.

The AFM topographies of polymer blends (**P1**-**P6**:PCBM=1:1 w/w) were investigated by the casting films of DCB solutions as shown in Figure 4.9, where the images were obtained in a surface area of $2 \times 2 \ \mu m^2$ by the tapping mode. The phase image of blended copolymer **P4** showed coarse chain-like features across the surface, which were attributed to the domains of the highly stacked polymer chains of **P4**. In comparison with blended copolymers **P1**-**P3**, the solid film of blended copolymer **P4** revealed a rather uneven surface with a root mean square (RMS) roughness of 7.3 nm. The rougher surface of blended copolymer **P4** was caused by the better self-assembled stacking between the bithiazole and thiophene units, which enhanced both hole mobility and photocurrent.[51] Furthermore, the solid film of blended copolymer **P1** showed the moderate rough surface with a RMS roughness of 5.2 nm. However, increasing the numbers of bithiazole units with alkyl side-chains in **P2** and **P3**, the surfaces of polymer blends (**P2** and **P3**) showed RMS roughnesses of 3.3 and 2.1 nm, respectively. The smoother surfaces of blended copolymers **P2** and **P3**

compared with that of blended copolymer **P1** indicated that more side chains of copolymers **P2** and **P3** would disrupt the polymer crystallization in the polymer blends and led to lower photocurrents. It is worthy to mention that the solid films of blended copolymers **P5** and **P6** showed rather rough surfaces, but the large values of RMS roughnesses (6.9 and 9.3 nm) were contributed from the aggregation of polymer chains due to their poor solubilities, which reduced the interfaces between donor (copolymers) and acceptor (PCBM) significantly. Owing to the unfavorable morphologies for charge transport offered by poor solubilities, the PSC devices based on **P5** and **P6** gave relatively low current densities (I_{sc}) as shown in Table 4. Therefore, excluding **P5** and **P6**, the blended copolymers (**P1-P4**:PCBM=1:1 w/w) have the same order of PCE values as those of root mean square (RMS) roughnesses in AFM, i.e., **P4** (7.3 nm) > **P1** (5.2 nm) > **P2** (3.3 nm) > **P3** (2.1 nm).

Since the best performance of PSC devices fabricated by polymer blends **P1-P6**:PCBM (1:1 w/w) was made of **P4**, current-voltage characteristics of PSC devices as a function of blended copolymer **P4**:PCBM in various weight compositions are shown in Figure 4.10 and Table 4.5. The optimum photovoltaic performance with the maximum PCE value of 3.04% (V_{oc} = 0.70 V, I_{sc} = 8.00 mA/cm^2, *FF* = 53.7%) was obtained in the PSC device having a weight ratio of **P4**:PCBM=1:2. Using lower weight ratios of PCBM in blended copolymers **P4**:PCBM (**P4**:PCBM=1:0.5 and 1:1 w/w) led to reductions in the I_{sc} values due to the inefficient charge separation and electron transporting properties, resulting in the lower PCE results.[131b] However, loading larger weight ratios of PCBM in blended copolymers **P4**:PCBM (1:3 and 1:4 w/w) also reduced the I_{sc} and PCE values, which could be probably attributed to the increased aggregation of PCBM so as to influence the separation of charges. Furthermore, an unbalanced charge transporting property was introduced due to the

large PCBM ratio. Hence, both I_{sc} and PCE values decreased with larger PCBM molar ratios of 1:3 and 1:4 (w/w) because of the two reasons described here.[133a] Therefore, the most efficient PSC device with the maximum PCE value of 3.04% was established by the blended copolymer **P4** with a weight ratio of **P4**/PCBM=1:2 in this report, which has a similar result as the PSC devices containing thiophene-based polymers.[67,133b]

Table 4.4 Photovoltaic Properties of PSC Devices Containing an Active Layer of P1-P6:PCBM = 1:1 (w/w) with the Configuration of ITO/PEDOT:PSS/Polymer:PCBM/Ca/Al[a]

Active layer[b] (**Polymer**:PCBM=1:1)	V_{oc} (V)	I_{sc} (mA/cm^2)	FF (%)	PCE (%)	Mobility (cm^{2}V^{-1}s^{-1})	Max. EQE (%)
P1	0.730	6.34	53.0	2.45	$5.4×10^{-4}$	50
P2	0.777	5.26	51.9	2.12	$5.6×10^{-4}$	40
P3	0.822	4.43	49.3	1.78	$4.7×10^{-4}$	36
P4	0.683	7.70	53.0	2.79	$5.2×10^{-4}$	60
P5	0.729	3.03	36.1	0.80	$3.9×10^{-4}$	28
P6	0.630	2.68	32.0	0.54	$3.3×10^{-4}$	28

[a] Measured under 100 mW/cm^2 of AM 1.5 irradiation. [b] Active layer with the weight ratio of **P1-P6**:PCBM = 1:1.

Table 4.5 Photovoltaic Parameters[a] for Bulk-Heterojunction PSC Devices Containing Different Weight Ratios of Blended Copolymer P4:PCBM

Weight ratios of blended **P4**:PCBM	V_{oc} (V)	I_{sc} (mA/cm^2)	FF (%)	PCE (%)
1:0.5	0.675	5.32	61.0	2.19
1:1	0.683	7.70	53.0	2.79
1:2	0.700	8.00	53.7	3.04
1:3	0.700	6.96	48.3	2.35
1:4	0.705	6.25	51.0	2.25

[a] PSC devices with the configuration of ITO/PEDOT:PSS/Polymer:PCBM/Ca/Al were measured under AM 1.5 irradiation, 100 mW/cm^2.

(a)
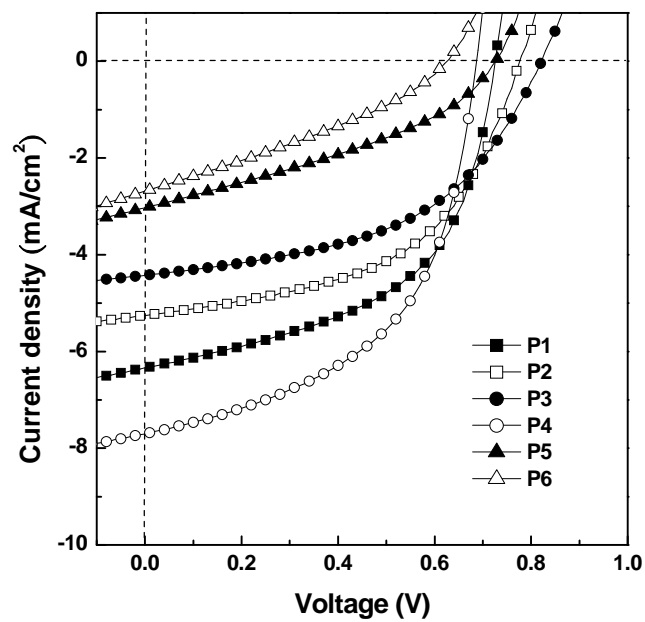
(b)

Figure 4.8 (a) *I*-V curves (under simulated AM 1.5 solar irradiation) and (b) EQE wavelength dependencies of PSC devices with an active layer of blended copolymers **P1**-**P6**:PCBM (1:1 w/w).
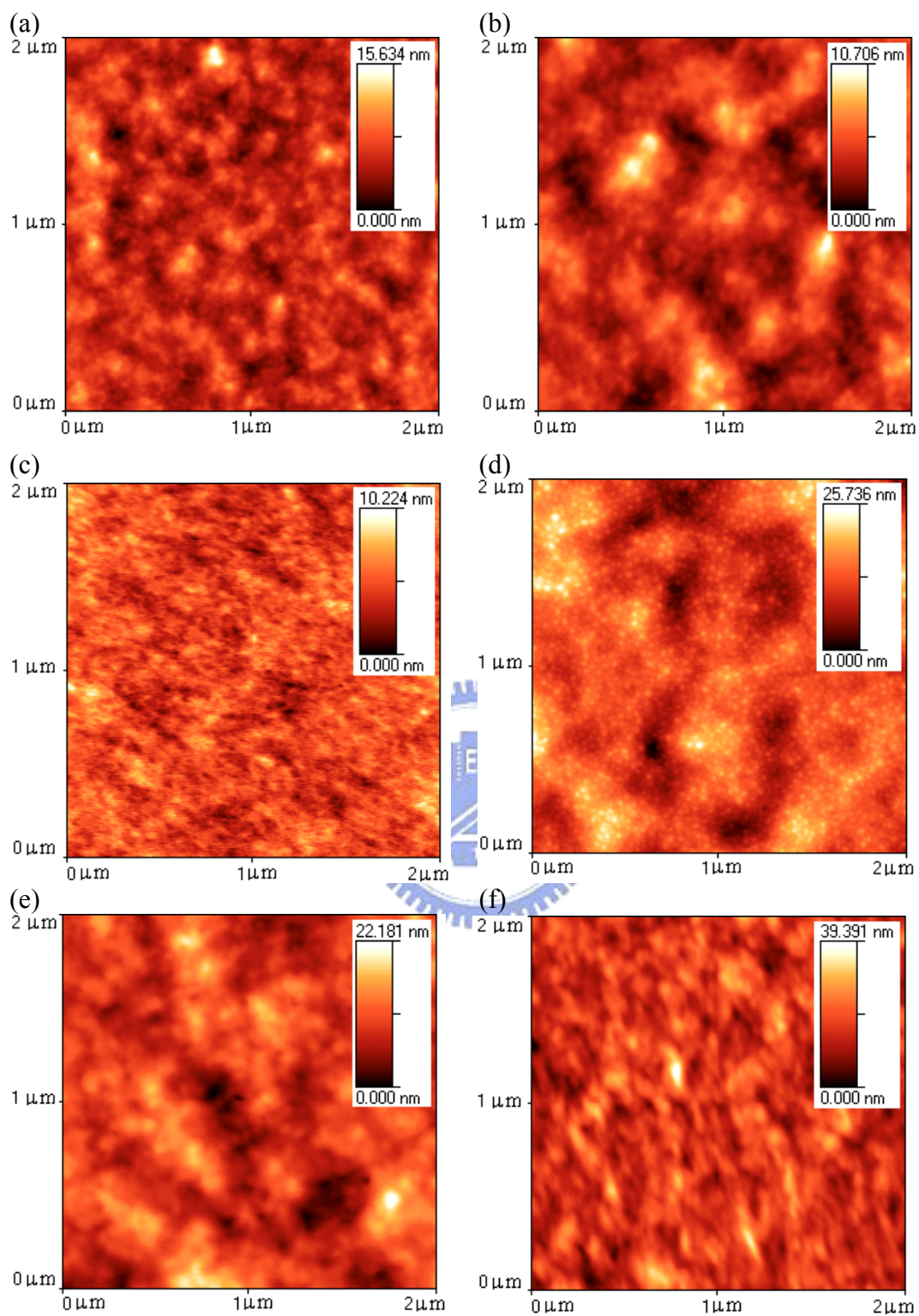
Figure 4.9 AFM images for solid films of blended copolymers (a) **P1**, (b) **P2**, (c) **P3**, (d) **P4**, (e) **P5**, and (f) **P6** with PCBM (1:1 w/w) as-cast from DCB solutions.

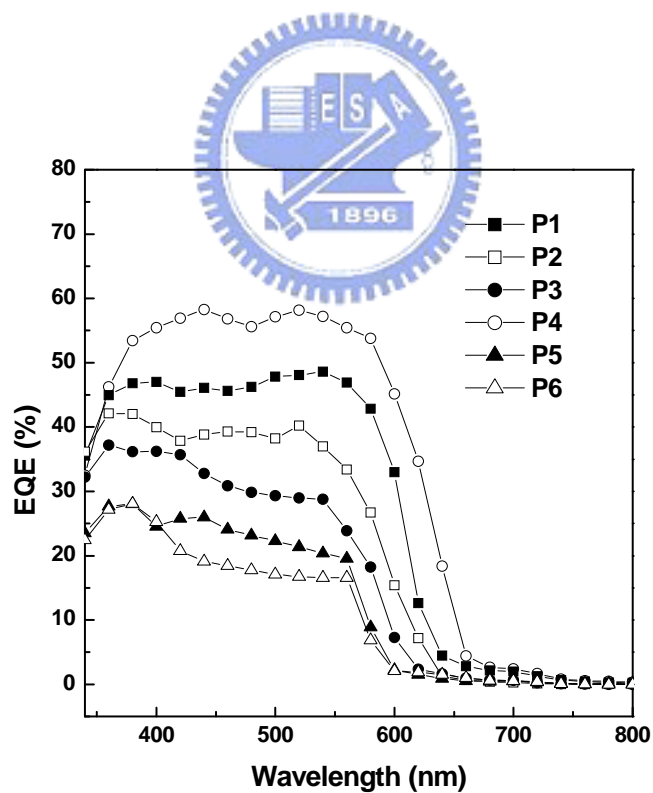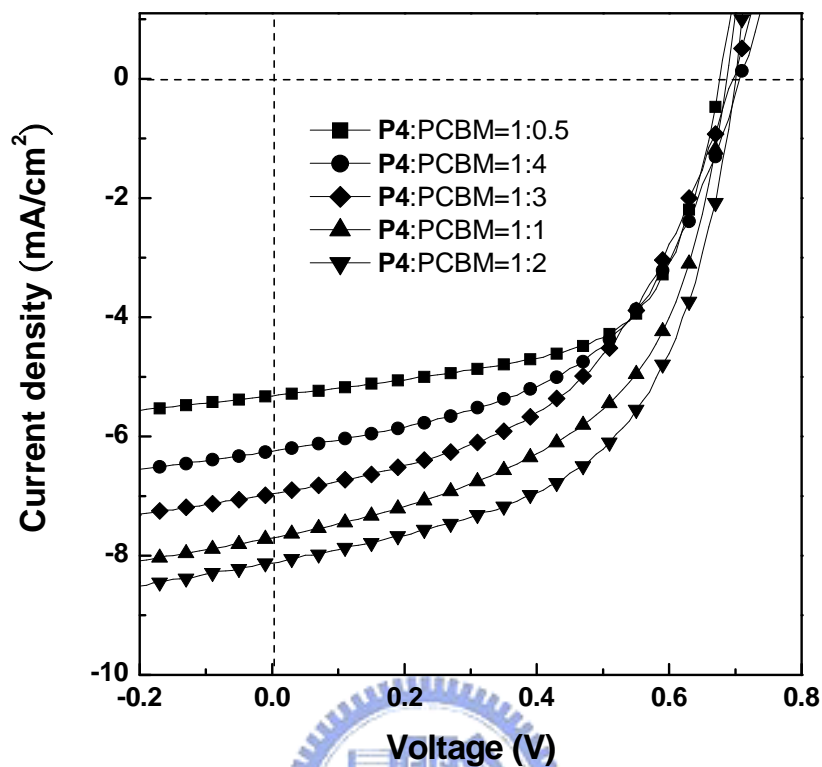**Figure 4.10** *I*-V curves of PSC devices containing an active layer of **P4**:PCBM (w/w) with different weight ratios under simulated AM 1.5 solar irradiation.

4.4 Conclusions

Using the concept of incorporating electron-withdrawing groups in the donor-acceptor conjugated copolymers, we have successfully synthesized six cyclopentadithiophene-bithiazole-based copolymers (**P1-P6**) employing oligo(bithiazole), bithiazole-oligo(thiophene), and diarylene-cyanovinylene-bithiazole groups by palladium (0)-catalyzed Stille coupling reactions. The band gaps and HOMO/LUMO levels of these resulting copolymers can be finely tuned as demonstrated in the exploration of optical absorption and electrochemical properties. In powder X-ray diffraction (XRD) measurements, these copolymers exhibited obvious diffraction features indicating highly ordered π-π stacking in the solid state. These copolymers also showed excellent charge-transporting properties with hole

mobilities of 3.3 - 5.6×10^{-4} $cm^2V^{-1}s^{-1}$ and good processabilities for PSC applications. A preliminary PSC device based on the blended copolymer **P4**:PCBM=1:2 (w/w) had the maximum power conversion efficiency (PCE) value up to 3.04%, which gave the best photovoltaic performance with the values of I_{sc} = 8.00 mA/cm^2, FF = 53.7%, and V_{oc} = 0.70 V as well as a peak EQE value of 60% under simulated AM1.5 solar illumination. These copolymers demonstrate a novel family of conjugated copolymers along the path toward achieving low cost PSC applications. Currently, deeper investigation for better photovoltaic properties is underway to further optimize the PSC performance.

Chapter 5 Conclusion

Souble conjugated donor-acceptor low-band-gap copolymers derived from 9,9-dihexylfluorene (FO) and phenothiazine-arylcyanovinyl units were synthesized by palladium (0)-catalyzed Suzuki coupling reactions and characterized by NMR, FTIR, and elemental analyses. The more heterocyclic units and cyano-groups incorporated into phenothiazine derivatives, the stronger strength of intramolecular charge-transfer interaction. Thus, the optical and electrochemical properties of the copolymers were induced to visible and even further to near infrared absorption with narrow band gaps, which the lowest result were 1.55 eV. Bulk heterojunction PVC devices fabricated from a thin film composed of a blend of **FO$_1$-PT** polymer derivatives and PCBM, with the configuration of ITO/PEDOT:PSS/(**FO$_1$-PT**:PCBM = 1:4)/LiF/Al, showed the preliminary results of the PVC devices, and their optoelectronic performance can also be much improved in the future.

Using the concept of incorporating electron-withdrawing groups in the donor-acceptor conjugated polymers, we have successfully synthesized five cyclopentadithiophene-based copolymers employing arylcyanovinyl and keto groups in different molar ratios by palladium (0)-catalyzed Suzuki coupling reactions. In powder X-ray diffraction (XRD) measurements, these copolymers exhibited obvious diffraction features indicating a highly ordered π-π stacking in the solid state. Preliminary PSC devices based on these five copolymers blended with PCBM acceptors (1:4 w/w) had the power conversion efficiency up to 0.77%, which gave the best performance with the values of I_{sc} = 2.36 mA/cm^2, FF = 38%, and V_{oc} = 0.84 V. Furthermore, this study provides novel conception that the HOMO energy levels can be reduced via the syntheses of merging with electron-withdrawing functional groups and thus the open-circuit voltage can be considerably enhanced, which will

significantly improve the low V_{oc} values mainly possessed by most CPDT-based narrow band-gap polymers.

Using the concept of incorporating electron-withdrawing groups in the donor-acceptor conjugated copolymers, we have successfully synthesized six cyclopentadithiophene-bithiazole-based copolymers (**P1-P6**) employing oligo(bithiazole), bithiazole-oligo(thiophene), and diarylene-cyanovinylene-bithiazole groups by palladium (0)-catalyzed Stille coupling reactions. In powder X-ray diffraction (XRD) measurements, these copolymers exhibited obvious diffraction features indicating highly ordered π-π stacking in the solid state. These copolymers also showed excellent charge-transporting properties with hole mobilities of 3.3 - 5.6×10^{-4} cm^{2}V^{-1}s^{-1} and good processabilities for PSC applications. A preliminary PSC device based on the blended copolymer **P4**:PCBM=1:2 (w/w) had the maximum power conversion efficiency (PCE) value up to 3.04%, which gave the best photovoltaic performance with the values of I_{sc} = 8.00 mA/cm^2, FF = 53.7%, and V_{oc} = 0.70 V as well as a peak EQE value of 60% under simulated AM1.5 solar illumination. These copolymers demonstrate a novel family of conjugated copolymers along the path toward achieving low cost PSC applications. Currently, deeper investigation for better photovoltaic properties is underway to further optimize the PSC performance.

References

(1) Spanggaard, H.; Krebs, F. C. *Solar Energy Materials & Solar Cells* **2004**, *83*, 125.

(2) Becquerel, A.E. *Compt. Rend. Acad. Sci. 1839,* **9,** 145.

(3) Smith, W. *Nature* **1873,** *7,* 303.

(4) Pochettino, A. *Acad. Lincei Rend.* **1906,** *15,* 355.

(5) Volmer, M. *Ann. Physik 1913,* **40,** 775.

(6) Borsenberger, P.M.; Weiss, D.S. *Organic Photoreceptors For Imaging Systems, Marcel Dekker,* New York, **1993**.

(7) Bube, R.H. *Photoconductivity of Solids,* Wiley, New York, **1960**.

(8) Anthoe, S. *Rom. Rep. Phys.* **2002,** *53,* 427.

(9) Tang, C. W. *Appl. Phys. Lett.* **1986,** *48,* 183.

(10) Cozzens, R.F. in: D.A. Seanor, (Ed.), *Electrical Properties of Polymer, Academic Press,* New York, **1982**, p. 93 (Chapter 3).

(11) Heeger, A.J. *J. Phys. Chem.* **2001,** *105,* 8475.

(12) Weinberger, B.R.; Akhtar, M.; Gau, S.C. *Synth. Met.* **1982,** *4,* 187.

(13) Glenis, S.; Tourillon, G.; Garnier, F. *Thin Solid Films* **1986,** *139,* 221.

(14) Karg, S.; Riess, W.; Dyakonov, V.; Schwoerer, M. *Synth. Met.* **1993,** *54,* 427.

(15) Marks, R.N.; Halls, J.J.M.; Bradley, D.D.C.; Friend, R.H.; Holmes, A.B. *J. Phys.-Condens. Matter* **1994,** *6,* 1379.

(16) Antoniadis, H.; Hsieh, B.R.; Abkowitz, M.A.; Jenekhe, S.A.; Stolka, M. *Synth. Met.* **1994,** *62,* 265.

(17) Kietzke, T.; Egbe, D. A. M.; Hörhold, H. H.; Neher, D. *Macromolecules* **2006,** *39,* 4018.

(18) Frankevich, E.L.; Zakhidov, A.; Yoshino, K. *Phys. Rev. B* **1996,** *53,* 4498.

(19) Brabec, C. J.; Sariciftci, N. S.; Hummelen, J. C. *Adv. Funct. Mater.* **2001,** *11,* 15.

(b) Chen, C. P.; Chan, S. H.; Chao, T. C.; Ting, C.; Ko, B. T. *J. Am. Chem. Soc.* **2008,** *130,* 12828-12833.

(20) Thompson, B. C.; Fréchet, J. M. J. *Angew. Chem. Int. Ed.* **2008,** *47, 58.

(21) Hoppe, H.; Sariciftci, N. S. *J. Mater. Res.* **2004,** *19,* 1924.

(22) Günes, S.; Neugebauer, H.; Sariciftci, N. S. *Chem. Rev.* **2007,** *107,* 1324.

(23) Rostalski, J.; Meissner, D. *Sol. Energy Mater. Sol. Cells* **2000**, *61*, 87.

(24) Parker, I. *J. Appl. Phys.* **1994**, *75*, 1656.

(25) Brabec, C. J.; Cravino, A.; Meissner, D.; Sariciftci, N. S.; Fromherz, T.; Minse, M.; Sanchez, L.; Hummelen, J. C. *Adv. Funct. Mater.* **2001**, *11,* 374.

(26) Scharber, M.; Mu¨hlbacher, D.; Koppe, M.; Denk, P.; Waldauf, C.; Heeger, A. J.; Brabec, C. *Adv. Mater.* **2006**, *18*, 789.

(27) Mallairas, G. G.; Salem, J. R.; Brock, P. J.; Scott, J. C. *J. Appl. Phys.* **1998**, *84,* 1583.

(28) Liu, L.; Shi, Y.; Yang, Y. *Adv. Funct. Mater.* **2001**, *11*, 420.

(29) Sugiyama, K.; Ishi, H.; Ouchi, Y.; Seki, K. *J. Appl. Phys.* **2000**, *87*, 295.

(30) Brown, J. M.; Kim, J. S.; Friend, R. H.; Caciolli, F.; Daik, R.; Feast, W. J. *Appl. Phys. Lett.* **1999**, *75*, 1679.

(31) Brabec, C. J.; Shaheen, S. E.; Winder, C.; Sariciftci, N. S.; Denk, P. *Appl. Phys. Lett.* **2002**, *80*, 1288.

(32) Van Duren, J.; Yang, X.; Loos, J.; Bulle-Lieuwma, C. W. T.; Sievel, A. B.; Hummelen, J. C.; Janssen, R. A. J. *Adv. Funct. Mater.* **2004**, *14*, 425.

(33) Hoppe, H.; Niggemann, M.; Winder, C.; Kraut, J.; Hiesgh, R.; Hinsch, A.; Meissner, D.; Sariciftci, N. S. *Adv. Funct. Mater.* **2004**, *14*, 1005.

(34) Arias, A. C.; MacKenzie, J. D.; Stevenson, R.; Halls, J. M.; Inbasekaran, M.; Woo, E. P.; Richards, D.; Friend, R. H. *Macromolecules* **2001,** *34,* 6005.

(35) Dimitrakopoulos, C.D.; Mascaro, D.J. *IBM J. Res. Dev.* **2001,** *45,* 11.

(36) Schilinsky, P.; Waldauf, C.; Hauch, J.; Brabec, C.J. *J. Appl. Phys.* **2004,** *95,* 2816.

(37) Riedel, I.; Dyakonov, V. *Phys. Status Solidi A* **2004**, *201*, 1332.

(38) Maenning, B.; Drechssel, J.; Gebeyehu, D.; Simon, P.; Kozlowski, F.; Werner, A.; Li, F.; Gundmann, S.; Sonntag, S.; Koch, M.; Leo, K.; Pfeiffer, M.; Hoppe, H.; Meissner, D.; Sariciftci, S.; Riedel, I.; Dyakonov, V.; Parisi, J. *J. Appl. Phys. A* **2004**, *79*, 1.

(39) Hoppe, H.; Sariciftci, N.S. *J. Mater. Chem.* **2006,** *16,* 45.

(40) Bundgaard, E.; Krebs, F. C. *Solar Energy Materials & Solar Cells* **2007,** *91,* 954.

(41) Dhanabalan, A.; van Duren, J.K.J.; van Hal, P.A.; van Dogen, J.L.J.; Janssen, R.A.J. *Adv. Funct. Mater.* **2001,** *11,* 255.

(42) Winder, C.; Sariciftci, N.S. *J. Mater. Chem.* **2004,** *14,* 1077.

(43) Kitamura, C.; Tanaka, S.; Yamashita, Y. *Chem. Mater.* **1996,** *8,* 570.

(44) Karikomi, M.; Kitamura, C.; Tanaka, S.; Yamashita, Y. *J. Am. Chem. Soc.* **1995,** *117,* 6791.

(45) Jayakannan, M.; van Hal, P.A.; Janssen, R.A.J. *J. Pol. Sci. A Pol. Chem.* **2002,** *40,* 251.

(46) Yang, L.; Feng, J.K.; Ren, A.M. *Polymer* **2005,** *46,* 10970.

(47) Chen, M.; Perzon, E.; Andersson, M.R.; Marcinkevicius, S.; Jönsson, S.K.M.; Fahlman, M.; Berggren, M. *Appl. Phys. Lett.* **2004,** *84,* 3570.

(48) Ajayaghosh, A. *Chem. Soc. Rev.* **2003,** *32,* 181.

(49) Glenis, S.; Tourillon, G.; Garnier, F. *Thin Solid Films* **1984,** *122,* 9.

(50) Sariciftici, N. S.; Smilowitz, L.; Heeger, A. J. *Science* **1992,** *258,* 1474.

(51) Li, G.; Shrotriya, V.; Huang, J.; Yao, Y.; Moriarty, T.; Emery, K.; Yang, Y. *Nat. Mater.* **2005,** *4,* 864.

(52) (a) Ma, W.; Yang, C.; Gong, X.; Lee, K.; Heeger, A. J. *Adv. Funct. Mater.* **2005,** *15,* 1617. (b) Koppe, M.; Scharber, M.; Brabec, C.; Duffy, W.; Heeney, M.; McCulloch, I. *Adv. Funct. Mater.* **2007,** *17,* 1371

(53) Reyes-Reyes, M.; Kim, K.; Dewald, J.; Lópex-Sandoval, M.; Avadhanula, A.; Curran, S.; Carrol, D. S. *Org. Lett.* **2005,** *7,* 5749.

(54) Waltman, R. J.; Bargon, J.; Diaz, A. F. *J. Phys. Chem.* **1983,** *87,* 1459.

(55) Thompson, B. C.; Kim, Y. G.; Reynolds, J. R. *Macromolecules* **2005,** *38,* 5359.

(56) Colladet, K.; Fourier, S.; Clej, T. J.; Lutsen, L.; Gelan, J.; Vanderzande, D.; Nguyen, L. H.; Neugebauer, H.; Sariciftci, S.; Aguirre, A.; Janssen, G.; Goovaerts, E. *Macromolecules* **2007,** *40,* 65.

(57) Roncali, J. *Macromol. Rapid Commun.* **2007,** *28,* 1761.

(58) Coppo, P.; Turner, M. L. *J. Mater. Chem.* **2005,** *15,* 1123.

(59) Cho, N. S.; Park, J. H.; Lee, S. K.; Lee, J.; Shim, H. K. *Macromolecules* **2006,** *39,* 177.

(60) Tang, W.; Kietzke, T.; Vemulamada, P.; Chen, Z. K. *J. Polym. Sci. Part A: Polym. Chem.* **2007,** *45,* 5266.

(61) Zou, Y.; Wu, W.; Sang, G.; Yang, Y.; Liu, Y.; Li, Y. *Macromolecules* **2007,** *40,* 7231.

(62) Kraak, A.; Wieserma, A. K.; Jordens, P.; Wynberg, H. *Tetrahedron* **1968,** *24,* 3381.

(63) Berlin, A.; Brenna, E.; Pagani, G. A.; Sannicolo, F. *Synth. Met.* **1992**, *51*, 287.

(64) Coppo, P.; Cupertino, D. C.; Yeates, S. G.; Turner, M. L. *Macromolecules* **2003,** *36,* 2705.

(65) Cremer, L. D.; Vandeleene, S.; Maesen, M.; Verbiest, T.; Koeckelberghs, G. *Macromolecules* **2008,** *41,* 591.

(66) Mühlbacher, D.; Scharber, M.; Morana, M.; Zhu, Z.; Waller, D.; Gaudiana, R.; Brabec, C. *Adv. Mater.* **2006,** *18,* 2884.

(67) Peet, J.; Kim, J. Y.; Coates, N. E.; Ma, W. L.; Moses, D.; Heeger, A. J.; Bazan, G. *Nat. Mater.* **2007,** *6*, 497.

(68) Mamada, M.; Nishida, J.; Kumaki, D.; Tokito, S. *Chem. Mater.* **2007,** *19,* 5404.

(69) Osaka, I.; Sauvé, G.; Zhang, R.; Kowalewski, T.; McCullough, R. D. *Adv. Mater.* **2007**, *19,*.

(70) (a) Lee, J.; Jung, B. J.; Lee, S. K.; Lee, J. I.; Cho, H. J.; Shim, H. K. *J. Polym. Sci., Part A: Polym. Chem.* **2005,** *43,* 1845-1857. (b) Wong, W. Y.; Wang, X. Z.; He, Z.; Chan, K. K.; Djurii, A. B.; Cheung, K. Y.; Yip, C. T.; Ng, A. M. C.; Xi, Y. Y.; Mak, C. S. K.; Chan, W. K. *J. Am. Chem. Soc.* **2007,** *129,* 14372. (b) Wong, W. Y.; Wang, X. Z.; He, Z.; Chan, K. K.; Djurisic, A. B.; Cheung, K. Y.; Yip, C. T.; Ng, A. M. C.; Xi, Y. Y.; Mak, C. S. K.; Chan, W. K. *J. Am. Chem. Soc.* **2007,** *129,* 14372.

(71) Coakley, K. M.; McGehee, M. D. *Chem. Mater.* **2004,** *16,* 4533.

(72) Yu, G.; Gao, J.; Hummelen, J.C.; Wudl, F.; Heeger, A.J. *Science* **1995,** *270,* 1789.

(73) Zhang, F.; Svensson, M.; Andersson, M.R.; Maggini, M.; Bucella, S.; Menna, E.; Inganäs O. *Adv. Mater.* **2001,** *13,* 1871.

(74) van Mullekom, H. A. M.; Vekemans, J. A. J. M.; Havinga, E. E.; Meijer, E. W. *Mater. Sci. Eng.* **2001,** *32,* 1.

(75) Lai, R. Y.; Kong, X.; Jenekhe, S. A.; Bard, A. J. *J. Am. Chem. Soc.* **2003,** *125,* 12631.

(76) Roncali, J. *Chem. Rev.* **1997,** *97,* 173.

(77) Lee, J.; Cho, N. S.; Lee, J.; Lee, S. K.; Shim, H. K. *Synthetic Metals* **2005,** *155,* 73.

(78) Ranger, M.; Rondeau, D.; Leclerc, M. *Macromolecules* **1997,** *30,* 7686.

(79) Jin, S. H.; Kim, M. Y.; Koo, D. S.; Kim, Y. I. *Chem. Mater.* **2004,** *16,* 3299.

(80) Kong, X.; Kulkarni, A. P.; Jenekhe, S. A. *Macromolecules* **2003,** *36,* 8992.

(81) Xia, Y.; Luo, J.; Deng, X.; Li, X.; Li, D.; Zhu, X.; Yang, W.; Cao, Y. *Macromol. Chem. Phys.* **2006,** *207,* 511.

(82) Kulkarni, A. P.; Jenekhe, S. A. *Macromolecules* **2003,** *36,* 5285.

(83) Cao, D.; Liu, Q.; Zeng, W.; Han, S.; Peng, J.; Liu, S. *Macromolecules* **2006,** *39,* 8347.

(84) Huang, F.; Hou, L.; Wu, H.; Wang, X.; Shen, H.; Cao, W.; Yang, W.; Cao, Y. *J. Am. Chem. Soc.* **2004,** *126,* 9845.

(85) Wang, F.; Luo, J.; Yang, K.; Chen, J.; Huang, F.; Cao, Y. *Macromolecules* **2005,** *38,* 2253.

(86) Svensson, M.; Zhang, F.; Veenstra, S. C.; Verhees, W. J. H.; Hummelen, J. C.; Kroon, J. M.; Inganas, O.; Andersson, M. R. *Adv. Mater.* **2003,** *15,* 988.

(87) Chen, Y. Y.; Tao, Y. T.; Lin, H. C. *Macromolecules* **2006,** *39,* 855.

(88) Janietz, S.; Bradley, D. D.C.; Grelly, M.; Giebeler, C.; Inbasekaran, M.; Woo, E. P. *Appl Phys Lett* **1998,** *73,* 2453.

(89) Hou, Q.; Zhou, Q.; Zhang, Y.; Yang, W.; Yang, R.; Cao, Y. *Macromolecules* **2004,** *37,* 6299.

(90) Koster, L. J. A.; Mihailetchi, V. D.; Blom, P. W. M. *Appl. Phys. Lett.* **2006,** *88,* 093511.

(91) Coffey, D. C.; Reid, O. G.; Rodovsky, D. B.; Bartholomew, G. P.; Ginger, D. S. *Nano. Lett.* **2007,** *7,* 738.

(92) Kietzke, T.; Shin, R. Y. C.; Ayuk Mbi Egbe, D.; Chen, Z. K.; Sellinger, A. *Macromolecules* **2007,** *40,* 4424.

(93) Uhrich, C.; Schueppel, R.; Petrich, A.; Pfeiffer, M.; Leo, K.; Brier, E.; Kilickiran, P.; Baeuerle, P. *Adv. Funct. Mater.* **2007,** *17,* 2991.

(94) Bouclé, J.; Ravirajanac, P.; Nelson, J. *J. Mater. Chem.* **2007,** *17,* 3141.

(95) Beek, W. J. E.; Wienk, M. M.; Janssen, R. A. J. *Adv. Funct. Mater.* **2006,** *16,* 1112.

(96) Chabinyc, M. L.; Street, R. A.; Northrup, J. E. *Appl. Phys. Lett.* **2007,** *90,* 123508.

(97) Tsami, A.; Yang, X. H.; Farrell, T.; Neher, D.; Holder, E. *J. Polym. Sci. Part A: Polym. Chem.* **2008,** *46,* 7794.

(98) XIA, P. F.; Lu, J. P.; Kwok, C. H.; Fukutani, H.; Wong, M. S.; Tao, Y. *J. Polym. Sci. Part A: Polym. Chem.* **2009,** *47,* 137.

(99) Zhu, Z.; Waller, D.; Gaudiana, R.; Morana, M.; Mü1hlbacher, D.; Scharber, M.; Brabec, C. *Macromolecules* **2007,** *40,* 1981.

(100)   Moulé, A. J.; Tsami, A.; Bünnagel, T. W.; Forster, M.; Kronenberg, N. M.; Scharber, M.; Koppe, M.; Morana, M.; Brabec, C. J.; Meerholz, K.; Scherf, U. *Chem. Mater.* **2008,** *20,* 4045.

(101)   Xiao, S.; Zhou, H.; You, W. *Macromolecules* **2008,** *41,* 5688.

(102)   Zhan, X.; Tan, Z.; Domercq, B.; An, Z.; Zhang, X.; Barlow, S.; Li, Y.; Zhu, D.; Kippelen, B.; Marder, S. R. *J. Am. Chem. Soc.* **2007,** *129,* 7246.

(103)   Zhang, M.; Tsao, H. N.; Pisula, W.; Yang, C.; Mishra, A. K.; Müllen, K. *J. Am. Chem. Soc.* **2007,** *129,* 3472.

(104)   Lambert, T. L.; Ferraris, J. P. *J. Chem. Soc. Chem. Commun.* **1991,** 752.

(105)   Brzezinski, J. Z.; Reynolds, J. R. *Synthesis* **2002,** *8,* 1053.

(106)   Chen, C. P.; Chan, S. H.; Chao, T. C.; Ting, C.; Ko, B. T. *J. Am. Chem. Soc.* **2008,** *130,* 12828.

(107)   Asawapirom, U.; Scherf, U. *Macromol. Rapid. Commun.* **2001,** *22,* 746.

(108)   Liao, L.; Dai, L.; Smith, A.; Durstock, M.; Lu, J.; Ding, J.; Tao, Y. *Macromolecules* **2007,** *40,* 9406.

(109)   Yang, J. S.; Liau, K. L.; Tu, C. W.; Hwang, C. Y. *J. Phys. Chem. A* **2005,** *109,* 6450.

(110)   Pal, B.; Yen, W. C.; Yang, J. S.; Chao, C. Y.; Hung, Y. C.; Lin, S. T.; Chuang, C. H.; Chen, C. W.; Su, W. F. *Macromolecules* **2008,** *41,* 6664.

(111)   Leeuw, D. M.; Simenon, M. M. J.; Brown, A. R.; Einhard, R. E. F. *Synth. Met.* **1997,** *87,* 53.

(112)   Mihailetchi, V. D.; Duren, J. K. J. v.; Blom, P. W. M.; Hummelen, J. C.; Janssen, R. A. J.; Kroon, J. M.; Rispens, M. T.; Verhees, W. J. H.; Wienk, M. M. *Adv. Funct. Mater.* **2003,** *13,* 43.

(113)   Lu, G.; Usta, H.; Risko, C.; Wang, L.; Facchetti, A.; Ratner, M. A.; Marks, T. J. *J. Am. Chem. Soc.* **2008,** *130,* 7670.

(114)   Yasuda, T.; Sakai, Y.; Aramaki, S.; Yamamoto, T. *Chem. Mater.* **2005,** *17,* 6060.

(115)   Yamamoto, T.; Arai, M.; Kokubo, H.; Sasaki, S. *Macromolecules* **2003,** *36,* 7986.

(116)   Yamamoto, Y.; and Lee, B. L. *Macromolecules* **2002,** *35,* 2993.

(117)   Ong, B. S.; Wu, Y. L.; Liu, P.; Gardner, S. *J. Am. Chem. Soc.* **2004,** *126,* 3378.

(118)   Morana, M.; Wegscheider, M.; Bonanni, A.; Kopidakis, N.; Shaheen, S.; Scharber, M.; Zhu, Z.; Waller, D.; Gaudiana, R.; Brabec, C. *Adv. Funct. Mater.* **2008,** *18,* 1757.

(119)   Huo, L.; Tan, Z.; Wang, X.; Zhou, Y.; Han, M. F.; Li, Y. F. *J. Polym. Sci.*

Part A: Polym. Chem. **2008,** *46,* 4038.

(120)   Morteani, A. C.; Sreearunothai, P.; Herz, L. M.; Friend, R. H.; Silva, C. *Phys. Rev. Lett.* **2004,** *92,* 247402.

(121)   Blom, P. W. M.; deJong, M. J. M.; vanMunster, M. G. *Phys. Rev. B* **1997,** *55,* R656.

(122)   Dunlap, D. H.; Parris, P. E.; Kenkre, V. M. *Phys. Rev. Lett.* **1996,** *77,* 542.

(123)   Moulé, A. J.; Bonekamp, J. B.; Meerholz, K. *J. Appl. Phys.* **2006,** *100,* 094503.

(124)   Markov, D. E.; Hummelen, J. C.; Blom, P. W.; Sieval, A. B. *Phys. Rev. B* **2005,** *72,* 045216.

(125)   Kietzke, T.; Horhold, H.; Neher, D. *Chem. Mater.* **2005,** *17,* 6532.

(126)   (a) Hou, J. H.; Tan, Z.; Yan, Y.; He, Y.; Yang, C.; Li, Y. *J. Am. Chem. Soc.* **2006,** *128,* 4911. (b) Chang, Y. T.; Hsu, S. L.; Chen, G. Y.; Su, M. H.; Singh, T. A.; Diau, E. W. G.; Wei, K. H. *Adv. Funct. Mater.* **2008,** *18,* 1. (c) Demadrille, R.; Delbosc, N.; Kervella, Y.; Firon, M.; Bettignies, R. D.; Billon, M.; Rannou, P. Pron, A. *J. Mater. Chem.* **2007,** *17,* 4661. (d) Qin, Y.; Kim, J. Y.; Frisbie, C. D.; Hillmyer, M. A. *Macromolecules* **2008,** *41,* 5563.

(127)   (a) Hou, J. H.; Park, M.-H.; Zhang, S.; Yao, Y.; Chen, L.-M.; Li, J.-H.; Yang, Y. *Macromolecules* **2008,** *41,* 6012. (b) Chan, S. H.; Chen, C. P.; Chao, T. C.; Ting, C.; Lin, C. S.; Ko, B. T. *Macromolecules* **2008,** *41,* 5519. (c) Liu, C. L.; Tsai, J. H.; Lee, W. Y.; Chen, W. C.; Jenekhe, S. A. *Macromolecules* **2008,** *41,* 6952.

(128)   (a) Naraso.; Wudl, F. *Macromolecules* **2008,** *41,* 3169. (b) Cao, J.; Kampf, J. W.; Curtis, M. D. *Chem. Mater.* **2003,** *15,* 404. (c) Politis, J. K.; Curtis, M. D.; Gonzalez, L.; Martin, D. C.; He, Y.; Kanicki, J. *Chem. Mater.* **1998,** *10,* 1713.

(129)   (a) Yamamoto, T.; Suganuma, H.; Maruyama, T.; Inoue, T.; Muramatsu, Y.;

Arai, M.; Komarudin, D.; Ooba, N.; Tomaru, S.; Sasaki, S.; Kubota, K. *Chem. Mater.* **1997,** *9,* 1217. (b) Yamamoto, T.; Otsuka, S.; Namekawa, K.; Fukumoto, H.; Yamaguchi, I.; Fukuda, T.; Asakawa, N.; Yamanobe, T.; Shiono, T.; Cai, Z. *Polymer* **2006,** *47,* 6038.

(130)   (a) Street, RA. *Nat. Mater.* **2006,** *5,* 171-172. (b) Kokubo, H.; Sato, T.; Yamamoto, T. *Macromolecules* **2006,** *39,* 3959-3963. (c) Yamamoto, T.; Komarudin, D.; Arai, M.; Lee, B. L.; Suganuma, H.; Asakawa, N.; Inoue, Y.; Kubota, K.; Sasaki, S.; Fukuda, T.; Matsuda, H. *J. Am. Chem. Soc.* **1998,** *120,* 2047-2058. (d) Chen, T. A.; Wu, X.; Rieke, R. D. *J. Am. Chem. Soc.* **1995,** *117,* 233-244.

(131)   (a) Savenije, T. J.; Kroeze, J. E.; Yang, X. N.; Loos, J. *Adv. Funct. Mater.* **2005**, *15,* 1260. (b) Baek, N. S.; Hau, S. K.; Yip, H. L.; Acton, O.; Chen, K. S.; Jen, A. K. Y. *Chem. Mater.* **2008,** *20,* 5734.

(132)   (a) Shrotriya, V.; Li, G.; Yao, Y.; Chu, C. W.; Yang, Y. *Applied Physics Letters* **2006,** *88,* 073508. (b) Malliaras, G. G.; Salem, J. R.; Brock, P. J.; Scott, C. *Phys. Rev. B* **1998**, *58,* 13411. (c) Chirvase, D.; Chiguvare, Z.; Knipper, M.; Parisi, J.; Dyakonov, V.; Hummelen, J. C. *Phys. Rev. B* **2004**, *70*, 235207.

(133)   (a) Huang, J. H.; Ho, Z. Y.; Kekuda, D.; Chang, Y.; Chu, C. W.; Ho, K. C. *Nanotechnology* **2009,** *20,* 025202. (b) Li, G.; Shrotriy, V.; Yao, Y.; Huang, J.; Yang, Y. *J. Mater. Chem.* **2007,** *17,* 3126.

Publication

1. <u>K. C. Li</u>, Y. C. Hsu, J. T. Lin, C. C. Yang, K. H. Wei, H. C. Lin*, **"Novel Narrow-Band-Gap Conjugated Copolymers Containing Phenothiazine-Arylcyanovinyl Units for Organic Photovoltaic Cell Applications"**, *Journal of Polymer Science: Part A: Polymer Chemistry* **2008,** *46,* 4285-4304.

2. <u>K. C. Li</u>, Y. C. Hsu, J. T. Lin, C. C. Yang, K. H. Wei, H. C. Lin*, **"Soluble Narrow-Band-Gap Copolymers Containing Novel Cyclopentadithiophene Units for Organic Photovoltaic Cell Applications"**, *Journal of Polymer Science: Part A: Polymer Chemistry* **2009,** *47,* 2073-2092.

3. <u>K. C. Li</u>, J. H. Huang, Y. C. Hsu, P. J. Huang, C. W. Chu, J. T. Lin, K. H. Wei, H. C. Lin*, **"Tunable Novel Cyclopentadithiophene-Based Copolymers Containing Various Numbers of Bithiazole and Thienyl Units for Organic Photovoltaic Cell Applications"**, *Macromolecules* **2009,** (ASAP).

學經歷資料表

姓　　　名	李光潔
性　　　別	女
出生日期	1980 年 08 月 07 日
婚姻狀況	未婚
E-mail 信箱	u9318830.mse93g@nctu.edu.tw
聯絡電話	0921031375
通訊地址	300 新竹市大學路 100 號工程六館 EF707 室
永久地址	830 高雄縣鳳山市五福里五福二路 70 巷 4 號
學　經　歷	1998 年 9 月 - 2002 年 6 月 私立高雄醫學大學化學系 學士 2002 年 9 月 - 2004 年 7 月 私立高雄醫學大學醫藥暨 應用化學系 碩士 2004 年 9 月 - 2009 年 4 月 國立交通大學材料科學與 工程學系 博士
專　　　長	有機太陽能電池材料開發、合成與物性鑑定
學術著作	1. K. C. Li, Y. C. Hsu, J. T. Lin, C. C. Yang, K. H. Wei, H. C. Lin*, **"Novel Narrow-Band-Gap Conjugated Copolymers Containing Phenothiazine-Arylcyanovinyl Units for Organic Photovoltaic Cell Applications"**, *J. of Polymer Sci. Part A: Polymer Chem.* **2008,** *46,* 4285-4304. 2. K. C. Li, Y. C. Hsu, J. T. Lin, C. C. Yang, K. H. Wei, H. C. Lin*, **"Soluble Narrow-Band-Gap Copolymers Containing Novel Cyclopentadithiophene Units for Organic Photovoltaic Cell Applications"**, *J. of Polymer Sci. Part A: Polymer Chem.* **2009,** *47,* 2073-2092. 3. K. C. Li, J. H. Huang, Y. C. Hsu, P. J. Huang, C. W. Chu, J. T. Lin, K. C. Ho, K. H. Wei, H. C. Lin*, **"Tunable Novel Cyclopentadithiophene-Based Copolymers Containing Various Numbers of Bithiazole and Thienyl Units for Organic Photovoltaic Cell Applications"**, *Macromolecules* **2009,** (ASAP).